University of Manitoba

THE MAGNETIC PROPERTIES OF IRON-ZINC FERRITES

by

P. A. Dickof

in partial fulfillment of the
requirements for the degree of
Master of Science

Department of Physics

August, 1978

THE MAGNETIC PROPERTIES
OF IRON-ZINC FERRITES

BY

PETER ALEXANDER DICKOF

A dissertation submitted to the Faculty of Graduate Studies of the University of Manitoba in partial fulfillment of the requirements of the degree of

MASTER OF SCIENCE

ABSTRACT

Experimental studies of the magnetic properties of mixed Fe-Zn ferrites of the form $Zn_xFe_{3-x}O_4$ are presented. Magnetization measurements were performed as a function of temperature, field, and composition. The value of the moments on different sites of the compound was determined. Mössbauer measurements were taken for various temperatures and fields in order to obtain the temperature and field dependance of the canting angle and hyperfine fields. Relaxation effects were observed for x = 0.8 well below the ordering temperature. These effects were found to be suppressed in a magnetic field.

A modifies version of the localized canting model which considers second and third nearest neighbour interactions for some cases was developed. This model was used with the Mössbauer data to provide a fit of the spin structure to the bulk magnetic properties of the material.

ACKNOWLEDGEMENTS

I would like to thank Dr. A. H. Morrish for his supervision of this thesis and Dr. P. J. Schurer for his active and invaluable involvement in the research. In addition, I would like to express my gratitude to Dr. C. M. Srivastava for the generous loan of the samples used in this investigation. Thank you also to Ms. J. S. Vaisey for editing and Mrs. R. A. Bobie for typing this thesis.

TABLE OF CONTENTS

LIST OF FIGURES

LIST OF TABLES

Page

CHAPTER 1

1-1. INTRODUCTION

Mixed Zn ferrites of the type $Zn_x M_{3-x} O_4$ where M is a magnetic ion have been the subject of numerous investigations in the past, especially with regard to their magnetic properties [1,2]. The metallic ions occupy the tetrahedral A or octahedral B sites in the spinel crystal structure. The Zn ions preferentially occupy the A sites because of their tendency to form covalent bonds involving sp^3 orbitals. The magnetic moments at $x = 0$ on the A sites are aligned anti-parallel while those on the more numerous B sites are parallel to the magnetization direction. Therefore, the substitution of diamagnetic Zn ions for the M ions on the A sublattice is expected to result in an increase in the magnetic moment of the sample at 0K proportional to the amount of substitution. Such is indeed the case in the region where $x < 0.5$, although the increase is less than expected if free ion magnetic moments for the M ions are assumed. At higher Zn concentrations, i.e., $x \gtrsim 0.5$, the moment begins to decrease and for $x = 1.0$, an antiferromagnetic structure is observed.[3] Several explanations have been offered for the behaviour of the magnetization for $x \gtrsim 0.5$,[4,5,6] but spin canting has been determined to be primarily responsible. The canting angles have been measured for several systems using the neutron diffraction[7] or the Mössbauer effect techniques.[8,12] By using the measured values of the canting angles it is possible in principle to fit quantitatively the magnetization results. No such work has yet been done. Magnetization results and Mössbauer results have primarily been determined for different samples, and at differing temperatures and fields. A study to fit quantitatively the canting angles should allow a decision on whether or not the spin canting is solely responsible for the magnetization behaviour. It should be noted that a Mössbauer study can only give information about canting of the Fe magnetic moments. Therefore, the only mixed Zn system for which a correlation between magnetization and Mössbauer effect measurements is possible is the $Zn_x Fe_{3-x} O_4$ system.

Another interesting phenomenon in mixed Zn ferrites is the occurence of relaxation effects in the Mössbauer spectra. This is usually explained as being caused by ionic spin flipping[8,13]; however, superparamagnetic clusters[6] and domain wall oscillations[14,15] have also been proposed. Frequently, one finds that the Curie temperatures, as measured by the Mössbauer effect, neutron diffraction, and magnetization measurements, differ from each other.[16-23] This is probably correlated with the relaxation phenomena in the high Zn region, and the measurement time for each technique.

The present study consists of magnetization and Mössbauer effect measurements for ferrites of the type

$$[Zn^{2+}_{x}\ Fe^{3+}_{1-x}]\ (Fe^{2+}_{1-x}\ Fe^{3+}_{1+x})\ O_4$$

The system was first studied by Stuijts et al[24] for $x \lesssim 0.7$. As with other mixed Zn ferrites, the magnetization M was shown to increase with increasing x until $x \simeq 0.5$ after which it began to decrease. Also of interest was a peak in the magnetization versus temperature curve for $x = 0.7$ at 40K. Similar peaks were also observed by Ishikawa[6] in the Ni-Zn system. This maximum has not yet been explained.

A more recent study has been published by Srivastava et al[14,15] on samples with $x = 0.0, 0.2, 0.4, 0.6$, and 0.8. Their work showed magnetization results from 77K and 300K, and permeability spectra at 300K. The primary focus of their study was the relaxation phenomena which were found to occur well below the Curie temperature at the higher Zn concentrations ($x > 0.5$). These samples were prepared in a way similar to those of Stuijts et al[24], and were generously made available to us for the present study. X-ray diffraction techniques showed the samples to be free of impurity phases. The lattice parameters were measured using a Debye-Scherrer powder diffraction camera, and are plotted as a function of Zn concentration in fig. 1.1. The linear increase in lattice

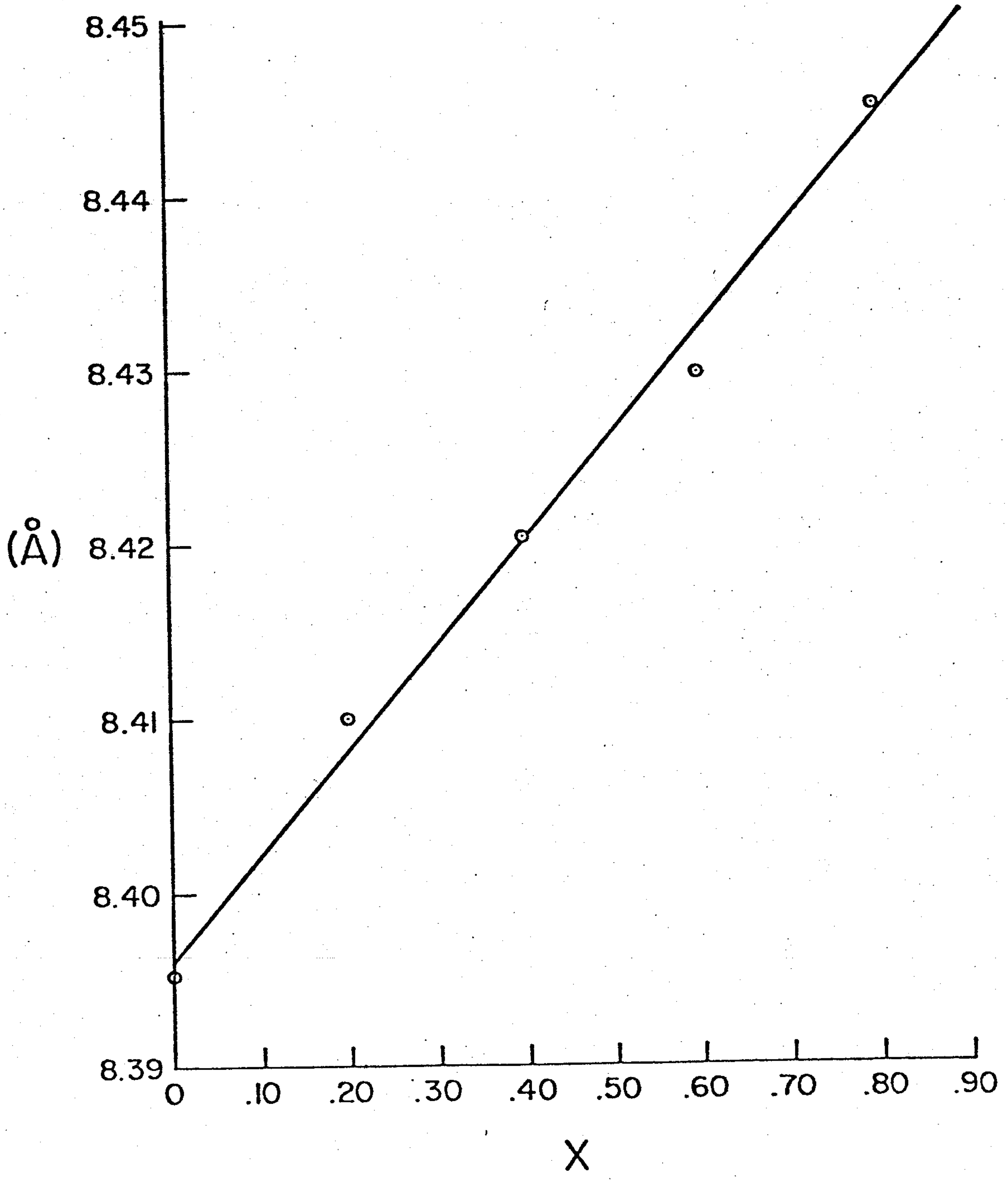

Fig. 1.1 Lattice parameter as a function of Zn concentration.

parameter with Zn concentration derives from the larger size of the Zn^{2+} ions as compared to the Fe^{3+} ions. The high angle lines were not broadened, indicating that the samples had a uniform Zn distribution. This thesis will compare our measured magnetization values with those calculated from the microscopic spin structure as determined from our Mössbauer study.

REFERENCES, INTRODUCTION

1. J. Smit and H. P. J. Wijn, Ferrites (Wiley, New York 1959).
2. Y. Hoshino et al (Eds.) Ferrites, Proceedings of the International Conference 1970 (Univ. Park Press, Baltimore London, Tokyo, 1971).
3. U. König et al, Sol. Stat. Comm., 8 (1970) 759.
4. M. A. Gilleo, Phys. Chem. Solids, 13 (1960) 33.
5. I. Nowik, J. Appl. Phys., 40 (1969) 872.
6. Y. Ishikawa, J. Phys. Soc. Japan, 17 (1962) 1877.
7. N. S. Satya Murthy et al, Phys. Rev., 181 (1969) 969.
8. J. M. Daniels and A. Rosencwaig, Can. Journal Phys., 48 (1970) 381.
9. L. K. Leung et al, Phys. Rev. B, 8 (1973) 29.
10. A. H. Morrish and P. J. Schurer, Physica, 86-88B (1977) 921.
11. P. E. Clark and A. H. Morrish, Phys. Stat. Sol. (a), 19 (1973) 687.
12. A. H. Morrish and P. E. Clark, Phys. Rev. B, 11 (1975) 278.
13. P. K. Iyengar and S. C. Bhargava, Phys. Stat. Sol. (b), 53 (1972) 359.
14. C. M. Srivastava et al, Phys. Rev. B, 14 (1976) 2032.
15. C. M. Srivastava et al, Phys. Rev. B, 14 (1976) 2041.
16. H. Szydlowski et al, Phys. Stat. Sol. (a), 2 (1970) K37.
17. H. Szydlowski et al, Phys. Stat. Sol. (a), 3 (1970) 769.
18. J. G. Booth and J. Crangle, Proc. Phys. Soc. Lond., 79 (1962) 1271.

19. G. A. Petitt and D. W. Forrester, Phys. Rev. B, 4 (1971) 3912.

20. P. K. Iyengar and S. C. Bhargava, Phys. Stat. Sol. (b) 46 (1971) 117.

21. J. G. Booth, Proc. Phys. Soc. Lond., 79 (1962) 1271.

22. S. C. Bhargava, Phys. Stat. Sol. (b) 53 (1972) 359.

23. C. Guilland and H. Crevaux, Compt. Rend., 230 (1950) 1256.

24. A. L. Stuijts et al, Ferrites, Proceedings of the International Conference 1970, p.236.

CHAPTER 2

THEORY

2-1. FERRIMAGNETISM IN FERRITES.

Ferrimagnets are ordered magnetic materials having two or more lattices antiferromagnetically aligned with a larger moment in one direction than the others. Ferrites, of which $[Fe^{3+}]\ (Fe^{2+}\ Fe^{3+})\ O_4$ is an example, are a class of ferrimagnetic metal oxides possessing a spinel structure. In this structure, metal ions occupy two different types of sites: A sites, indicated with brackets [ ]; and B sites, indicated with parentheses ( ). The A sites are tetrahedrally coordinated, and the B sites, of which there are twice as many occupied, are octahedrally coordinated as shown in figs. 2.1a and 2.1b.

The exchange interactions in the two lattices can be represented with 3 exchange parameters: J_{AB}, the intersublattice exchange parameter; and J_{BB} and J_{AA}, the intrasublattice exchange parameters. The molecular field for a spin on the ith lattice can then be written as

$$\vec{H}_i = \frac{2}{g\mu_B} \left(\vec{S}_j J_{ij} + \vec{S}_i J_{ii}\right)$$

where $\vec{S}_i$ and $\vec{S}_j$ represent the sum of the 6 neighbouring moments on either lattice, i.e.:

$$\vec{S}_A = \frac{6\mu_\alpha}{g\mu_B} \quad ; \quad \vec{S}_B = \frac{6\mu_\beta}{g\mu_B} \quad .$$

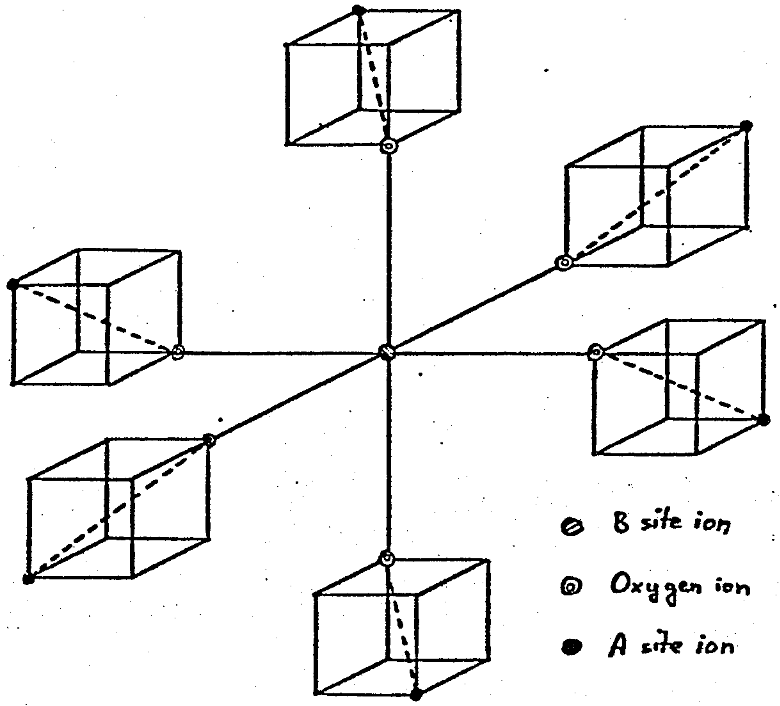

Fig. 2.1a Central B-site iron ion in a spinel structure surrounded by the six nearest oxygen ions and the six nearest A-site metal ions.

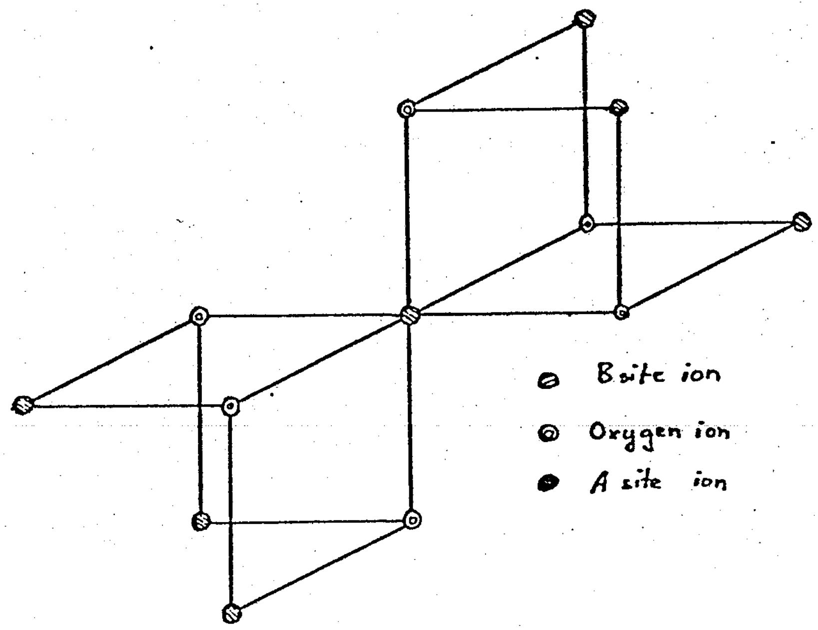

Fig. 2.1b Central B-site iron ion in a spinel structure surrounded by the six nearest oxygen ions and the six nearest B-site iron ions.

Here μ_α and μ_β are the magnetic moments of spins on the A and B lattices respectively. From the chemical formula of the example above, and using the free ion magnetic moments of $5\mu_B$ for Fe^{3+} ions and $4\mu_B$ for Fe^{2+} ions, we get $\mu_\alpha = 5\mu_B$ and $\mu_\beta = 4.5\mu_B$. As $|J_{AB}| > |J_{BB}| > |J_{AA}|$, and the exchange parameter J_{AB} is negative because of the antiferromagnetic nature of the superexchange interaction in ferrites, the two sublattices are arranged in an antiparallel fashion as shown in figure 2.2.

In $[Zn^{2+}_x\ Fe^{3+}_{1-x}]\ (Fe^{2+}_{1-x}\ Fe^{3+}_{1+x})O_4$, diamagnetic Zn^{2+} ions are randomly substituted onto the A sublattice, resulting in a change in $\vec{S}_A$ and $\vec{S}_B$, and in a breaking of exchange interactions. Geller et al[1] proposed that random canting occurred on the unsubstituted lattice under these conditions, on the basis of their experimental data. This proposal was mathematically developed by Rosencwaig[2], and is outlined here.

Random substitution of diamagnetic ions is assumed on the A site, and some average canting angle ϕ, with respect to the magnetization direction, is assumed for the B site. This allows us to write the local molecular field for a given B site ion called B_i, as

$$\vec{H}_i = \frac{2}{g\mu_B}\left(\vec{S}_A\ J_{AB} + \vec{S}_B\ J_{BB}\right).$$

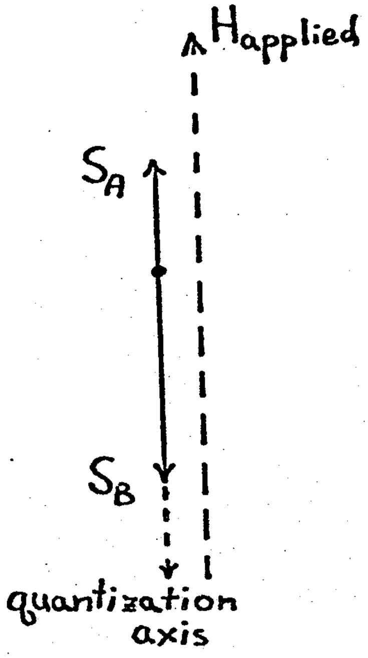

Fig. 2.2 Ferrimagnetic spin structure of Fe_3O_4.

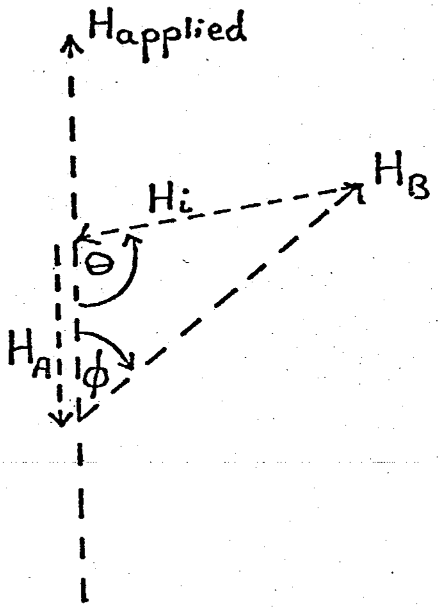

Fig. 2.3a Angular relationship between magnetic and hyperfine fields.

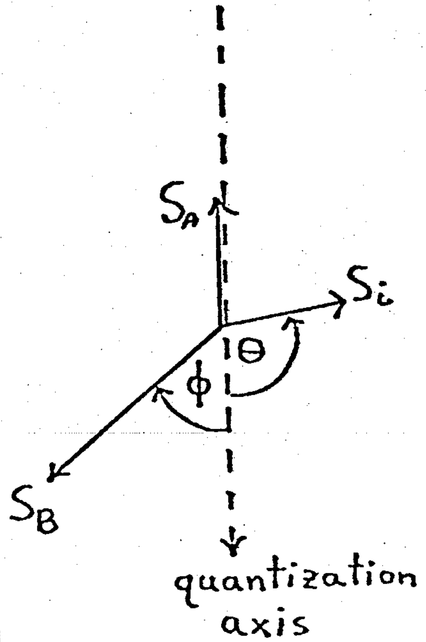

Fig. 2.3b Angular relationship of spins in fields of fig. 2.3a.

Since there is diamagnetic substitution on the A lattice, we may write

$$|\vec{S}_A| = \frac{(6-m)\mu_\alpha}{g\mu_B}$$

where m is the number of neighbouring A sites occupied by diamagnetic ions. Similarily, we have

$$|\vec{S}_B| = \frac{6\mu_\beta(x)}{g\mu_B} ,$$

where

$$\mu_\beta(x) = (1-x)\ \mu_\beta^{2+} + (1+x)\ \mu_\beta^{3+} ,$$

and μ_β^{2+} and μ_β^{3+} represent the moments of the B site Fe^{2+} and Fe^{3+} ions respectively. In fig. 2.3a, $\vec{H}_i$ as well as the component terms $\vec{H}_A$ and $\vec{H}_B$ are shown. The resultant spin structure, with the moment S_i taking a canting angle of θ with respect to the magnetization direction, is shown in fig. 2.3b. By using fig. 2.3a, and the formula for the local molecular field, we may write

$$\cos\theta = \frac{S_A - S_B\delta\cos\phi}{[S_A{}^2 + (S_B\delta)^2 + 2S_A\, S_B\cos\phi]^{\frac{1}{2}}}$$

where

$$\delta = \frac{J_{BB}}{J_{AB}} .$$

It is clear that θ can take on any value between 0° and 180° depending on the value of the term $S_A - S_B\delta\cos\phi$. If

$S_A > S_B\delta \cos \phi$, i.e., if the net intersublattice interaction on a spin is greater than the net intrasublattice interaction, then θ will be smaller than the average canting angle ϕ. If $S_A < S_B\delta \cos \phi$, then θ will be larger than the average canting angle ϕ, and if $S_A = 0$, then the B_i spin will be aligned antiparallel to the B sublattice and the magnetization direction.

In order to calculate any bulk properties of the mixed Zn ferrite, we must calculate the probability of a spin having m of its six A sites occupied by Zn^{2+} ions. This is determined by the binomial distribution:

$$P(x,m) = \binom{6}{m} x^{6-m} (1-x)^m$$

which allows us to write the 0 K magnetic moment as

$$\mu(x,T=0) = 2\sum_{m=0}^{6} P(x,m) \cos [\theta(x,m)]\mu_\beta(x)-(1-x)\mu_\alpha .$$

The first term indicates the decrease in moment due to random canting on the B sublattice, and the second represents the increase in moment due to diamagnetic substitution on the antiparallel A sublattice.

This model has been successfully applied to the substituted Yttrium Iron Garnets, and gives a qualitative agreement with the experimental data for Zn substituted ferrites. Neutron diffraction[3] and Mössbauer effect[4] data show canting angles in these systems for Zn substitution in excess of $x \approx 0.5$.

However, no quantitative correlation has been published as yet. Reasons for this include the facts that magnetization, neutron diffraction and Mössbauer results have largely come from different samples. Also, canting angles, as determined by the Mössbauer effect, have been measured in relatively large fields and not compared with magnetization results in the same field.

2.2 MODEL REVISIONS

The major flaw of the localized canting model is that only first nearest neighbour interactions are considered. In most cases, this is a justifiable approximation, but for cases in which there are spins having canting angles $\theta > 90^0$, a revision is required, considering second and even third nearest neighbour interactions.

Spins which have canting angles $\theta > 90^0$ will be referred to as "reversed" spins. If all or nearly all of the B site neighbours of one of these reversed spins are themselves reversed, then that spin will have been reversed twice. Similarily, if all the neighbours to a reversed spin are themselves doubly reversed, that spin will have been triply reversed. Since $|J_{AB}|$ is known to be much larger than $|J_{BB}|$ we will assume that only those spins with all six nearest neighbour A sites occupied by Zn ions can be reversed. The probabilities for such multiple reversals occurring are higher than might at first be expected. This is because the B site nearest neighbours of a spin having six

Zn A site nearest neighbours each have three Zn A site nearest neighbours which are shared with the central spin. The remaining A site neighbours are shared among each other. The calculations for multiple reversal (single and double reversal for x = 0.6 and single and triple reversal for x = 0.8) are given in Appendix A, where the notation used in the following discussion is defined. The probabilities for multiple reversals are extremely small for all other cases. The results of these calculations are as shown in table 2.1.

TABLE 2.1

Multiple reversal probabilities for x = 0.6 and x = 0.8.

Sample	Unreversed (B_0-B_5)	Single Reversal B_6	Double Reversal B_6	Triple Reversal B_6
x = 0.6	0.95334	0.04274	0.00392	---
x = 0.8	0.73786	0.15219	0.08121	0.02874

This allows determination of the total number of spins reversed or unreversed with respect to the magnetization direction, as shown in table 2.2.

TABLE 2.2

Probabilities for reversed and unreversed spins in samples with x = 0.6 and x = 0.8.

Sample	Unreversed (B_{05})	Reversed (B_6')	Unreversed (B_6)
x = 0.6	0.95334	0.00392	0.04274
x = 0.8	0.73786	0.08121	0.18093

The bulk magnetic moment at T = 0 K may now be written as

$$\mu(x,T=0)= \sum_{m=0}^{5}\Big\{P(m,x)\cos[\theta(m,x)]+P(6',x)\cos[\theta(6',x)] + P(6,x)\cos[\theta(6,x)]\Big\}2\mu_\beta-(1-x)\mu_\alpha$$

One would expect $\theta(6,x)$ to be quite close to zero, since the only interaction that a B_6 site has is with B_6' sites, each having the same canting angle with respect to the quantization axis. An average of the six B_6' spins, will therefore be of the form:

$$\overline{S}_{6'} = S\,\frac{\cos\theta}{6}\sum_{i=1}^{6}\cos\psi_i\,\hat{x} + S\,\frac{\cos\theta}{6}\sum_{i=1}^{6}\sin\psi_i\,\hat{x} + S\sin\theta\,\hat{y}.$$

Since the spins will be randomly distributed over the azimuthal angle ψ_i, the first two terms will be close to zero.

This analysis will be used in Chapter 5 of this thesis to compare the Mössbauer and magnetization results.

2.3 MÖSSBAUER EFFECT

General Theory

The energy difference for a given nuclear transition is a well defined quantity, but in general, the energy distribution of gamma rays emitted or absorbed in such a transition is quite broad due to the recoil of the nucleus involved. In solids however, where the nucleus in question is strongly bound to the lattice, the recoil can be absorbed by the crystal as a whole for a significant fraction called the recoil-free fraction, of such transitions. In such a case, due to the enormous mass of the crystal compared to that of a single atom, the energy lost in the recoil is very small, and the energy of the emitted γ-ray is well-defined. This is referred to as the Mössbauer effect, and is of interest in solid state physics because the emitted γ-ray energy is well enough defined ($\frac{\Delta E}{E} \sim 10^{-12}$ for Fe^{57}) to allow observation of the shifting of the nuclear levels due to the so-called "hyperfine interactions" arising from the distribution of the electron cloud surrounding the nucleus. In the case of Fe^{57}, the nucleus of interest in this thesis, the Mössbauer transition is the transition between the first excited state with spin 3/2 and the ground state with spin 1/2, having an energy of 14.36 keV.

The first hyperfine interaction is the electric monopole interaction between the s-electron charge cloud and the nucleus. This is referred to as the isomer shift because it shifts the energy of the 3/2-1/2 transition when the nucleus is placed in the different electronic environments found in different chemical bondings of Fe atoms. The energy shift due to this interaction may be written as

$$\Delta E = \frac{2\pi}{5} Ze^2 \, |\Psi(o)|^2 \, (R_{ex}^2 - R_{gd}^2)$$

where R_{ex} and R_{gd} are the radii of the excited and ground states of the nucleus respectively; Z is the nuclear charge; and $-e|\Psi(o)|^2$ is the electronic charge density.

The second hyperfine interaction is the electric quadrupole interaction which represents the interaction of the nuclear quadrupole moment with the electric field gradient due to the other charges in the crystal. The Hamiltonian for this interaction may be written as

$$H_Q = \frac{V_{zz} Qe}{4I(2I-1)} [3 I_z^2 - I(I+1) + \frac{\eta}{2} (I_+^2 + I_-^2)]$$

where

$$\eta = \frac{V_{xx} - V_{yy}}{V_{zz}} ;$$

and the V_{ii} are the principle axes of the electric field gradient tensor chosen such that

$$| V_{zz} | > | V_{xx}| > | V_{yy} |;$$

Q is the quadrupole moment of the nucleus, and I the nuclear spin. This gives eigenvalues

$$\Delta E_Q = \frac{V_{zz} Qe}{4I(2I-1)} [3M_I^2 - I (I+1)] (1+\frac{\eta^2}{3})^{\frac{1}{2}}$$

where $M_I = I, I-1, \ldots, -I.$

The ground state of Fe^{57} is spherically symmetrical and thus has no quadrupole moment, but the first excited state has some of its (2I+1) degeneracy lifted and is split into two states: $M_I = \pm 3/2$ and $M_I = \pm 1/2$.

The final hyperfine interaction is the magnetic dipole interaction which gives the interaction between the nuclear magnetic dipole moment μ and the magnetic field at the nucleus. The Hamiltonian for this interaction may be written as

$$\mathcal{H} = -gu_n \vec{I}\cdot\vec{H}_{hf}$$

where H_{hf} is the hyperfine field at the nucleus, μ_n is the nuclear Bohr magneton (eh/2Mc) and g is the nuclear g factor. This gives eigenvalues

$$\Delta E_{hf} = -gu_n H_{hf} M_I$$

In general, H_{hf} may be written as

$$H_{hf} = H_S + H_L + H_D + \frac{4}{3}\pi \text{ M-DM} + H_{ext}$$

where $H_S = \frac{16\pi}{3}\mu_B \langle\Sigma(S\uparrow - S\downarrow)\rangle$, the fermi contact interaction between the nucleus and the unbalanced s electron spin density caused by exchange interactions with the partially filled 3d shell;

$H_L = -2\mu_B \frac{\langle L\rangle}{\langle r^3\rangle}$, the orbital magnetic component. (For Fe^{3+} L=0, and thus makes no contribution.)

$H_D = -2\mu_B \frac{3\vec{r}(\vec{S}\cdot\vec{r})}{r^5 - \vec{S}/r^3}$, the dipolar interaction with the electronic spin of the atom;

$\frac{4}{3}\pi\vec{M}$ and $-D\vec{M}$ are the Lorentz fields and demagnetizing fields respectively; and, H_{ext} is the externally applied field.

All three of the hyperfine interactions can occur simultaneously giving the energy levels shown in figure 2.4. In this case, standard absorption spectroscopy gives a six line spectrum as shown in figure 2.5.

The relative intensities of the line pairs 1-6: 2-5: 3-4 are given by $\frac{9}{4}(1+\cos^2\theta) : 3\sin^2\theta : \frac{3}{4}(1+\cos^2\theta)$ where θ is the angle between the direction of the magnetic field, and the incident direction of the absorbed gamma ray. For an iron foil absorber, all the domains are aligned in the plane of the foil, while the gamma rays are perpendicular to that plane. The intensity ratio is therefore 3:4:1. A powdered sample with a random orientation of spins would have intensities 3:2:1 as calculated by averaging over the angle θ. For an aligned material, with the magnetization direction parallel to the incident gamma rays, the canting angle can be calculated from the line intensities using the following equation:

$$\theta = \arcsin\left[\frac{(\frac{3}{2} A_{2,5}/A_{1,6})}{(1+\frac{3}{4}(A_{2,5}/A_{1,6}))}\right]^{\frac{1}{2}}$$

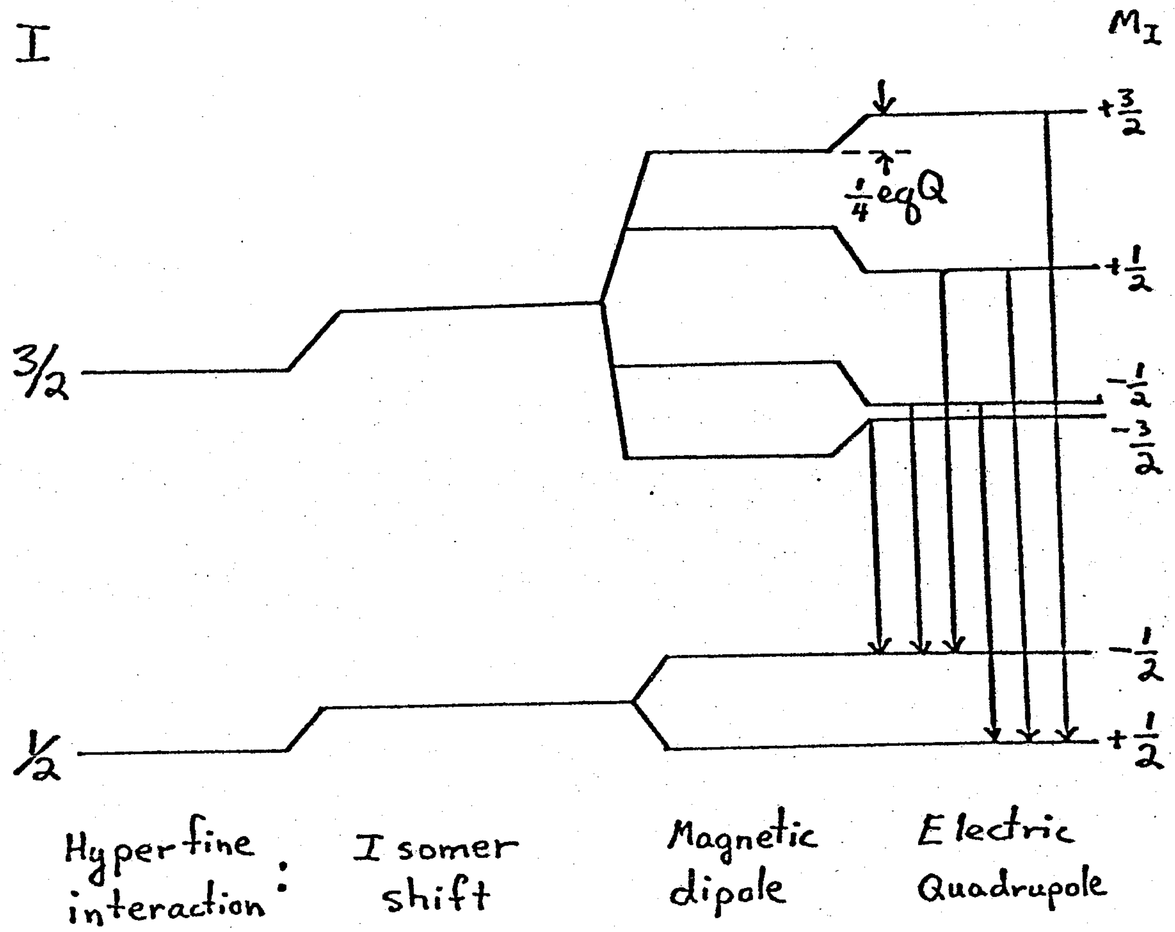

Fig. 2.4 Hyperfine field splitting for an axially symmetric electric field gradient tensor with symmetry axis parallel to H.

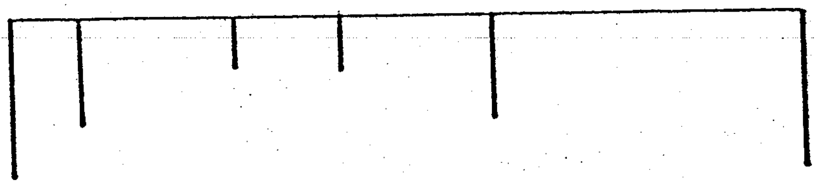

Fig. 2.5 Hyperfine spectrum for an axially symmetric electric field gradient tensor with symmetry axis parallel to H.

2.4 RELAXATION EFFECTS

All of the above results assume that the hyperfine field is a constant in time. This is not always the case, and in general, there is a relaxation time τ_r of the atomic spin to states other than the ground state, causing fluctuations in the hyperfine field. The effect of such fluctuations on Mössbauer spectra has been analysed by several authors[5,7] by assuming that individual spins relax by a stationary Markoff process.

The analysis has shown that if the relaxation time is long, compared with the Larmor precession time of the nucleus, a well-defined six line spectrum is observed for an ordered material. However, if the relaxation time is short, compared with the Larmor precession time of the nucleus, we observe a time-averaged spectrum. Thus, for an ordered material with spin waves (which have a precession time much shorter than the Larmor precession time), we observe a single six line spectrum with a hyperfine field proportional to the average z-component of the spin. For materials in which the spins are relaxing between various states such that the average z-component of the spin is zero, a central paramagnetic peak will be observed.

In the intermediate region, where the relaxation time is comparable to the Larmor precession frequency, we observe a "relaxed" spectrum in which the six-line spectrum begins to broaden. Simultaneously, the inner lines gain area at the expense of the outer lines. This type of spectrum is found in the transition region between the ordered and the disordered state of some ferromagnets[8].

There are several mechanisms by which relaxation can proceed. Spin-spin and spin-lattice processes are the sources of relaxation for individual random spins, and are the accepted cause of the relaxation found in some ferromagnetically ordered materials in the immediate vicinity of the Curie temperature[8]. However, in the Zn substituted ferrites, relaxation is found well below the temperature where the material is completely disordered. There would no longer appear to be a Curie temperature as such because the magnetic order breaks up over a wide temperature range. Two new processes have been proposed to explain this. Ishikawa[8] proposed superparamagnetic cluster relaxation, the relaxation of small, single-domain clusters of spins acting as one large spin, and Srivastava[9] proposed relaxation due to domain wall oscillations. Neither model has been conclusively validated or invalidated.

REFERENCES, THEORY

1. S. Geller et al, Bell Systems Tech. J., 43 (1964) 565.
2. A. Rosencwaig, Can. Jour. Phys., 48 (1970) 2857.
3. N. S. Satya Murthy et al, Phys. Rev., 181 (1969) 969.
4. A. H. Morrish and P. J. Schurer, Physica, 86-88B (1977) 921.
5. N. Blume and J. A. Tjon, Phys. Rev., 165 (1968) 446.
6. F. van der Woude and A. J. Dekker, Phys. Stat. Sol., 9 (1965) 775.
7. A. M. Afanasev and Y. Kagan, Soviet Physics, JETP, 18 (1964) 1139.
8. F. Van der Woude et al, Proceedings of the Conference on the Application of the Mössbauer Effect (Tihany 1969) P. 133.
9. Y. Ishikawa, J. Phys. Soc. Japan, 17 (1976) 1877.
10. C. M. Srivastava et al, Phys. Rev. B, 14 (1976) 2032.

CHAPTER 3

MAGNETIZATION MEASUREMENTS

3.1 EQUIPMENT

The magnetization measurements were performed using a vibrating sample magnetometer, usually within the field of a regulated, water-cooled electromagnet. For fields in excess of 18kOe, a super-conducting solenoid was used for which a set of sensing coils was developed. The system was calibrated using a sphere of spectroscopically pure nickel and the values of Crangle and Goodman[1].

The coil system was constructed on the basic design suggested by Mallinson[2] and is shown in figure 3.1. The individual coils were made up of 880 turns of #36 wire on a plexiglass former, the dimensions of which are shown in figure 3.2.

Fig. 3.2 Plexiglass Coil Former

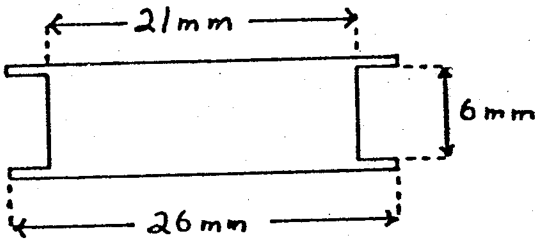

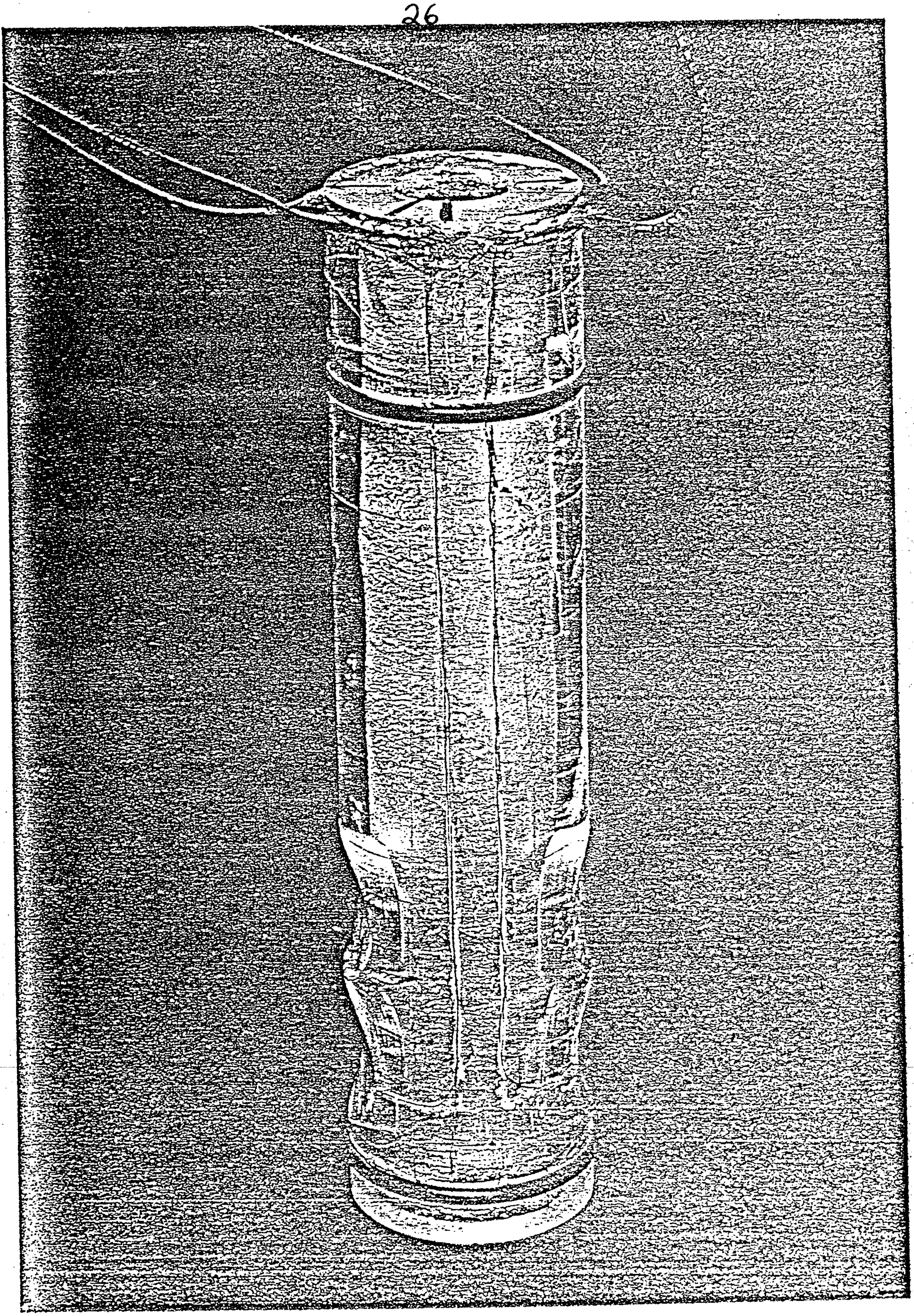

Fig. 3.1 Magnetometer coil system for use with superconducting solenoid.

The coils were wired in series in order to obtain the maximum output voltage, and mounted onto a plexiglass tube, perpendicular to the axis of the magnetic field. The lead wires were recessed in vertical grooves along the sides of the tube. There were o-rings near the top and the bottom of the tube to allow a friction fit to the magnet bore. The sample was vibrated closely about an equilibrium position at the centre of the four coils and the voltage generated in the coils was monitored to obtain the relative magnetization of the sample. The temperature of the sample, for measurements from 4.2K to 300K, was controlled using a flow-through liquid helium cryostat with a temperature stability of ±0.5K. Above room temperature, a vacuum furnace with a temperature stability of ±2K was used.

3.2 MEASUREMENTS

The magnetic moment was primarily measured in fields between 0kOe and 18kOe, with a few extra measurements in fields up to 50kOe. Spontaneous magnetization values were calculated using a least squares fit of the flat, saturated region (greater than 10kOe) of the magnetization versus magnetic field plots, to extrapolate to zero field. Curie temperatures were measured by using a least squares fit, to extrapolate the last few points before the "tail" on the spontaneous magnetization curve to the temperature axis.

3.3 RESULTS

The values of the magnetization for the various samples are shown as a function of field at 4.2K in figure 3.3. This figure indicates a qualitative difference in the behaviour of the various samples. For the samples with $x = 0.0$ and 0.2, saturation occurs in a field of approximately 8kOe. Above 10kOe, the susceptibility for these samples is less than 0.05 emu/gm-kOe. The samples $x = 0.8$ and 0.6 however, are clearly not saturated even at 50kOe, having susceptibilities at that field of 0.57 emu/gm-kOe and 0.33 emu/gm-kOe respectively. The $x = 0.4$ sample represents an intermediate case. The susceptibility in the samples with higher Zn concentrations is attributable to localized canting angles which are field dependent, as will be seen from the Mössbauer results in Chapter 4.

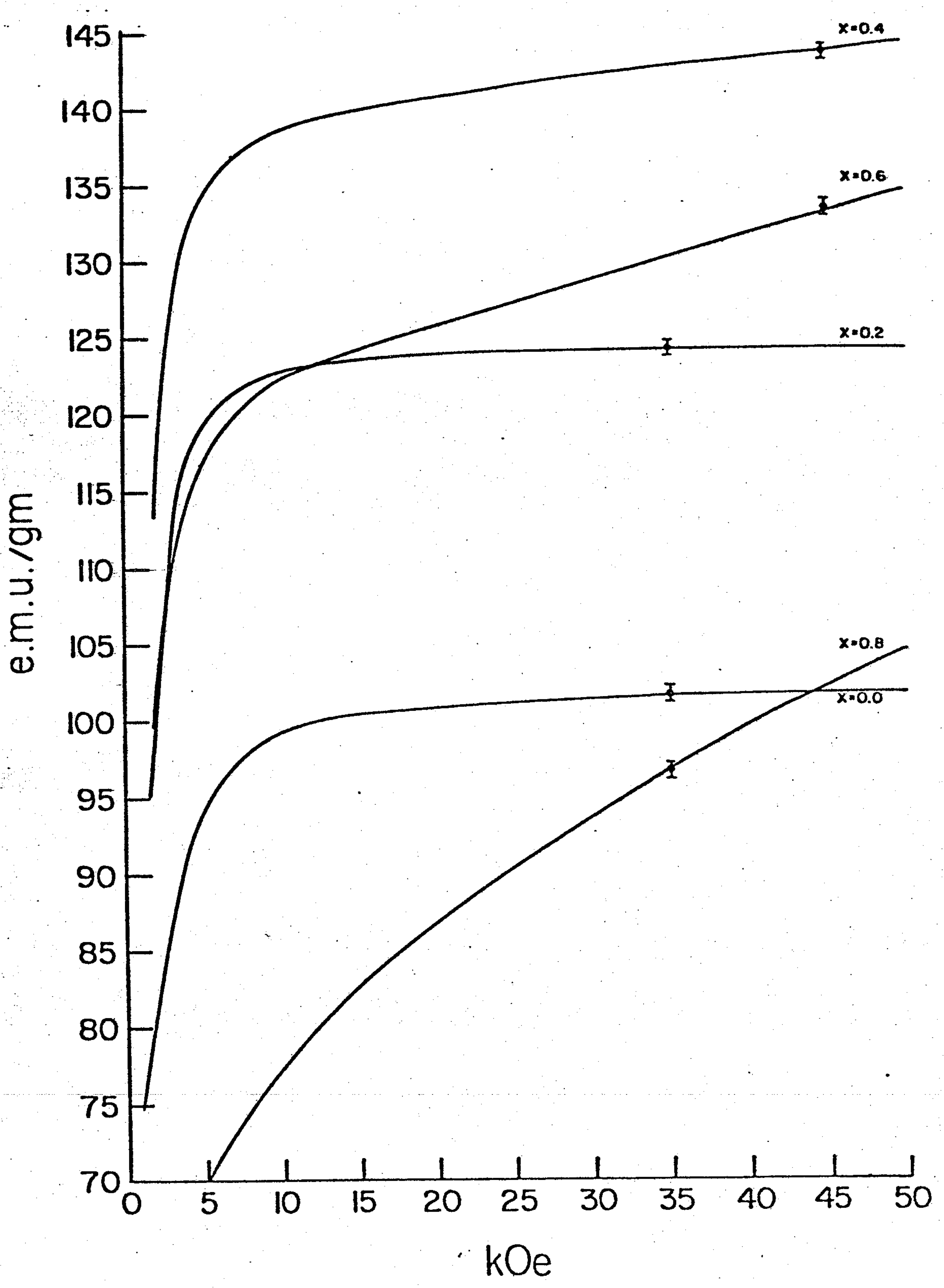

Fig. 3.3 Magnetization of $Zn_x Fe_{3-x}O_4$ versus applied field for $x = 0.0, 0.2, 0.4, 0.6$ and 0.8.

The magnetization at 4.2K is plotted as a function of x for fields of 0, 10, 35 and 50kOe in figure 3.4. The moments calculated by assuming no canting and free ion magnetic moments for the Fe^{2+} and Fe^{3+} ions are also plotted, as are the values of Stuijts et al, for 10kOe at 5K. The measured values rise to a maximum in the vicinity of $x = 0.5$, and then begin to decrease. The difference in susceptibility for the various samples is reflected in the increase in the spread of the moments at various fields with increasing Zn concentration. The results of Stuijts et al are in qualitative agreement with ours, differences probably being due to inhomogeneities in their samples. In the region below $x \simeq 0.5$ the free ion calculations give a moment that rises much more rapidly than observed in the data, although the $x = 0.0$ value is in agreement with the data. This discrepancy can be ascribed to covalency effects in the solid changing the magnetic moments from the free ion values and will be discussed in Chapter 5 of this thesis.

A plot of the extrapolated zero field magnetization as a function of temperature for all the samples is shown in figure 3.5. Once again, qualitative differences can be found between the samples. The samples with low Zn concentrations appear to be largely ordered up to a significant fraction of

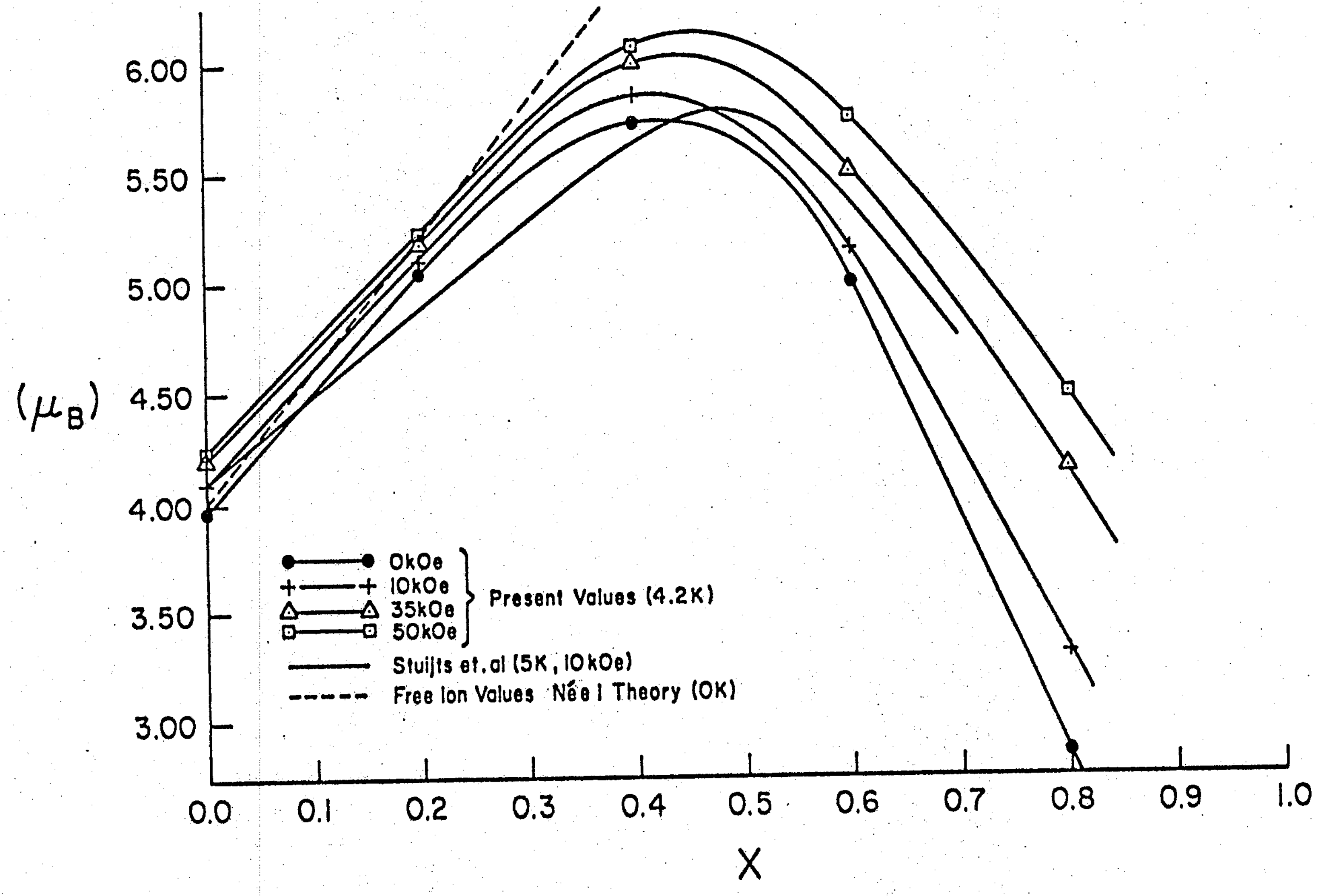

Fig. 3.4 Magnetization versus Zn concentration.

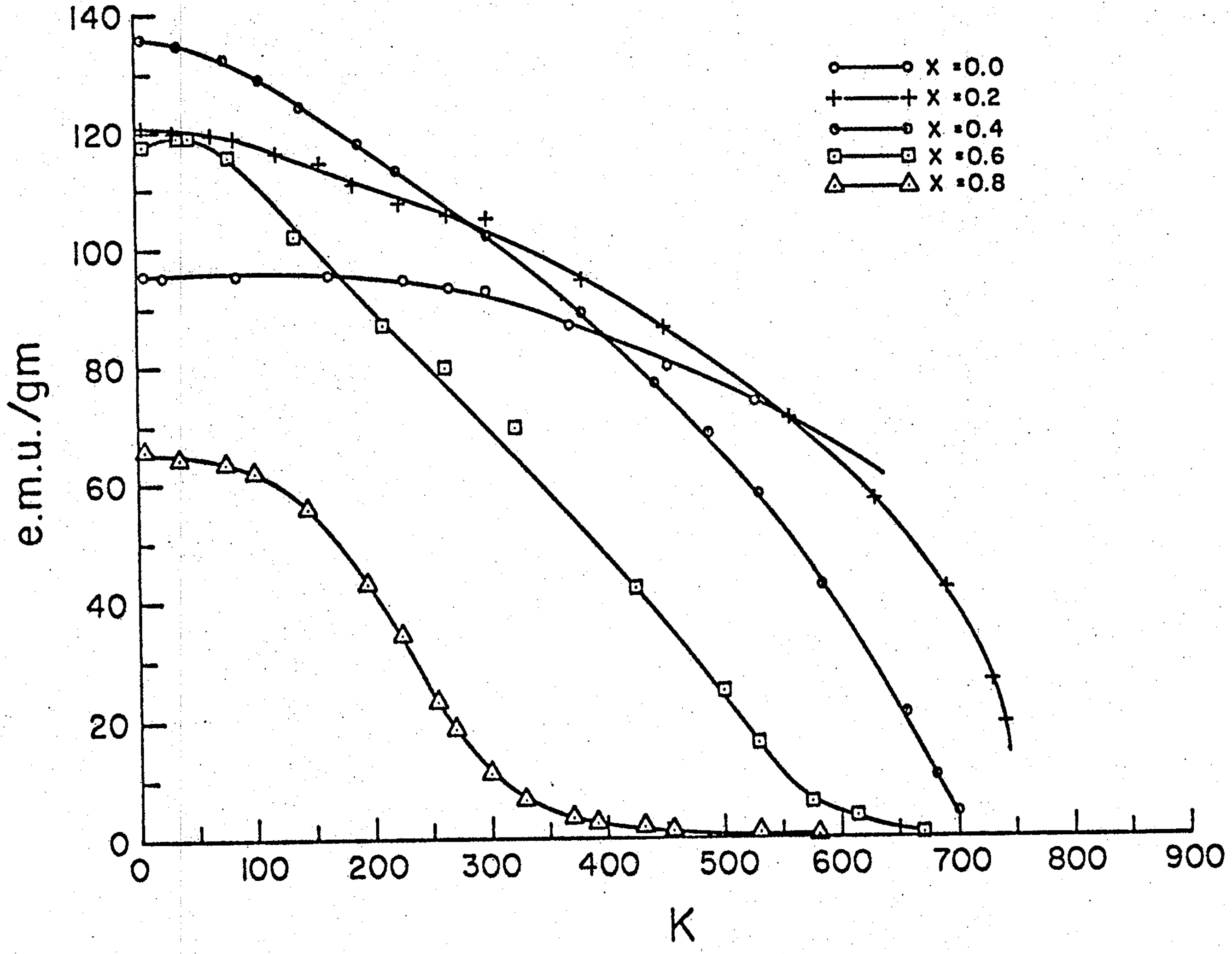

Fig. 3.5 Spontaneous magnetization versus temperature.

their Curie temperature. The higher the Zn concentration however, the more rapidly the moment decreases, and the less the curve resembles a Brillouin curve. For the x = 0.8 sample, the moment decreases almost linearly from ∿ 80K to ∿ 300K, while the x = 0.6 sample behaves similarly between ∿70K and ∿550K. This is linked to the relaxation effects occurring in these compounds at these temperatures (see Chapter 5). The Curie points measured are given in table 3.1, where they are compared with those of Stuijts[3] and Srivastava[4].

TABLE 3.1

Curie temperatures derived from magnetization measurements.

	Stuijts (10kOe)	Srivastava (7kOe)	Present (0kOe)
0.0	838	875	---
0.2	763	788	784
0.4	695	732	709
0.6	532	624	597
0.8	---	335	330

The agreement of our data with that of Srivastava is quite good, any differences probably being due to the difference in the magnetic fields in which the measurements were made.

Another effect of interest is shown in figures 3.6 and 3.7. These figures give the plots of magnetization versus temperature at fields of 0, 10, 18, 35 and 50kOe for the samples x = 0.6

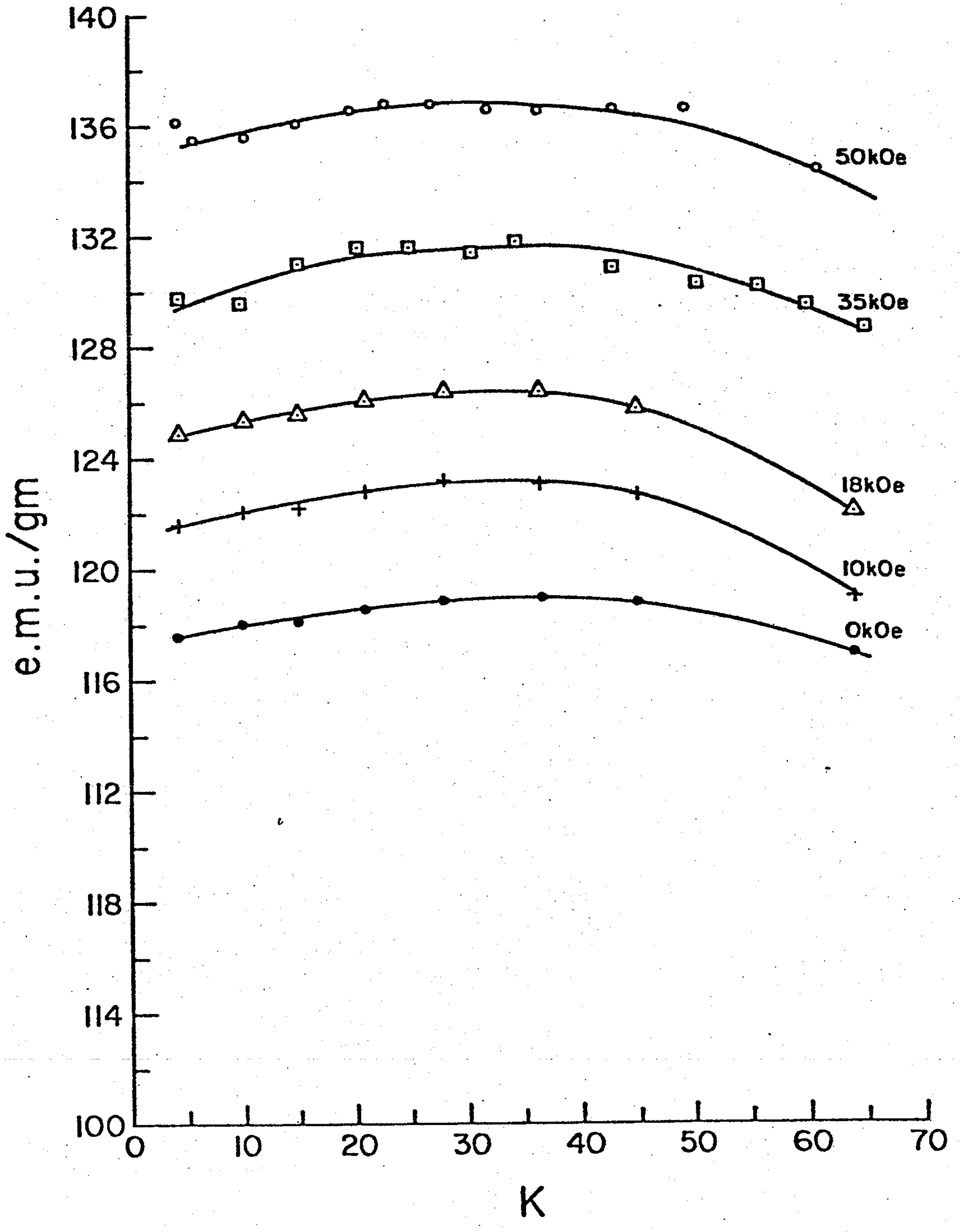

Fig. 3.6 Magnetization versus temperature for $Zn_{0.6}Fe_{2.4}O_4$.

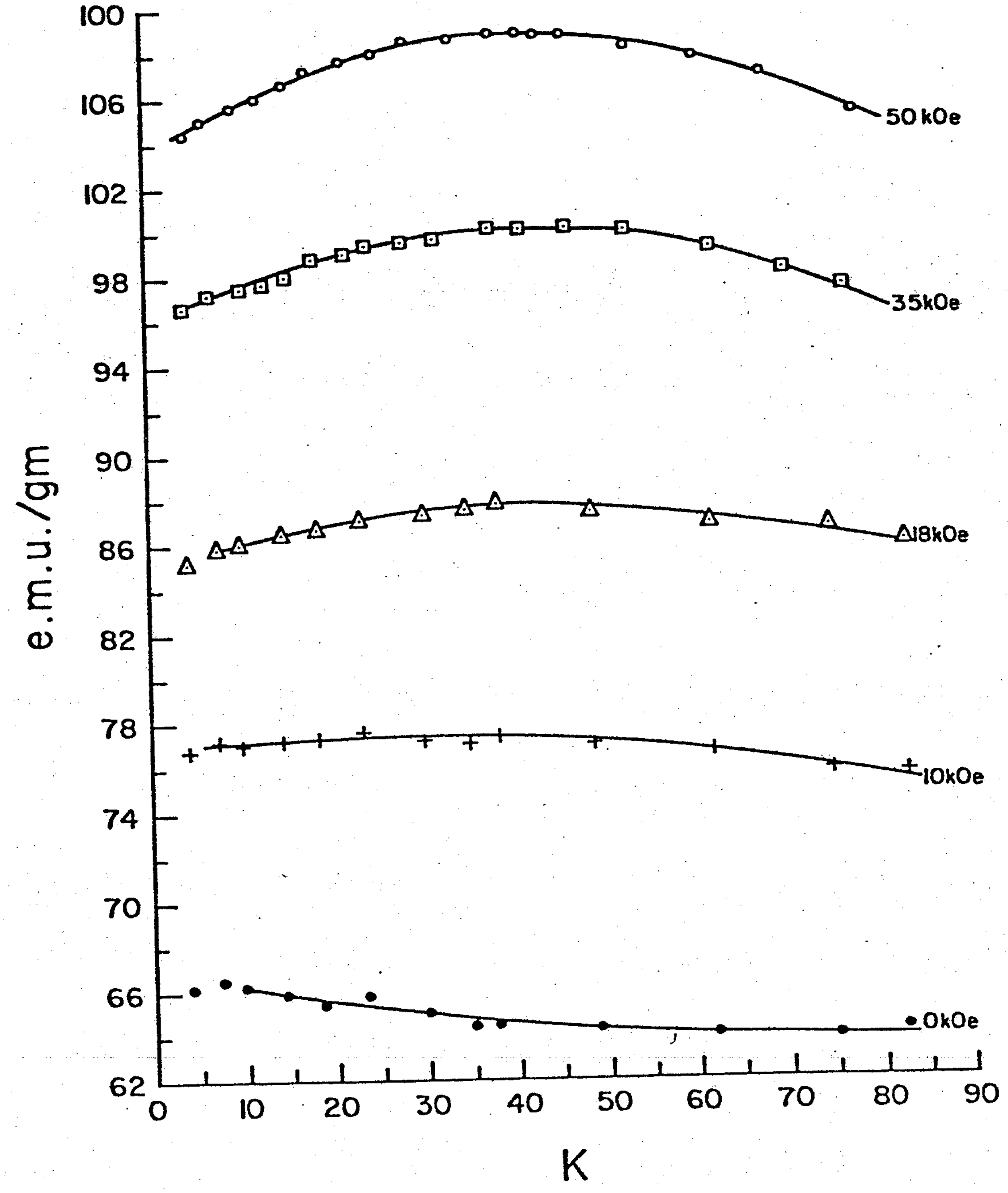

Fig. 3.7 Magnetization versus temperature for $Zn_{0.8} Fe_{2.2}O_4$.

and x = 0.8 respectively. For the x = 0.6 sample, a peak, with a maximum ∿ 1% higher than the value at 4.2K, is present at 33K for all fields. For the x = 0.8 sample, a similar peak is found at 40K for fields 18kOe or larger. The percentage increase in the moment at the maximum is a function of the applied field, being largest (∿4%) for the largest field applied (50kOe). With the help of data from Mössbauer experiments, these peaks will be explained in Chapter 5 as being due to a combination of factors: a more rapid decrease for some moments than for others; and, a change in canting angles with temperature.

In figure 3.8 we have plotted the x = 0.8 moment in fields of 10kOe, 18kOe, 35kOe and 50kOe and at temperatures of 4.2K and 40K. At 40K, one can see that the average high field susceptibility above 10kOe has risen 15% above the value at 4.2K. (See table 3.2.)

TABLE 3.2

The average high field susceptibility above 10kOe for x = 0.8 at 4.2K and 40K.

High field susceptibility	4.2K	0.69 emu/gm-kOe
High field susceptibility	40K	0.79 emu/gm-kOe

These values will be compared with the Mössbauer results in Chapter 5.

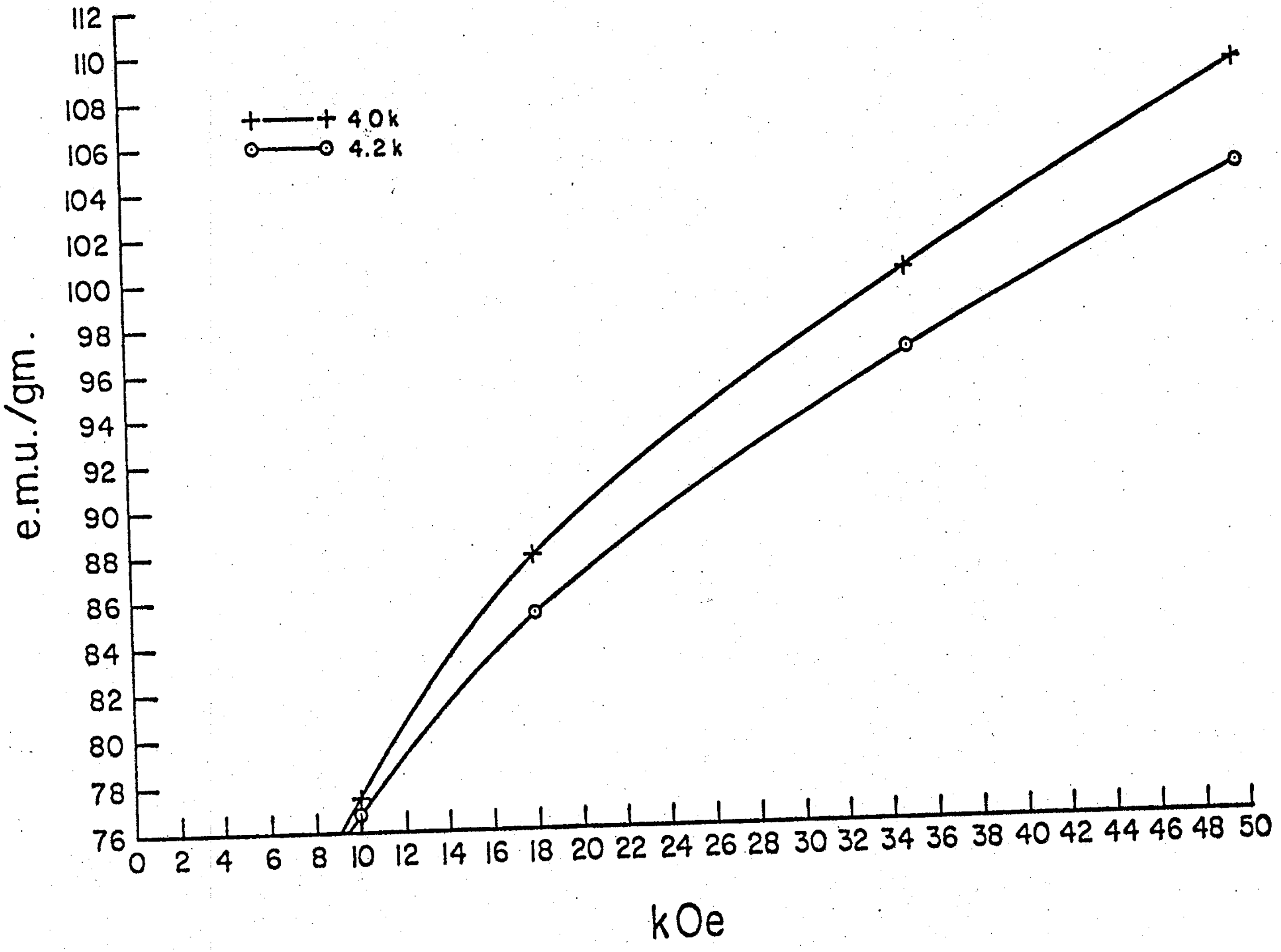

Fig. 3.8 Magnetization versus applied field for $Zn_{0.8}Fe_{2.2}O_4$, T=4.2K, 40K.

REFERENCES

1. J. Crangle and G. M. Goodman, Proc. Roy. Soc. Lond. A, 321 (1971) 477.
2. J. Mallinson, J. Appl. Phys., 37 (1966) 2514.
3. A. L. Stuijts et al, Ferrites Proceedings of the International Conference 1970, P. 236.
4. C. M. Srivastava et al, Phys. Rev. B, 14 (1976) 2032.

CHAPTER 4

MÖSSBAUER EFFECT MEASUREMENTS

4.1 EXPERIMENTAL TECHNIQUES

A standard transmission Mössbauer spectrometer was employed in a constant acceleration mode, giving a linear energy scale for the spectra. The system was calibrated by using either an iron foil or α-Fe_2O_3 absorber, taking the separation of the outer lines of iron, as 10.6570 mm/sec or 330kOe[1]. All isomer shifts are given with respect to iron. These calibrations also allowed us to measure the linewidth (0.28 mm/sec for iron linearity. The linearity was such that for an iron foil spectrum, the splittings Δ_{12}, Δ_{23}, Δ_{45} and Δ_{56} were 48.78, 48.91, 48.86 and 48.90 channels respectively.

The temperature of the absorber was controlled below room temperature with a stability better than ±0.1K using a liquid helium Dewar, custom-built by Oxford Instrument Company. A high temperature vacuum furnace with a temperature stability better than ±0.5K was used for measurements above room temperature. The absorber could also be placed in fields of up to 50kOe by using a super-conducting solenoid. Another liquid helium Dewar, custom-built by Thor Cryogenics Ltd., was available to control samples temperatures from 4.2K to room temperature, with a stability better than ±0.1K, while the sample was in the field of the super-conducting solenoid.

Spectra were fit using a program "Monkey" which performs a least squares fit of the equation:

$$I(\nu) = \left[I(o)\sum_{i=o}^{m} k_i(\nu-\nu_o)^i\right]\left[1-\sum_{j=1}^{n}\frac{\alpha_j}{\frac{(\nu-\nu_j)^2}{(0.5\beta_j)^2}+1}\right]$$

to the experimental data by using the technique of variable matrix minimization. The first term represents the background, and the second term subtracts up to 24 Lorentzian peaks from the background. As many as 72 linear combinations of the Lorentzian parameters may be simultaneously constrained.

The constraints used in fitting the parameters are outlined here. All component spectra were symmetrically constrained, i.e., the linewidth and depth of the first peak equal the linewidth and depth of the sixth peak. The splitting ratios for the 2-5 lines as compared to the 1-6 lines were constrained to the theoretical values. All spectra used quadratic background functions. In addition to these general constraints, special constraints were used for specific spectra. These will be discussed later.

Canting angles were calculated for the various component spectra in order that the values could be used for the calculation of the bulk magnetization. Two methods were used to calculate these angles: the intensities method; and, the hyperfine fields method. The intensities method uses the ratios of the areas of the 2-5 and 1-6 lines of the various spectra and the formula

$$\theta = \arcsin \left[\frac{\frac{3}{2}\,(A_{2,5}/A_{1,6})}{1 + \frac{3}{4}\,(A_{2,5}/A_{1,6})}\right]^{\frac{1}{2}}$$

This gives the angle between the total hyperfine field at the nucleus, and the incident direction of the absorbed gamma ray (here parallel to the applied magnetic field). This method is reasonably accurate (±10° or less) because the line intensities are usually well defined. For small angles ($\theta<20^{\circ}$) the relative error becomes large, but this has small effect on the calculated moments for the samples since these depend on $\cos\theta$ as was shown in Chapter 2. The cosine of an angle changes slowly in the region $\theta<30^{\circ}$.

The hyperfine fields method for calculating the canting angles uses the cosine rule to solve for the canting angle (figure 4.1) giving us

$$\theta = \mathrm{arcos} \left[\frac{H_{hpf}^{2} + H_{app}^{2} - H_{hpf\,total}^{2}}{2\,H_{hpf}\,H_{app}}\right].$$

This method has many associated problems. The required information for the calculation of an angle is: the value of the applied field, the internal hyperfine field, and the total measured hyperfine field. The internal hyperfine field must be measured in another spectrum, in which the applied field is zero. In general, the hyperfine fields for a spectrum where the applied field is small are unresolved and have errors which are

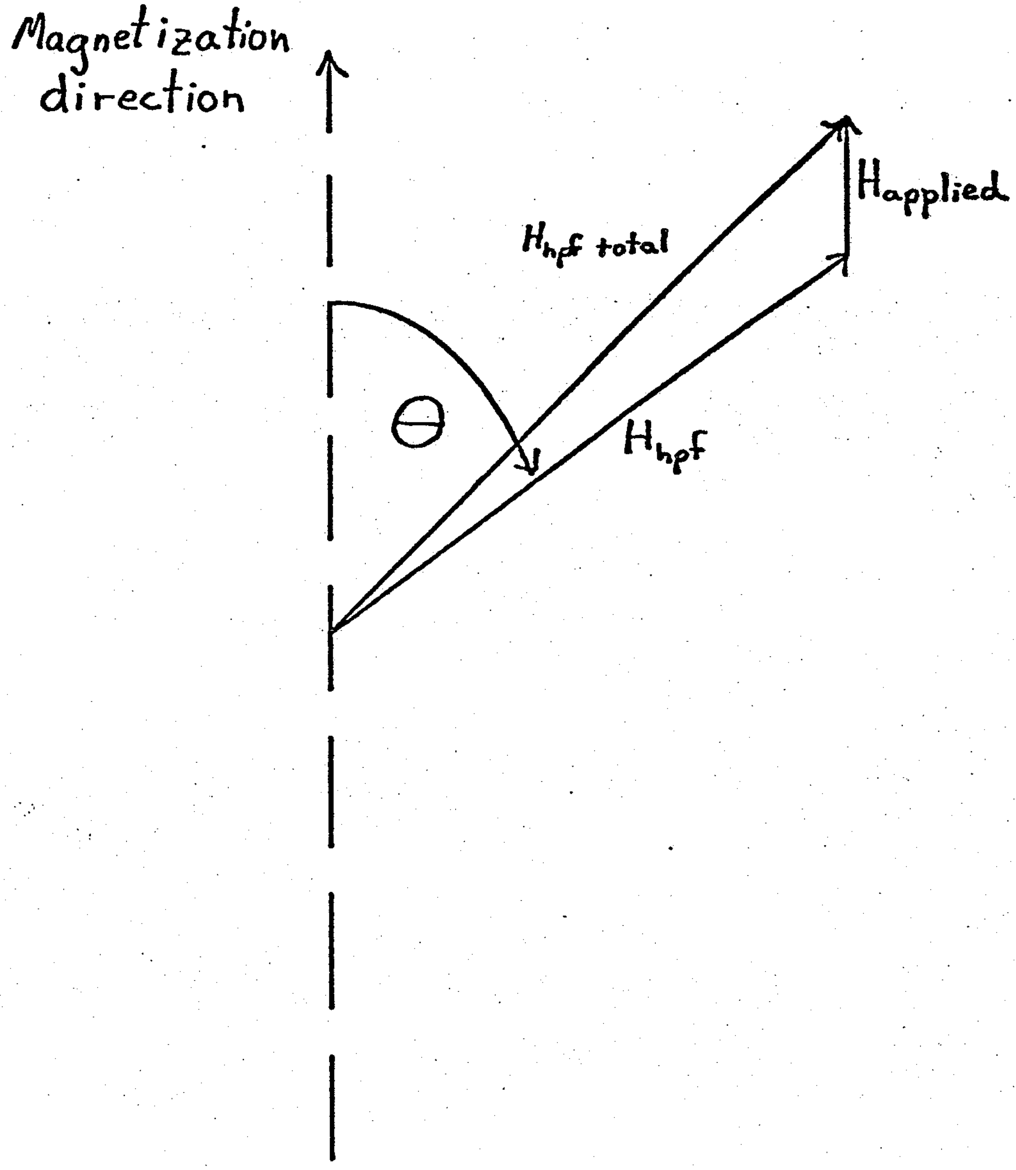

Fig. 4.1 Hyperfine fields and canting angle.

a significant percentage (up to 100% for low fields) of the applied field. Since the hyperfine field terms in the numerator dominate, and since the hyperfine fields can at most differ by H_{app}, this error can easily result in a very large canting angle error. There is also evidence, discussed in Chapter 5, that the internal hyperfine field changes in both orientation and magnitude when an external field is applied, in which case this method is inapplicable.

In general, the errors throughout this section are those given by the fitting program. However, for those cases where several subspectra are not resolved, and were fitted with a six line spectrum, a larger error of 5kOe was assigned due to the uncertainty of the placement of the unresolved subspectra within the fitted peaks. In those fits where all of the subspectra were fit with one six line spectrum, this placement error was raised to 10kOe. These figures represent approximately one quarter and one half the linewidth of the fitted lines respectively.

4.2 RESULTS AT 4.2K

We will now present the experimental data obtained from the Mössbauer study. In order to determine the canting angles on various sites, measurements were conducted in various fields at 4.2K. These results will be used in Chapter 5 to explain the behaviour of the bulk magnetization as a function of applied field (see fig. 3.3) and Zn concentration (see Fig. 3.4).

Below x = 0.5 the zero field spectra at 4.2K (figs. 4.2-4.4) may be resolved into two six-line components, one for the Fe^{2+} ions and one for the Fe^{3+} ions. The intensity ratios for these spectra were constrained to their theoretical values. The linewidth of the Fe^{3+} component ($\sim$ 0.6 mm/sec.) indicates a relatively small distribution in hyperfine fields. The Fe^{2+} component, however, has a linewidth of $\sim$1.0 mm/sec, indicating a fairly broad hyperfine field distribution. The Fe^{3+} spectrum is relatively unaffected by an increase in the Zinc concentration, but the Fe^{2+} spectrum shows a declining hyperfine field with increasing Zn concentration. This may be connected with other data, shown later, in which the Fe^{2+}/Fe^{3+} distinction ceases to exist for x = 0.6, 0.8.

No field measurements were made of the samples x = 0.0, 0.2 as the susceptibilities above 10kOe (described in Chapter 3) placed an upper limit of $\sim 10^{o}$ canting on these samples. Canting angles of such small size are extremely difficult to measure. For the x = 0.4 sample, the canting expected, assuming that all the high field susceptibility is due to the disappearance of canting, is 17^{o}. Spectra of this sample were taken in fields of 10kOe (fig. 4.5) and 50kOe (fig. 4.6). Canting angles were assumed only for the B sites, and were calculated both by the intensities (θ_I) and by the hyperfine fields (θ_H) method. The large errors in the hyperfine fields

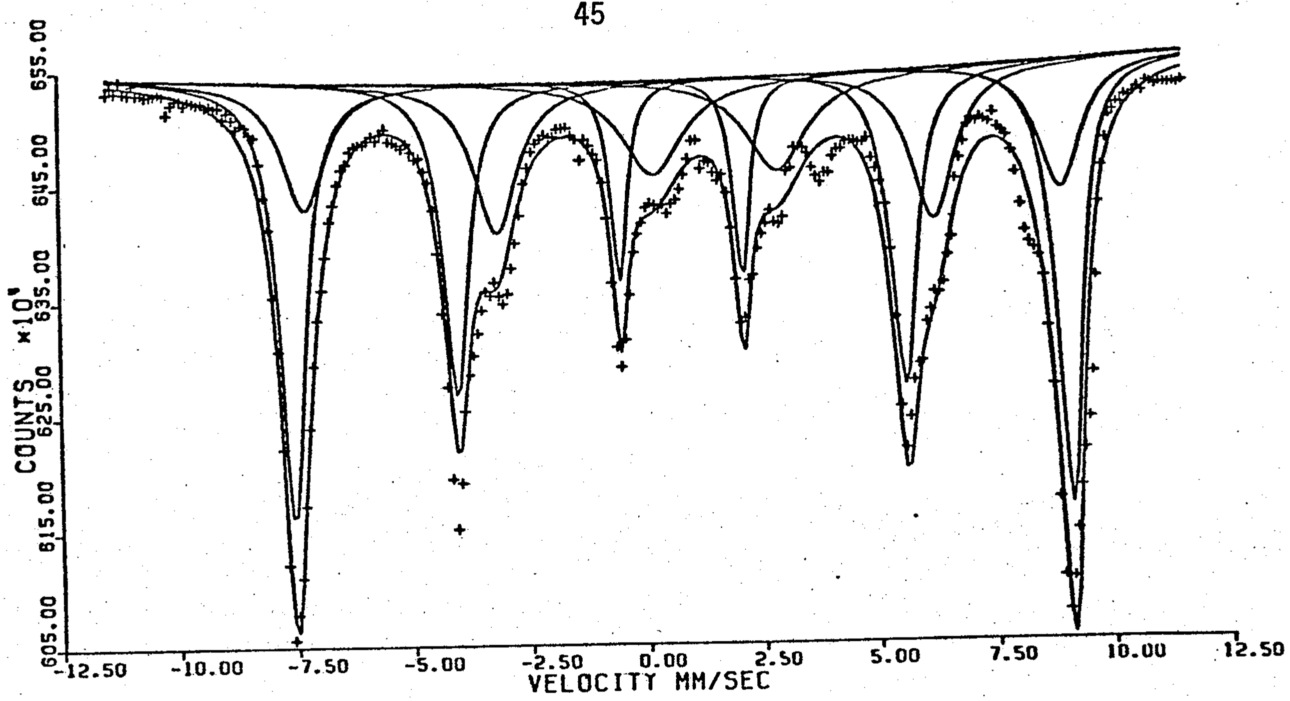

Fig.4.2 Mössbauer spectrum of x = 0.0 at 4.2K, 0kOe.

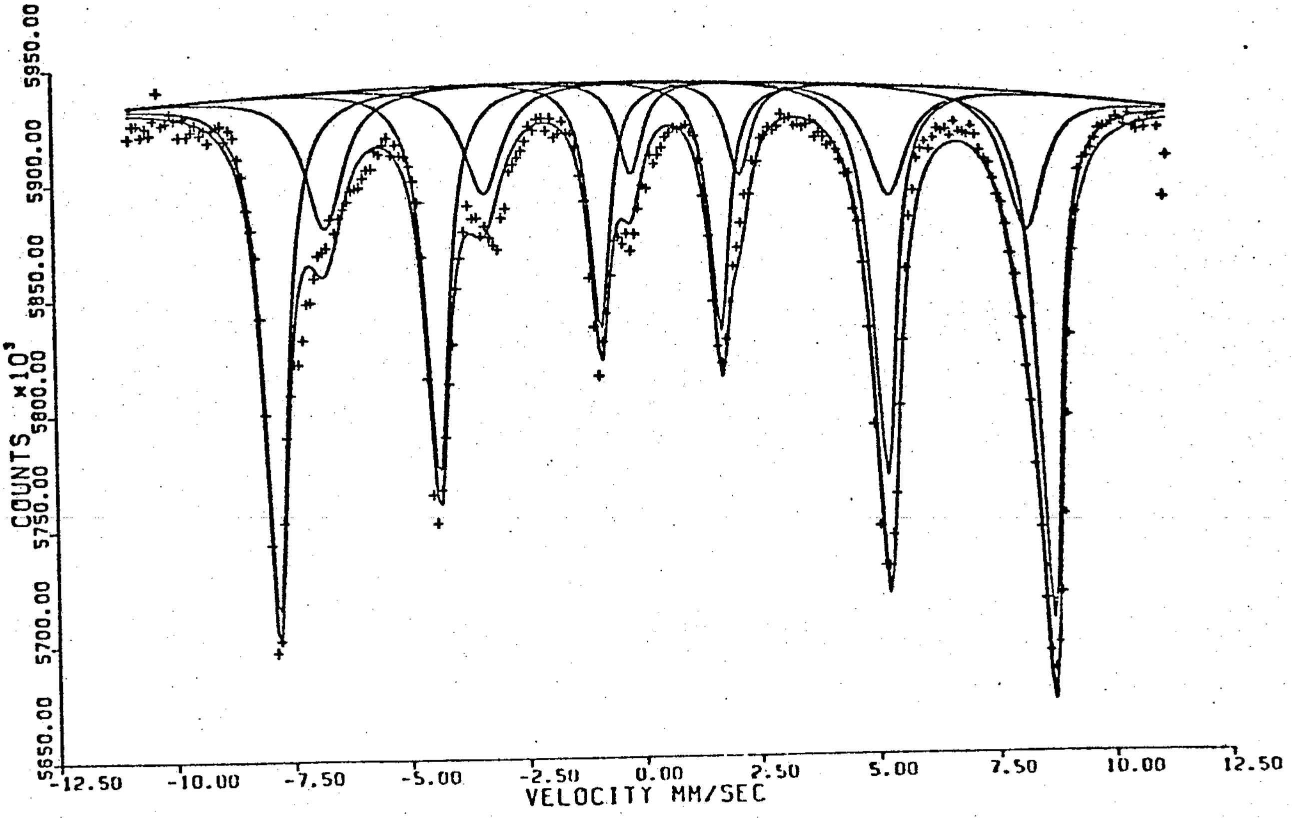

Fig.4.3 Mössbauer spectrum of x = 0.2 at 4.2K, 0kOe.

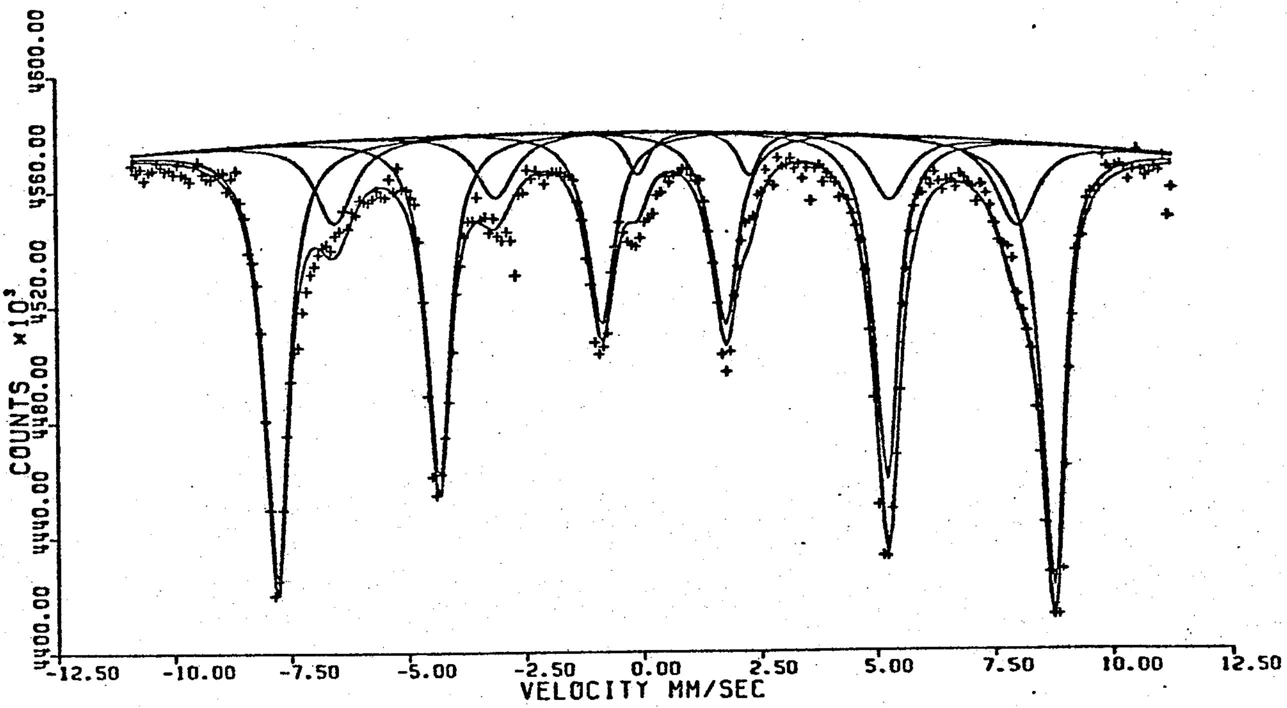

Fig. 4.4 Mössbauer spectrum of x = 0.4 at 4.2K, 0kOe.

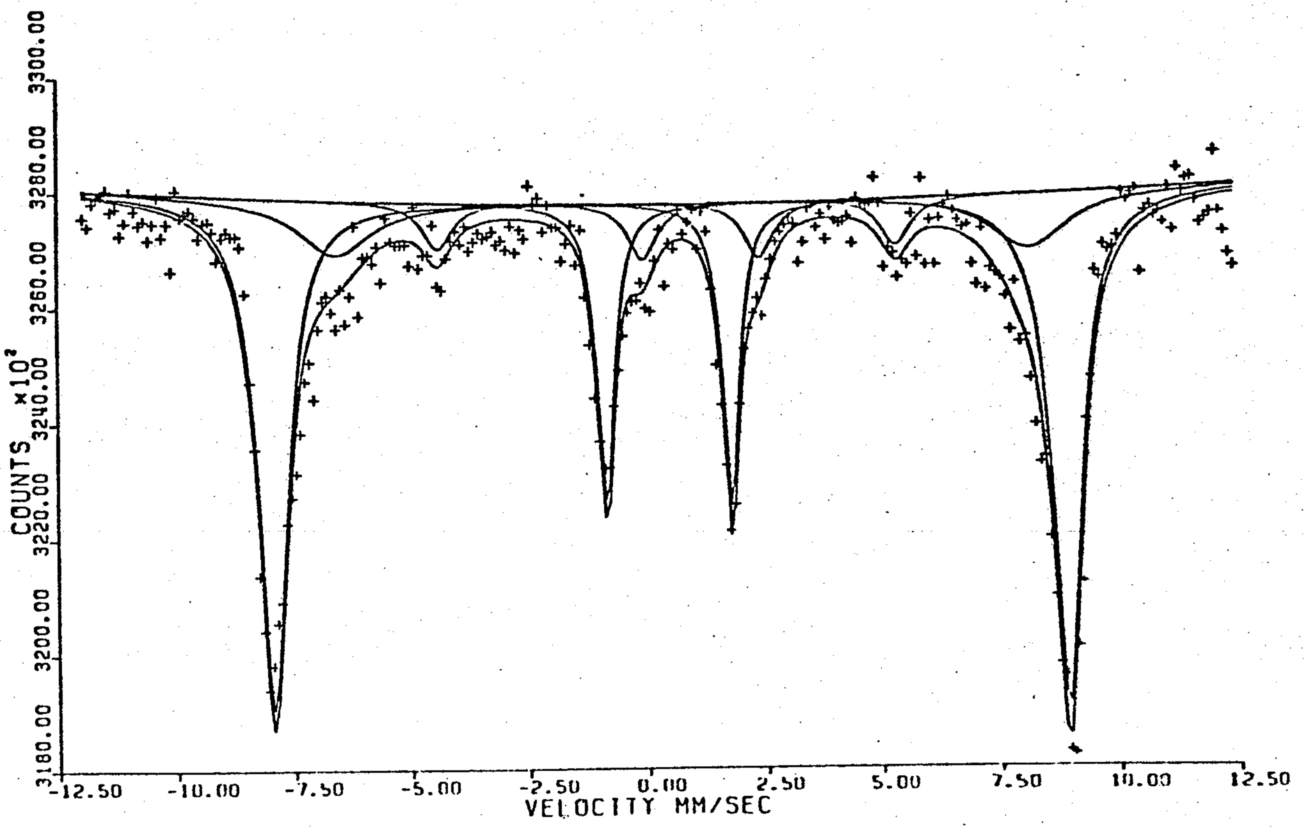

Fig. 4.5 Mössbauer spectrum of x = 0.4 at 4.2K, 10kOe.

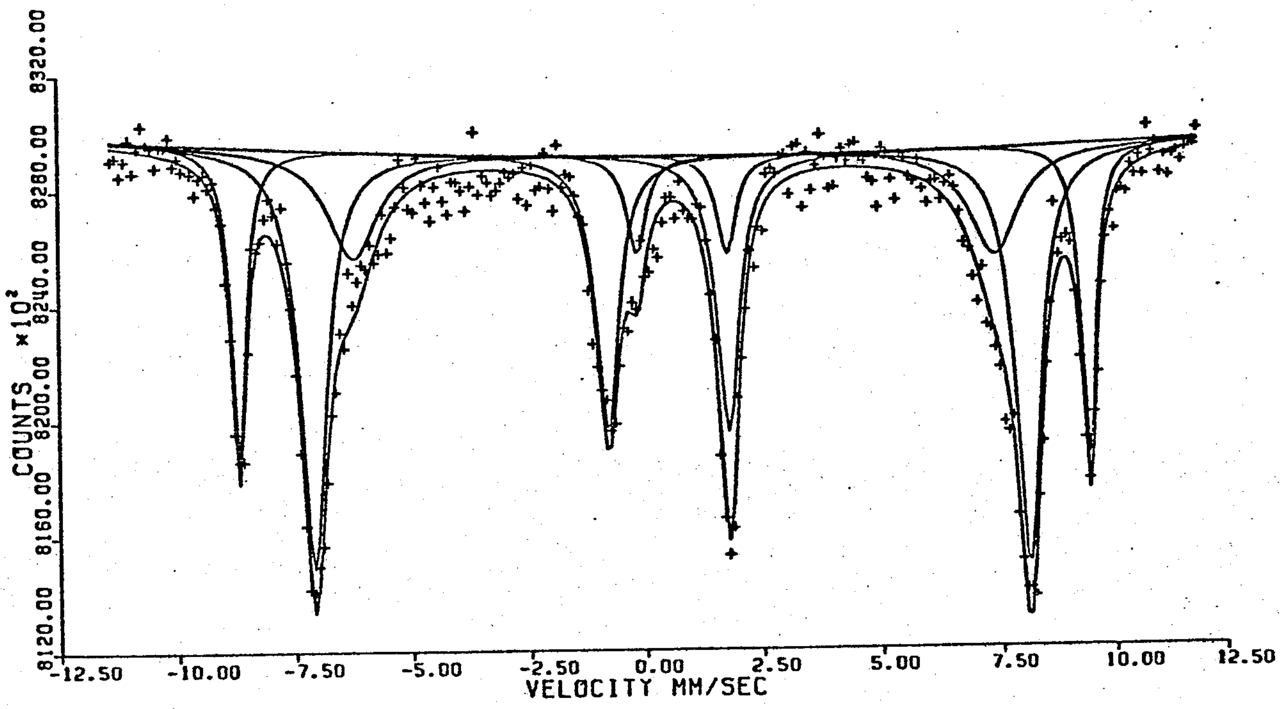

Fig. 4.6 Mössbauer spectrum of x = 0.4 at 4.2K, 50kOe.

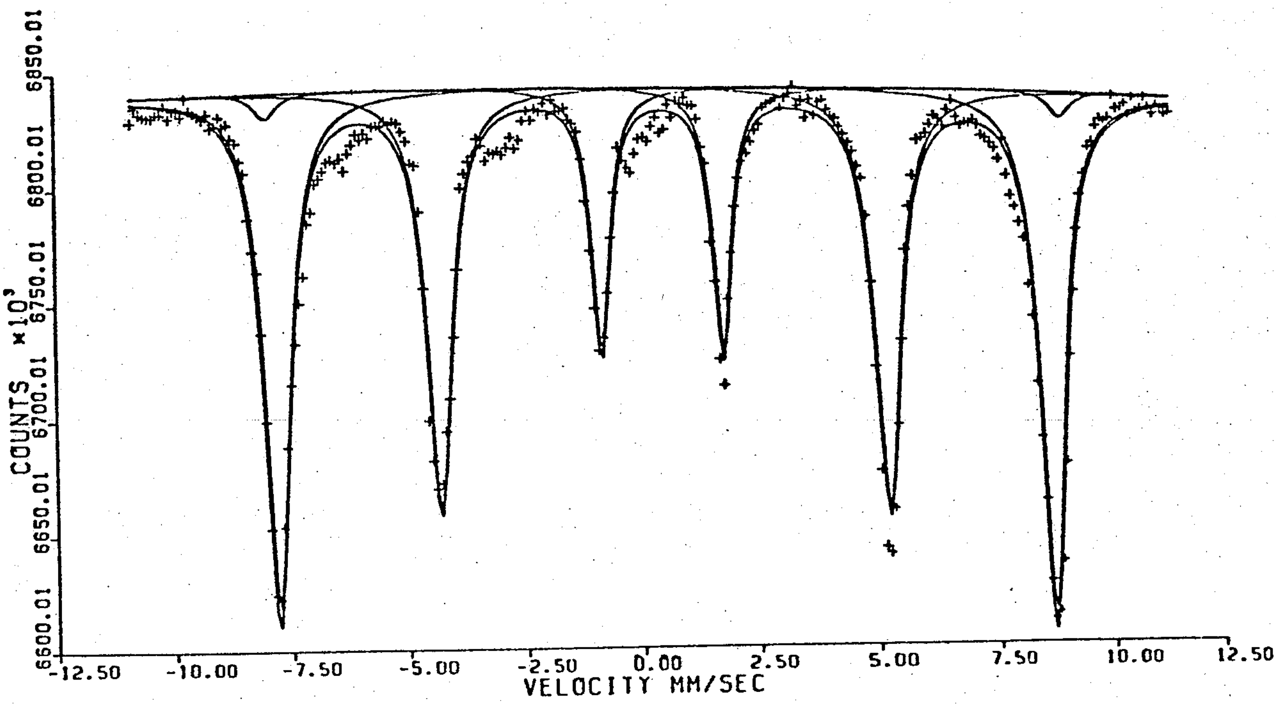

Fig. 4.7 Mössbauer spectrum of x = 0.6 at 4.2K, 0kOe.

in the 0kOe and 10kOe spectra are due to the A site Fe^{3+} ion spectrum and the B site Fe^{3+} ion spectrum not being resolved. The 2-5 lines for the Fe^{2+} ions are harder to resolve than the 2-5 lines for the Fe^{3+} because of their greater linewidth and smaller area, the error in the area being approximately 70%. Therefore, no canting angles for Fe^{2+} ions were determined using the intensities method. In Chapter 5 the B^{2+} site will be assumed to have a canting equal to the B^{3+} site. The data for all the measurements with $x<0.5$ are given in tables 4.1, 4.2.

The 4.2K spectra for $x = 0.6$ (figs. 4.7-4.10) were shown on analysis to contain subspectra for the A-sites and for the various B sites, given in table 4.3. The B_6 spectrum was too small to be resolved, so only spectra up to B_6' were fitted. The theoretical ratios for the various component spectra were constrained in order to facilitate their resolution. B site subspectra were constrained to have equal line widths and centroids, reflecting their common origin. Quadrupole splitting was constrained to be zero for all subspectra in field measurements as the sample was powdered and randomly oriented, causing the electric field gradient tensor to be at random orientation to the magnetic axis throughout the sample. Theoretically, this results in the quadrupole splitting being averaged to zero with some slight line broadening. At zero field, only two subspectra were resolved, one for B_{04}, B_5, and A, and one for B_6'.

TABLE 4.1

Mössbauer data for x = 0.0 and 0.2 at 4.2K

		Fe^{3+}			Fe^{2+}		
Fig.	Sample	H_{hf}	I.S.	Q.S.	H_{hf}	I.S.	Q.S.
4.2	0.0	515(1)	0.77(1)	-	502(1)	1.18(2)	-1.43(2)
4.3	0.2	511(1)	0.45(1)	-	464(1)	0.89(4)	-0.50(4)

TABLE 4.2

Mössbauer data for x = 0.4 at 4.2K.

		B Fe^{3+}				B Fe^{2+}					A	
Fig.	Field	H_{hf}	I.S.	θ_I	θ_H	H_{hf}	I.S.	Q.S.	θ_I	θ_H	H_{hf}	I.S.
4.4	0	511(5)	0.45(1)	-	-	450(1)	0.93(7)	-0.77(7)	-	-	511(5)	0.45(1)
4.5	10	521(5)	0.47(2)	21(2)	(40)	455(2)	0.90(2)	-0.6(2)	-	(10)	521(5)	0.47(2)
4.6	50	471(1)	0.50(2)	(10)	36(20)	422(5)	0.70(8)	-	-	55(25)	462(1)	0.39(1)

Note: Numbers in parentheses give the errors in the last digit (or two digits) of the tabulated value. No measurements were made of the boxes with slashes through them.

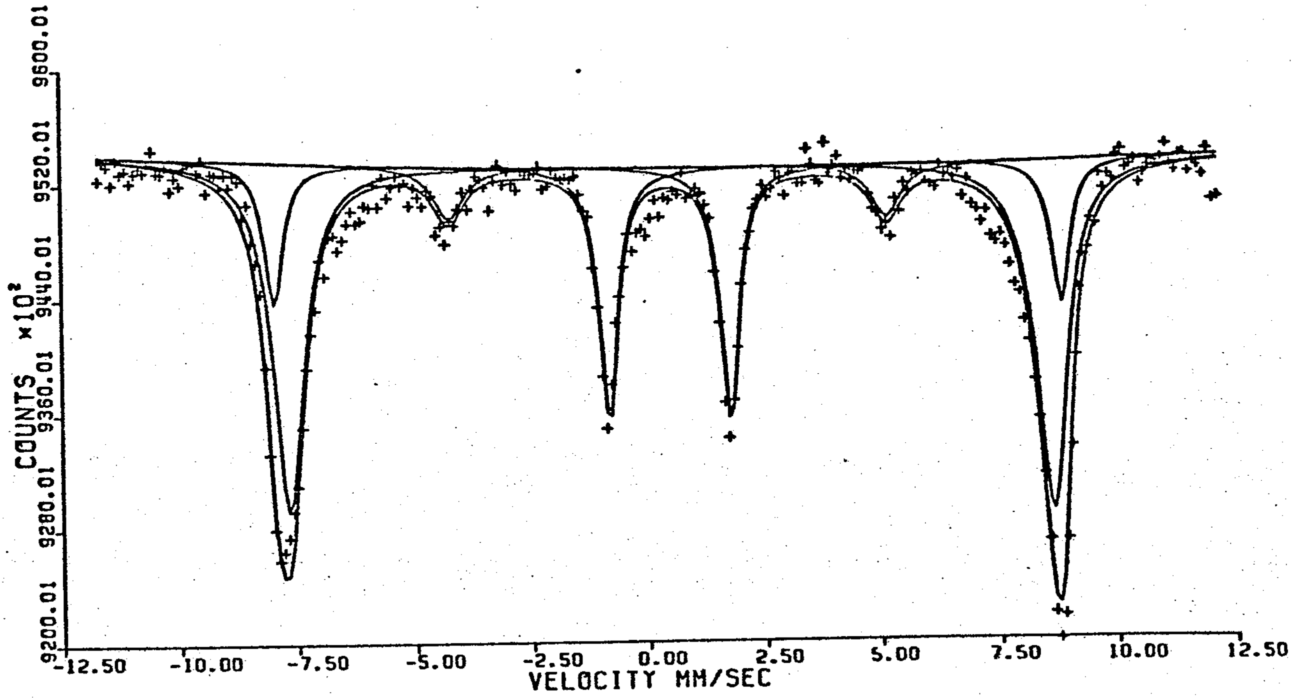

Fig. 4.8 Mössbauer spectrum of x = 0.6 at 4.2K, 10kOe.

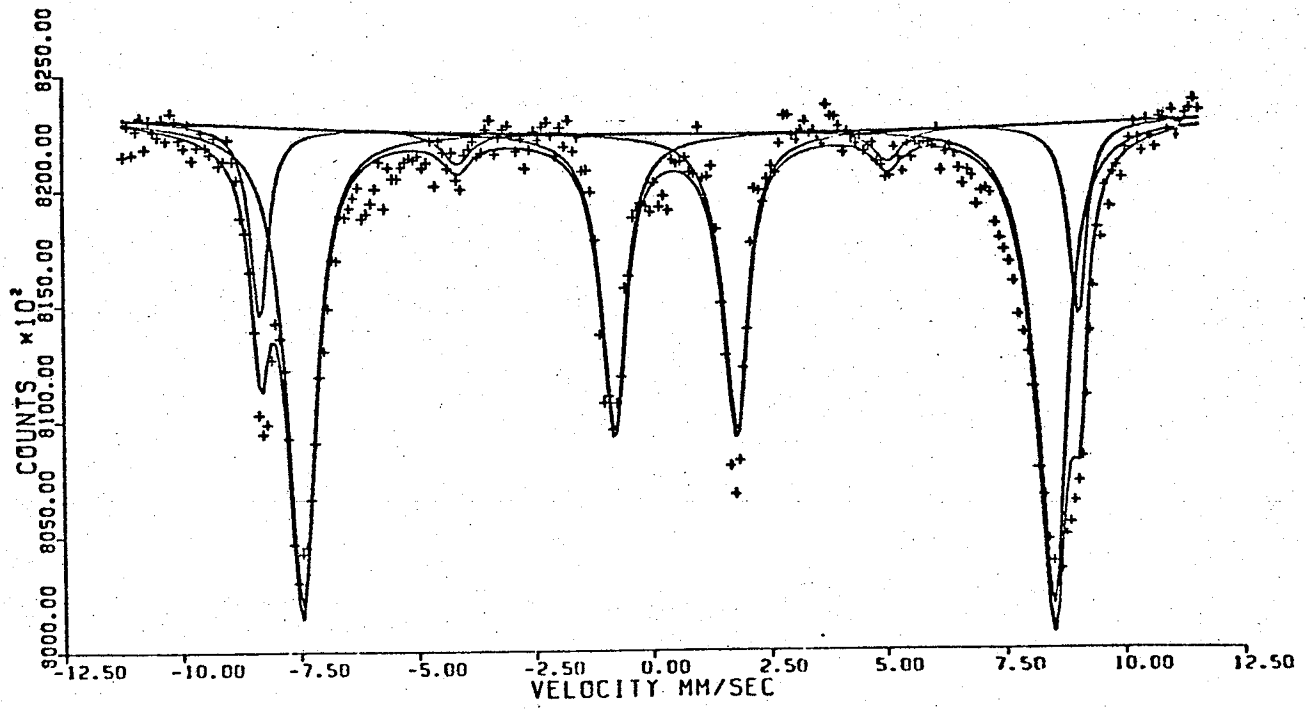

Fig. 4.9 Mössbauer spectrum of x = 0.6 at 4.2K, 25kOe.

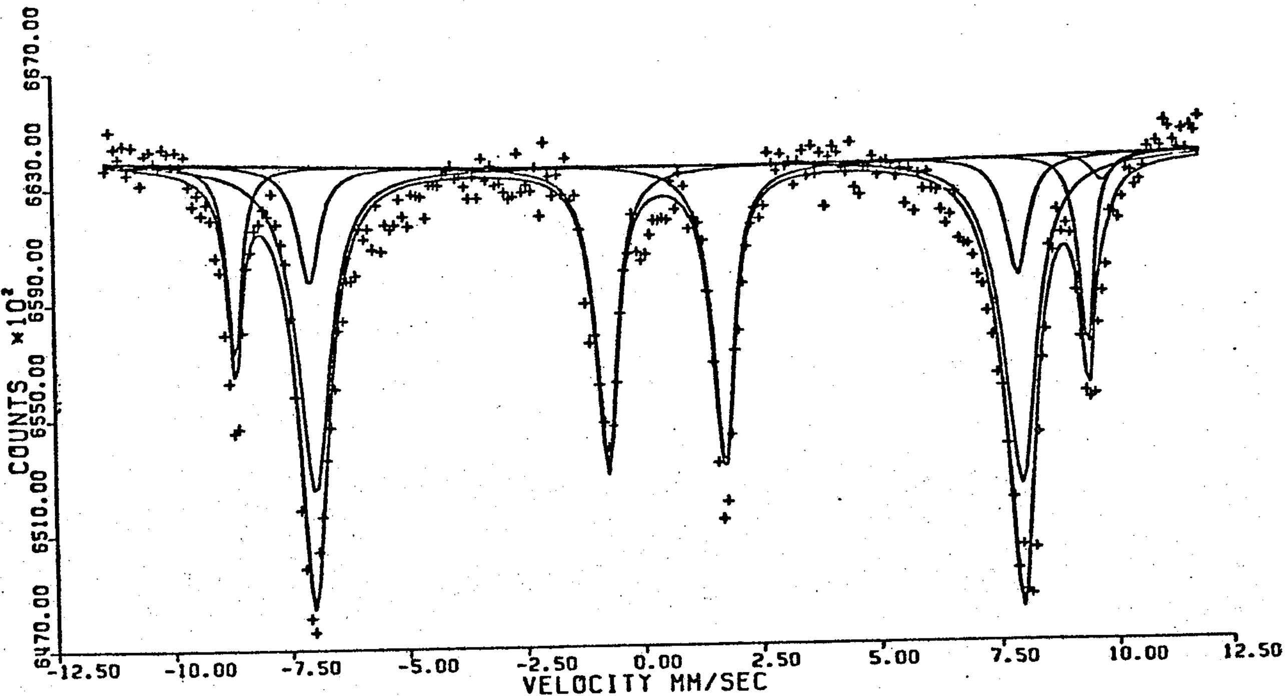

Fig. 4.10 Mössbauer spectrum of x = 0.6 at 4.2K, 50kOe.

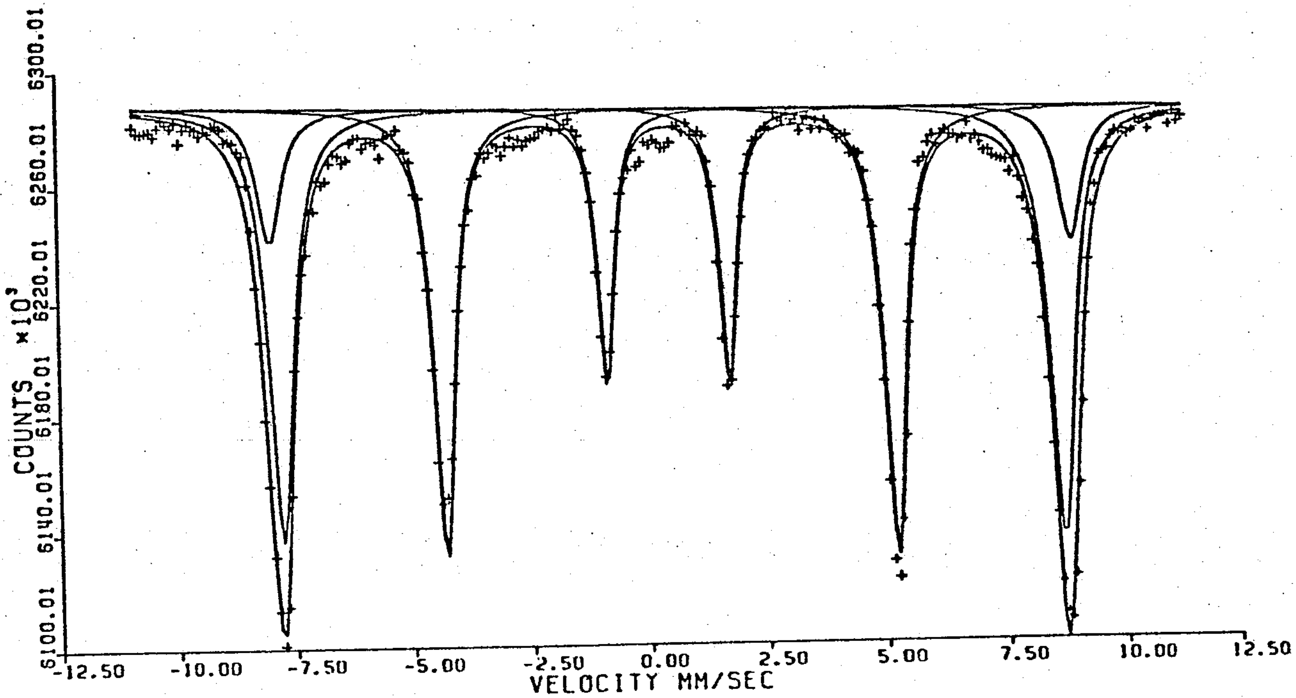

Fig. 4.11 Mössbauer spectrum of x = 0.8 at 4.2K, 0kOe.

TABLE 4.3

Definition of B site subspectra

B_{04} → B sites with 0 to 4 Zn A site nearest neighbours

B_5 → B sites with 5 Zn A site nearest neighbours

B'_6 → B sites with 6 Zn A site nearest neighbours which have canting angles $> 90^\circ$

B_6 → B sites with 6 Zn A site nearest neighbours which have canting angles $< 90^\circ$

The components of the first line mentioned, being unresolved, have large errors for the hyperfine fields. Similarly, at 10kOe and 50kOe, two spectra were used, one for B_{04}, B_5, and B_6, and the other for B_6' and A. All these subspectra, being parts of unresolved doublets, have large hyperfine field errors and large errors in θ . For the B_6' spectrum in the 50kOe field, it was not possible to calculate any canting angle using the hyperfine field method. No canting angles could be calculated for the B_6' spectrum at any field using the intensities method, due to resolution problems. Consequently, a value of 140° was assigned (indicated by the starred values in table 4.4), on the basis of measurements both at and above room temperature, for the sample x = 0.8 (tables 4.5, 4.8). The data for the sample x = 0.6 are given in table 4.4.

In table 4.5 we see a summary of the data gained from spectra of the x = 0.8 sample at 4.2K (figs. 4.11-4.15). These spectra were fitted with up to 4 B site and 1 A site subspectra. As was the case for the sample x = 0.6, B site linewidths and centroids were all constrained to be equal and quadrupole splittings were constrained to zero. The theoretical line intensities were constrained except for the B_6' intensities in the 30kOe and 50kOe spectra. For these spectra, one six line spectrum was used for B_6' and A, and three others for B_{04}, B_5, and B_6. The intensity of the first line was not constrained, and when the theoretical A intensity was subtracted, values of 0.17±0.3 of the total B

TABLE 4.4

Mössbauer data for x = 0.6 at 4.2K

		B_{04}		B_5				B_6'				A	
Fig.	Field	H_{hf}	I.S.	H_{hf}	I.S.	θ_I	θ_H	H_{hf}	I.S.	θ_I	θ_H	H_{hf}	I.S.
4.7	0	510(5)	0.45(3)	510(5)	0.45(3)	-	-	523(1)	0.45(3)	-	-	$510^{(5)}$	0.45(3)
4.8	10	503(5)	0.47(2)	503(5)	0.47(2)	$59^{(2)}$	$47^{(80)}$	519(5)	0.43(3)	140*	$66^{(70)}$	$519^{(5)}$	0.43(3)
4.9	25	492(1)	0.48(3)	492(1)	0.48(3)	$40^{(5)}$	$48^{(50)}$	537(3)	0.34(9)	140*	$123^{(20)}$	$537^{(3)}$	0.34(9)
4.10	50	462(2)	0.45(6)	464(2)	0.45(6)	(20)	$17^{(20)}$	576(2)	0.45(6)	140*	-	$559^{(2)}$	0.34(7)

TABLE 4.5

Mössbauer data for x = 0.8 at 4.2K

		B_{04}		B_5				B_6'				B_6		A	
Fig.	Field	H_{hf}	I.S.	H_{hf}	I.S.	θ_I	θ_H	H_{hf}	I.S.	θ_I	θ_H	H_{hf}	I.S.	H_{hf}	I.S.
4.11	0	509(5)	0.45(2)	509(5)	0.45(2)	-	-	522(1)	0.45(2)	-	-	522(1)	0.45(2)	509(5)	0.45(2)
4.12	8.6	511(10)	0.34(2)	511(10)	0.34(2)	65(12)	-	511(10)	0.34(2)	140*	-	511(10)	0.34(2)	511(10)	0.34(2)
4.13	15.4	505(10)	0.50(4)	505(10)	0.50(4)	60(2)	-	505(10)	0.50(4)	140*	-	505(10)	0.50(4)	505(10)	0.50(4)
4.14	30	476(4)	0.47(12)	494(3)	0.49(9)	54(5)	65(20)	540(4)	0.47(1)	140(5)	140(15)	496(6)	0.47(20)	540(4)	0.47(13)
4.15	50	460(1)	0.36(1)	478(1)	0.44(7)	$46^{(1)}$	$55^{(10)}$	566(5)	0.37(1)	142(1)	167(15)	477(1)	0.44(1)	566(5)	0.37(1)

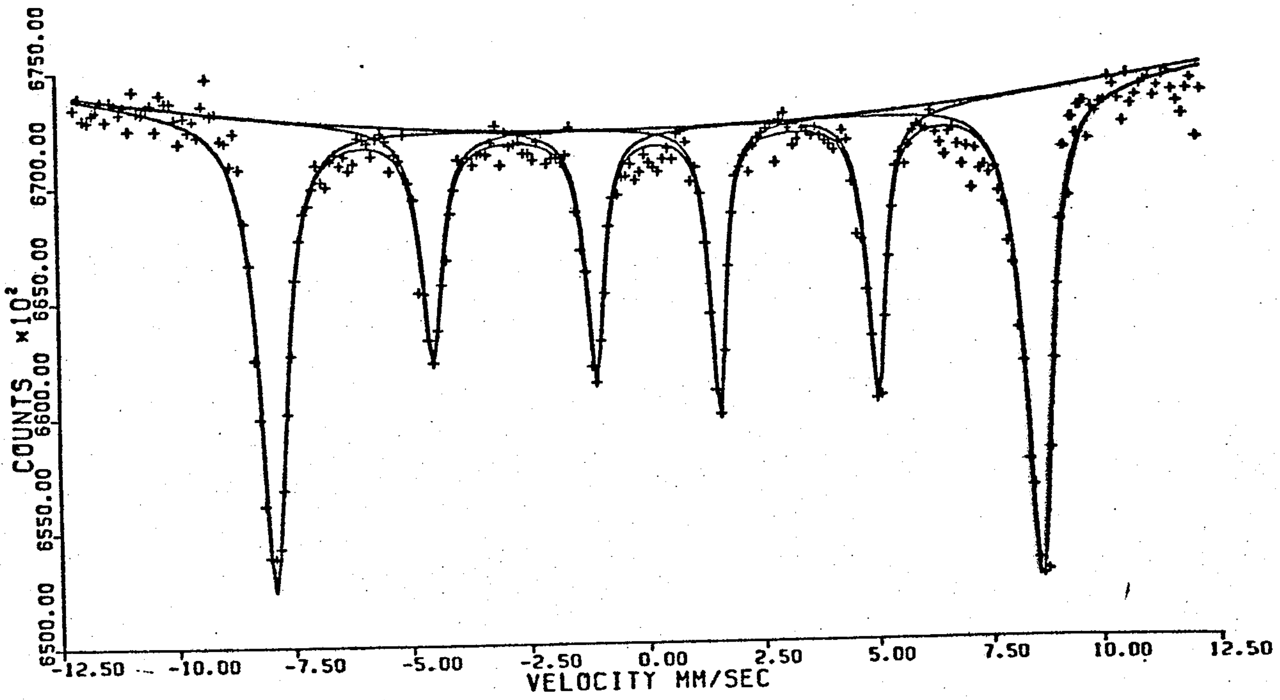

Fig. 4.12 Mössbauer spectrum of x = 0.8 at 4.2K, 8.6kOe.

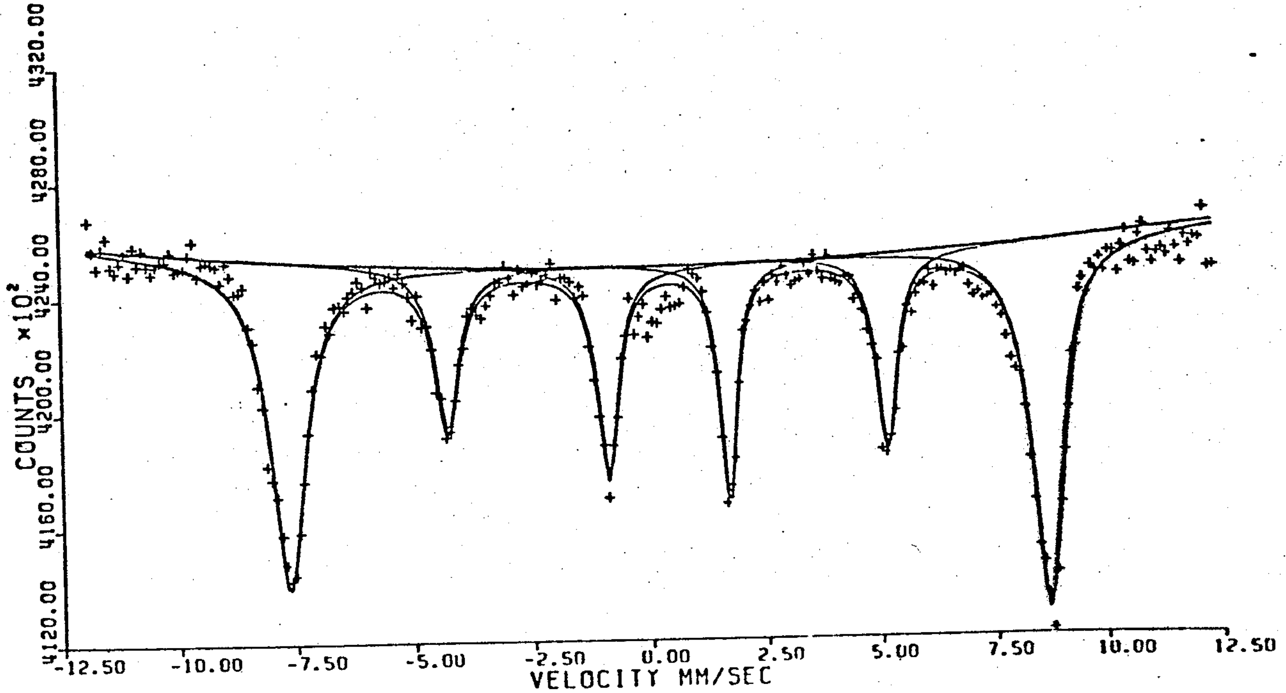

Fig. 4.13 Mössbauer spectrum of x = 0.8 at 4.2K, 15.4kOe.

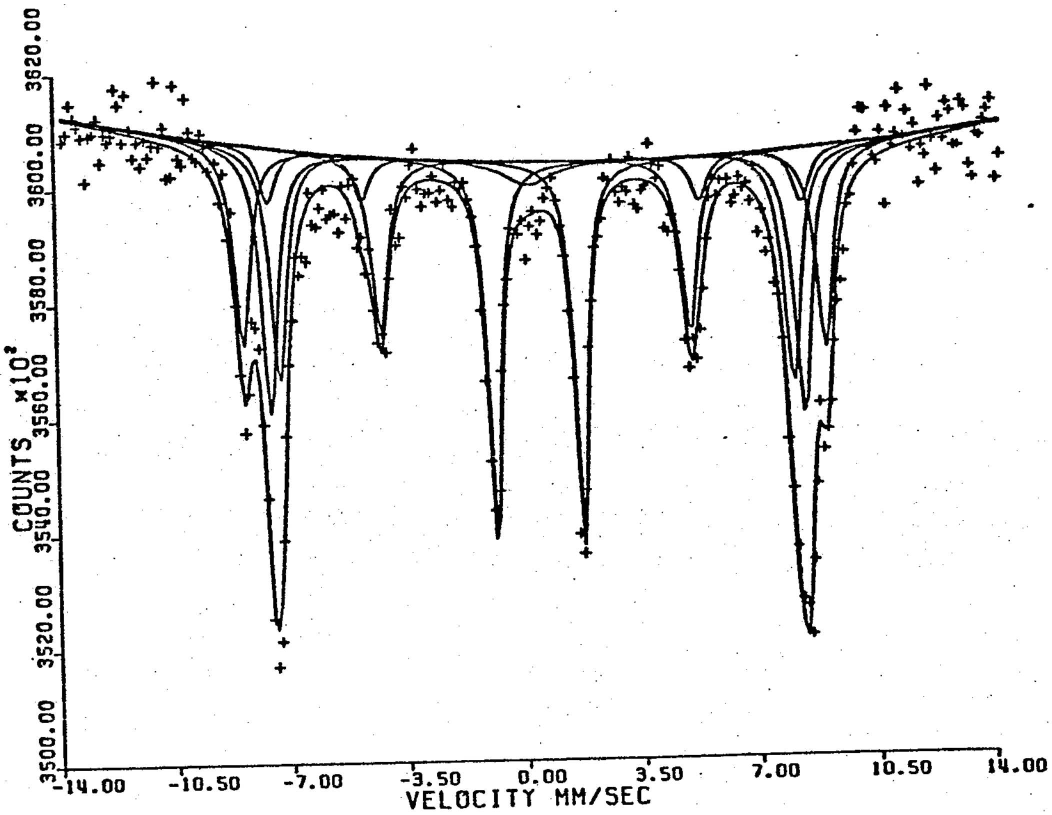

Fig. 4.14 Mössbauer spectrum of x = 0.8 at 4.2K, 30kOe.

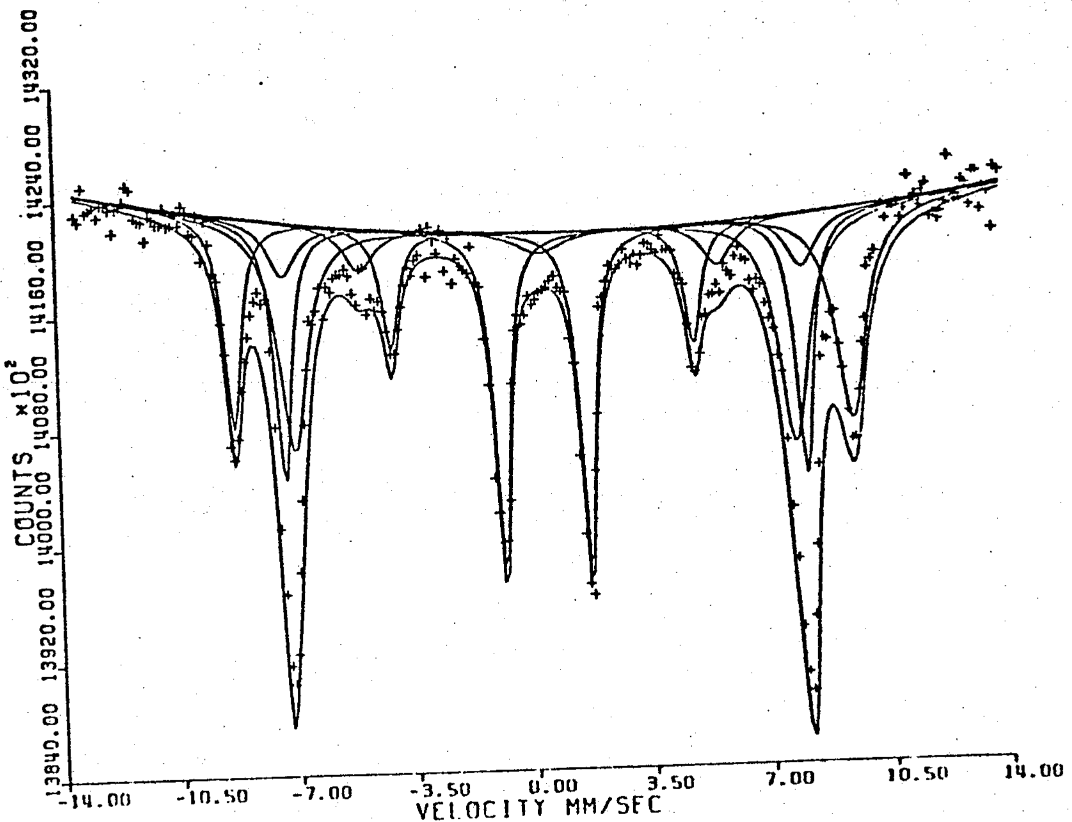

Fig. 4.15 Mössbauer spectrum of x = 0.8 at 4.2K, 50kOe.

intensity at 30kOe and 0.17±.01 of the total B intensity at 50kOe were found for the B_6' intensity. These values compare well with the theoretical intensity of 0.181, calculated in Appendix A. Canting angles were calculated for both the B_5 and B_6' spectra using both the intensity and hyperfine field methods. Agreement between the two methods was generally good, the intensity method, however, being the more reliable. In the low field spectra, the subspectra were not all resolved. For the zero field case, two six-line spectra were used: one for B_6' and B_6; and, one for all other sites. This splitting was chosen because the high field data showed that the B_6 and B_6' hyperfine field was larger than that of any of the other spectra, which were all close together. For the 8.6kOe and the 15.4kOe spectrum, only one six-line spectrum was used, as the lines were all poorly resolved. Because of this, no attempt was made to calculate any canting angles using the hyperfine fields method. The 2-5 lines of the B_6' spectrum were not resolved for low fields, and thus no B_6' canting angles were calculated using intensities. However, since θ_6' seemed to be unaffected by temperature and field (tables 4.5-5.8), we assigned (indicated with starred values) a canting angle value of 140°. The intensity of the unresolved 2-5 line of the B_6' canted at 140^0 was subtracted from the over all 2-5 intensity before calculating the B_5 canting angle.

4.3 RESULTS ABOVE 4.2K

Measurements have been performed at various temperatures

TABLE 4.6

Mössbauer data for x = 0.2 and x = 0.4 above 4.2K.

				Fe^{3+}			Fe^{2+}		
Fig.	Sample	Temp.	Field	H_{hf}	I.S.	Q.S.	H_{hf}	I.S.	Q.S.
4.3	0.2	4.2	0	511(1)	0.45(1)	-	464(1)	0.89(4)	-0.50(4)
4.16	0.2	85	0	506(1)	0.70(1)	-	466(1)	1.10(1)	-0.44(2)
4.4	0.4	4.2	0	511(5)	0.45(1)	-	450(1)	0.93(7)	-0.77(7)
4.17	0.4	85	0	502(1)	0.68(1)	-	454(1)	1.09(1)	-0.58(2)

TABLE 4.7

Mössbauer data for x = 0.6 above 4.2K

			B_{04}		B_5				B_6'				A	
Fig.	Temp.	Field	H_{hf}	IS.	H_{hf}	IS.	θ_I	θ_H	H_{hf}	IS.	θ_I	θ_H	H_{hf}	IS.
4.7	4.2	0	510(5)	0.45(3)	510(5)	0.45(3)	-	-	523(1)	0.45(3)	-	-	510(5)	0.45(3)
4.8	4.2	10	503(5)	0.47(2)	503(5)	0.47(2)	59(2)	47(80)	519(5)	0.43(3)	140*	66(70)	519(3)	0.43(3)
4.10	4.2	50	462(2)	0.45(6)	464(2)	0.45(6)	(20)	17(20)	576(2)	0.45(6)	140*	-	559(2)	0.34(7)
4.18	20	0	497(1)	0.49(1)	457(1)	0.49(3)	-	-	406(2)	0.49(6)	-	-	519(1)	0.49(2)
4.19	32	10	501(1)	0.52(1)	448(3)	0.52(4)	37(5)	-	391(10)	0.52(2)	140*	-	523(1)	0.43(2)
4.20	32	50	460(1)	0.50(1)	410(3)	0.50(3)	-	-	336(10)	0.50(2)	140*	-	559(9)	0.39(2)
4.21	85	0	482(1)	0.49(2)	429(1)	0.49(1)	-	-	381(1)	0.49(2)	-	-	502(1)	0.35(1)

TABLE 4.8

Mössbauer data for x = 0.8 above 4.2K.

			B_{04}		B_5				B'_6				B_6		A	
Fig.	Temp.	Field	H_{hf}	I.S.	H_{hf}	I.S.	θ_I	θ_H	H_{hf}	I.S.	θ_I	θ_H	H_{hf}	I.S.	H_{hf}	I.S.
4.11	4.2	0	509(5)	0.45(2)	509(5)	0.45(2)	--	--	522(1)	0.45(2)	--	--	522(1)	0.45(2)	509(5)	0.45(2)
4.14	4.2	30	476(4)	0.47(12)	494(3)	0.49(9)	$54^{(5)}$	$65^{(20)}$	540(4)	0.47(1)	$140^{(5)}$	$140^{(15)}$	496(1)	0.47(20)	540(4)	0.47(13)
4.15	4.2	50	460(1)	0.36(1)	478(1)	0.44(7)	$46^{(1)}$	$55^{(10)}$	566(5)	0.37(1)	$142^{(1)}$	$167^{(15)}$	477(1)	0.44(1)	566(5)	0.37(1)
4.22	11.6	0	500(5)	0.46(1)	500(5)	0.46(1)	--	--	473(5)	0.47(6)	--	--	473(5)	0.47(6)	500(5)	0.46(1)
4.23	20	0	478(5)	0.44(1)	469(1)	0.44(1)	--	--	433(5)	0.45(1)	--	--	433(5)	0.45(1)	478(5)	0.44(1)
4.24	20	30	476(1)	0.50(2)	467(1)	0.50(2)	$48^{(8)}$	$90^{(5)}$	429(2)	0.50(7)	$138^{(20)}$	$80^{(20)}$	378(2)	0.50(7)	532(1)	0.39(2)
4.25	20	50	459(2)	0.49(4)	442(2)	0.49(4)	$30^{(3)}$	$55^{(5)}$	459(2)	0.49(4)	$140^{(4)}$	$119^{(10)}$	380(2)	0.49(4)	558(1)	0.41(2)
4.26	40	0	381(2)	0.48(3)	337(3)	0.48(3)	--	--	249(4)	0.48(5)	--	--	249(4)	0.48(5)	413(2)	0.48(3)
4.27	40	30	449(3)	0.50(4)	420(3)	0.50(4)	$45^{(2)}$	--	350(6)	0.50(7)	$138^{(4)}$	--	294(6)	0.50(7)	504(3)	0.39(4)
4.28	40	50	443(1)	0.46(2)	411(1)	0.46(2)	$19^{(2)}$	--	368(1)	0.46(2)	$137^{(2)}$	--	281(1)	0.46(2)	548(1)	0.35(2)

and fields above 4.2K for the purpose of investigating the behaviour of the magnetization versus temperature curve. This behaviour will be discussed in Chapter 5 as being a function of several different effects: the change in canting angles with temperatures and fields; the decrease in hyperfine fields due to spin waves; and the collapse in hyperfine fields, change in the intensities of the various lines, and line broadening due to relaxation effects in some of the samples.

For samples with $x = 0.2, 0.4$, zero field spectra were gathered at 85K (figs 4.16, 4.17). These spectra were fitted with two six-line subspectra constrained to the theoretical Fe^{2+}/Fe^{3+} ratios. The linewidths were approximately equal to those at 4.2K. The hyperfine fields of the Fe^{3+} spectra were somewhat reduced from the 4.2K values while the Fe^{2+} values remained unchanged within the measurement error. The line intensities also remain unchanged from the 4.2K values, approximately 2.3: 1.8: 1 for the whole spectrum. In Chapter 5, the change in the spontaneous magnetization with temperature will be dealt with in terms of hyperfine field changes.

The $x = 0.6$ and $x = 0.8$ samples were more extensively studied as a function of temperature for an investigation of relaxation effects. In addition, the samples were studied in applied fields to investigate the maximum in the bulk magnetization curves (see fig. 3.5). Spectra were taken for $x = 0.6$ at several temperatures

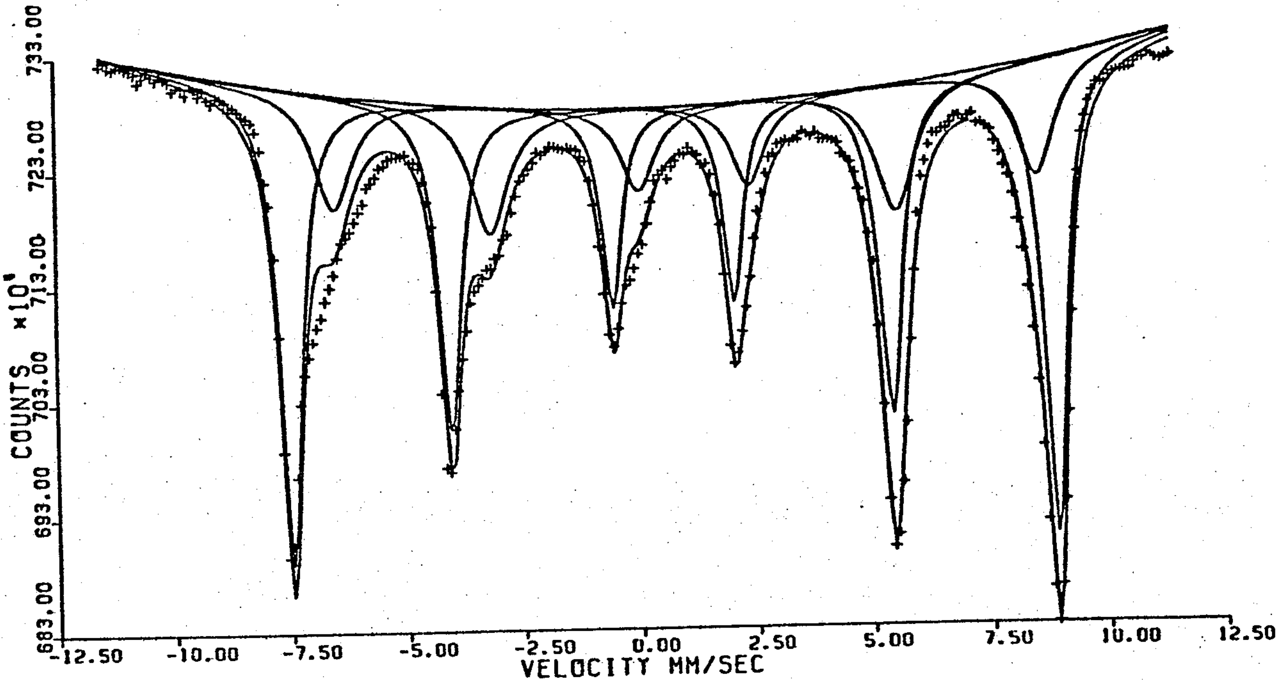

Fig. 4.16 Mössbauer spectrum of x = 0.2 at 85K, 0kOe.

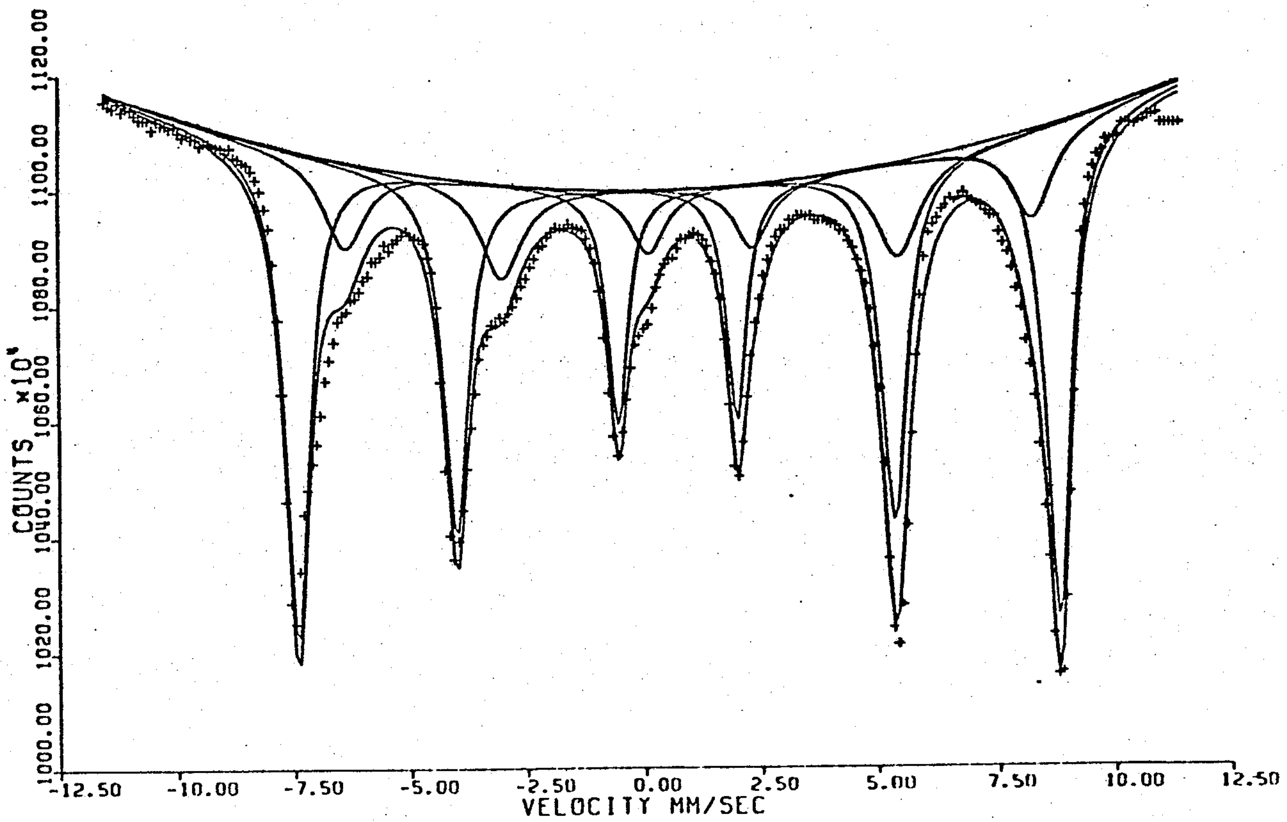

Fig. 4.17 Mössbauer spectrum of x = 0.4 at 85K, 0kOe.

and fields (figs. 4.18-4.21) and the data from these fits are given in table 4.7. All spectra were analysed to contain four subspectra, one for each of the B_{04}, B_5, B_6', and A sites. Constraints were identical to those at 4.2K. The intensities of the 2-5 lines for B_6' were too small to resolve, so only B_5 canting angles could be determined from the intensities method. Hyperfine field calculated canting angles could not be obtained because no zero field 32K spectrum was taken. Once again, a value of 140° was assigned (indicated with starred values) to the B_6' canting angle. The linewidth of the component spectra remained approximately 0.8 mm/sec. over the whole temperature and field range, but the hyperfine field decreased with increasing temperature.

The x = 0.8 sample was analysed at several temperatures and fields (figs. 4.22-4.28), the results of which are given in table 4.8. The theoretical line intensities were all constrained, as were the quadrupole splittings. All B site linewidths and centroids were constrained equal. Once again, the errors were large for those hyperfine fields where several subspectra were contained in one line. Canting angles were measured using both the hyperfine fields and the intensities method at 20K. At 40K, the hyperfine fields method could not be used; the increase in the total hyperfine field with applied fields was much too large to be explained in terms of canting angles. The hyperfine field calculated canting angles at 20K were themselves in relatively poor agreement with the

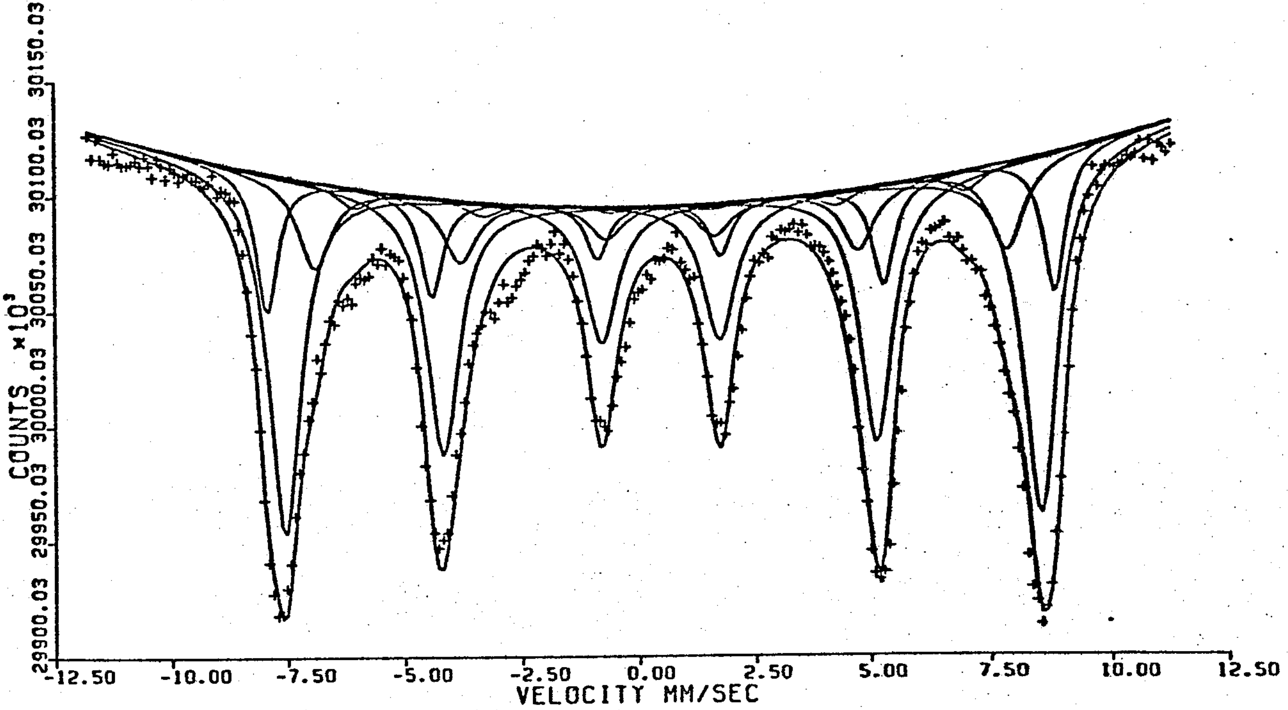

Fig. 4.18 Mössbauer spectrum of x = 0.6 at 20K, 0kOe.

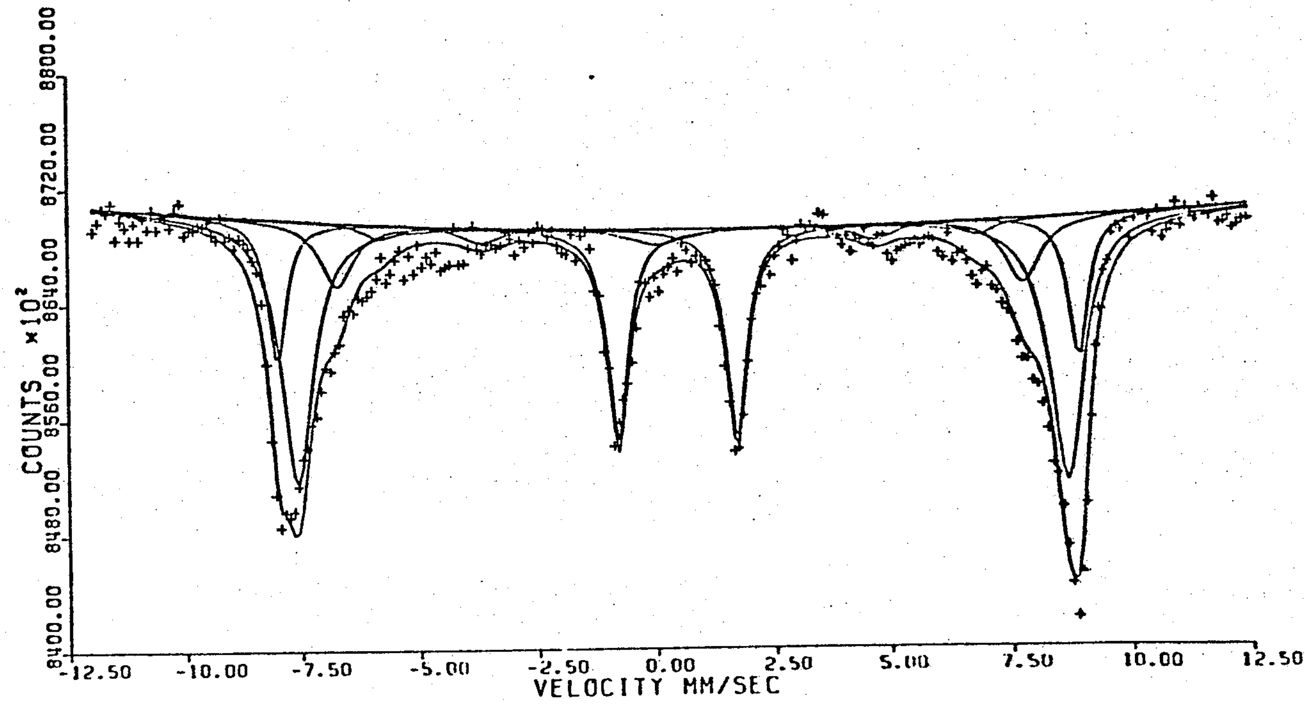

Fig. 4.19 Mössbauer spectrum of x = 0.6 at 32K, 10kOe.

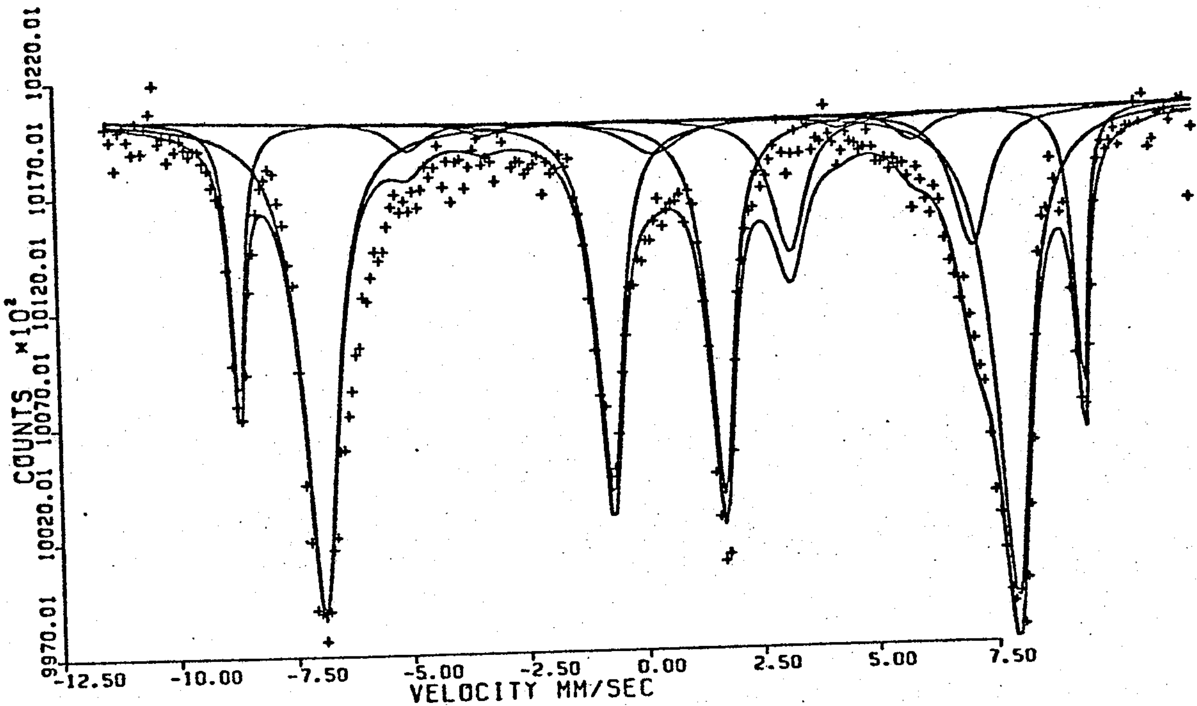

Fig. 4.20 Mössbauer spectrum of x = 0.6 at 32K, 50kOe.

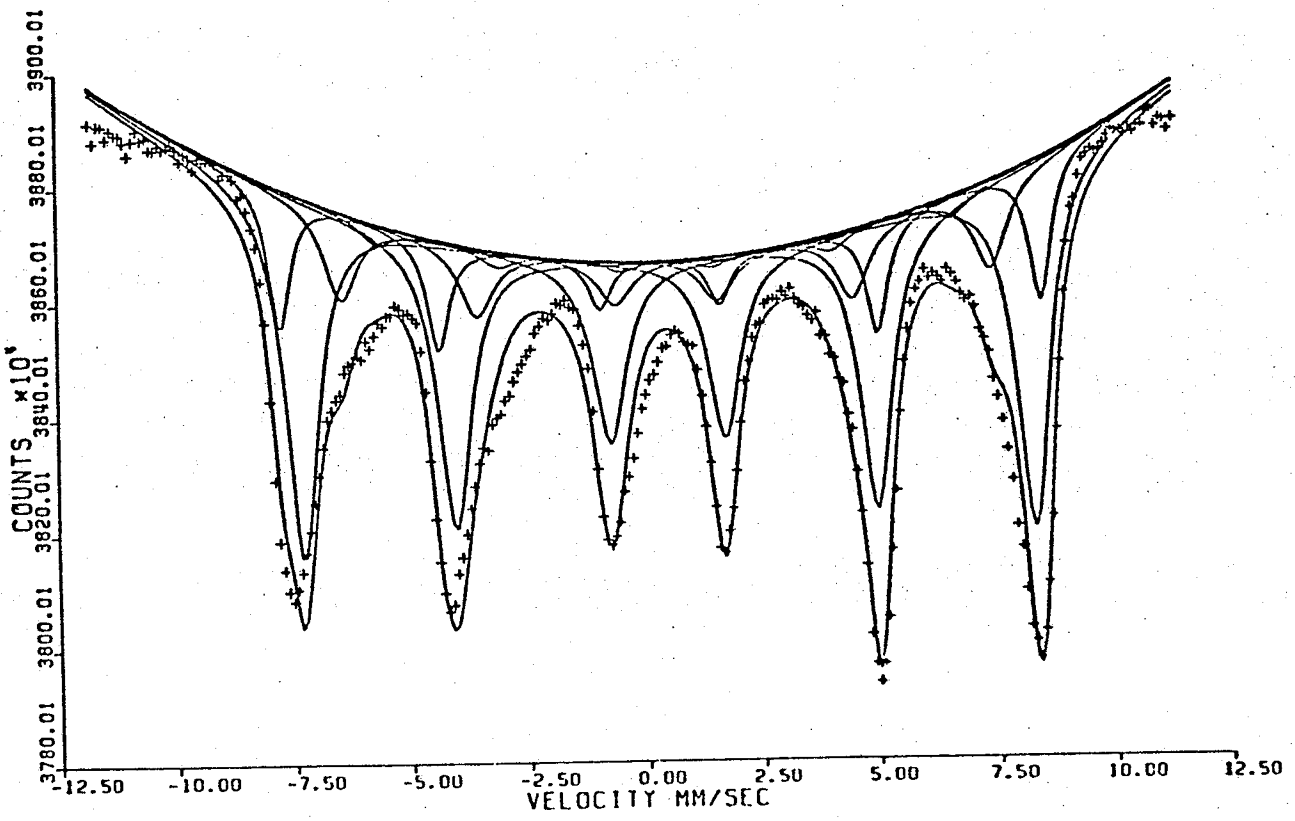

Fig. 4.21 Mössbauer spectrum of x = 0.6 at 85K, 0kOe.

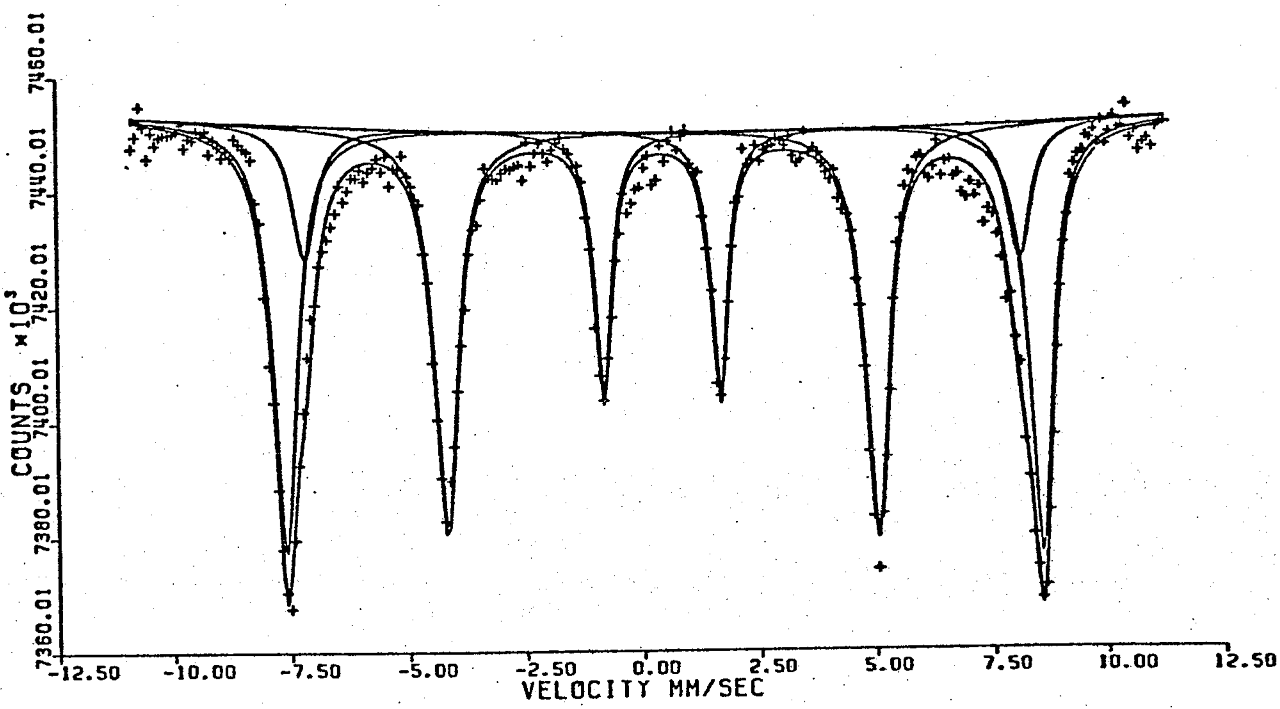

Fig. 4.22 Mössbauer spectrum of x = 0.8 at 11.6K, 0kOe.

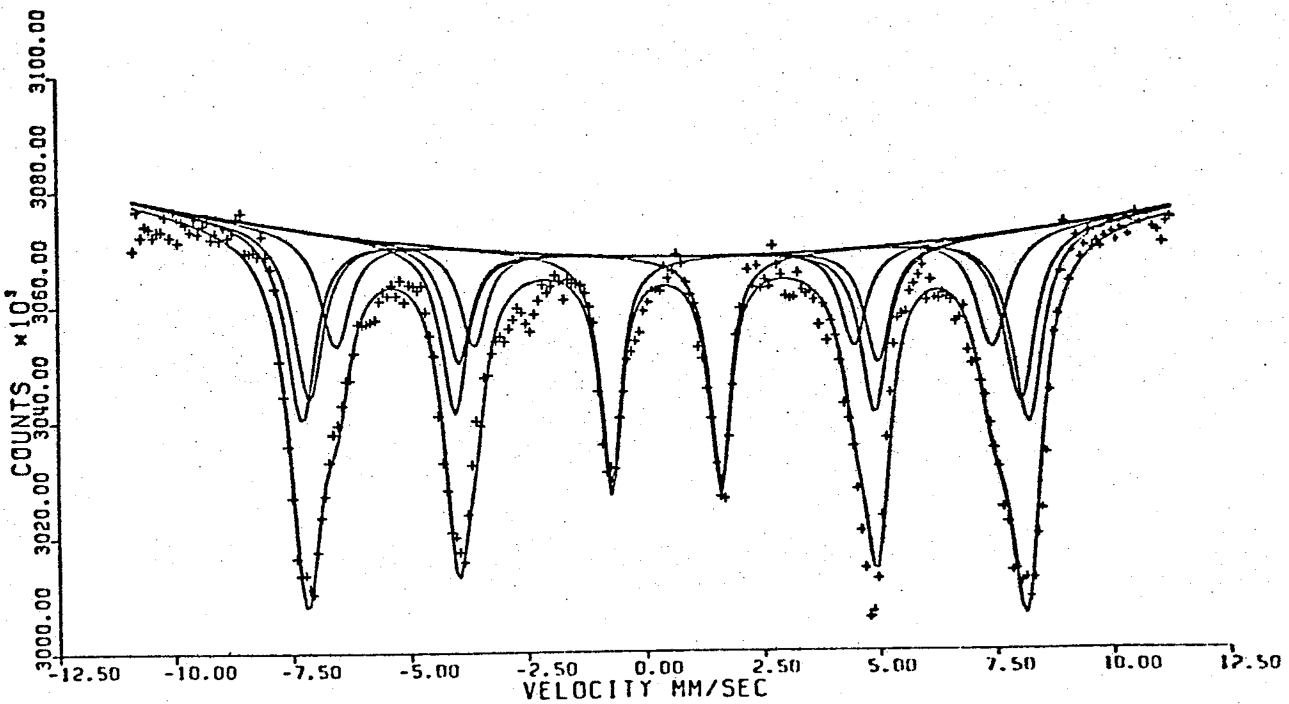

Fig. 4.23 Mössbauer spectrum of x = 0.8 at 20K, 0kOe.

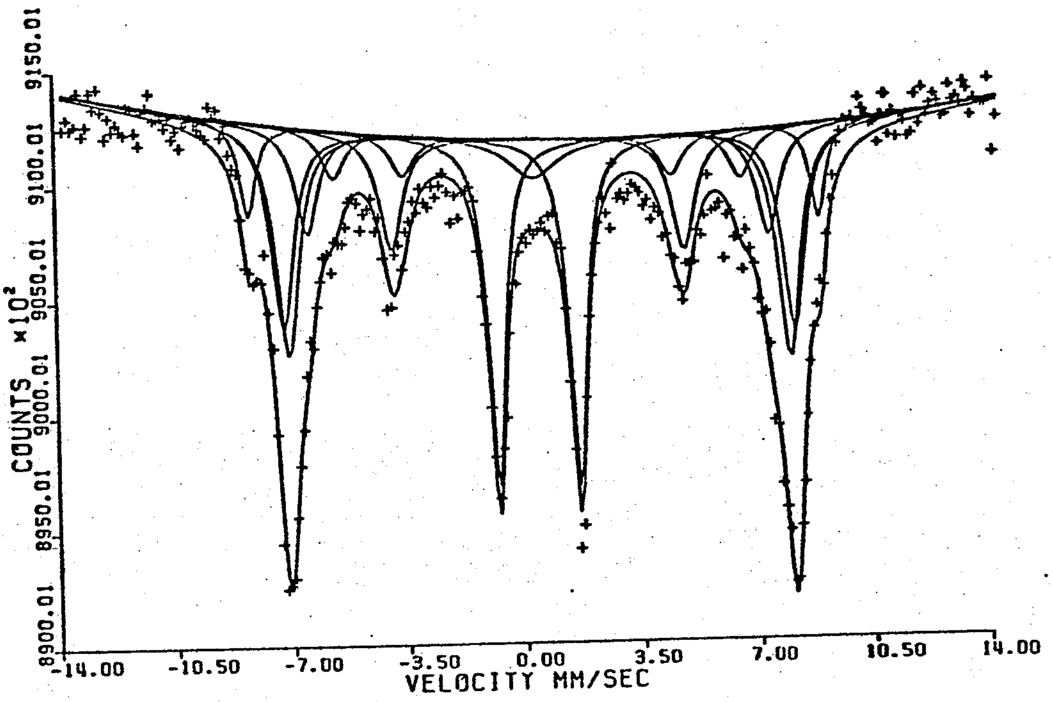

Fig. 4.24 Mössbauer spectrum of x = 0.8 at 20K, 30kOe.

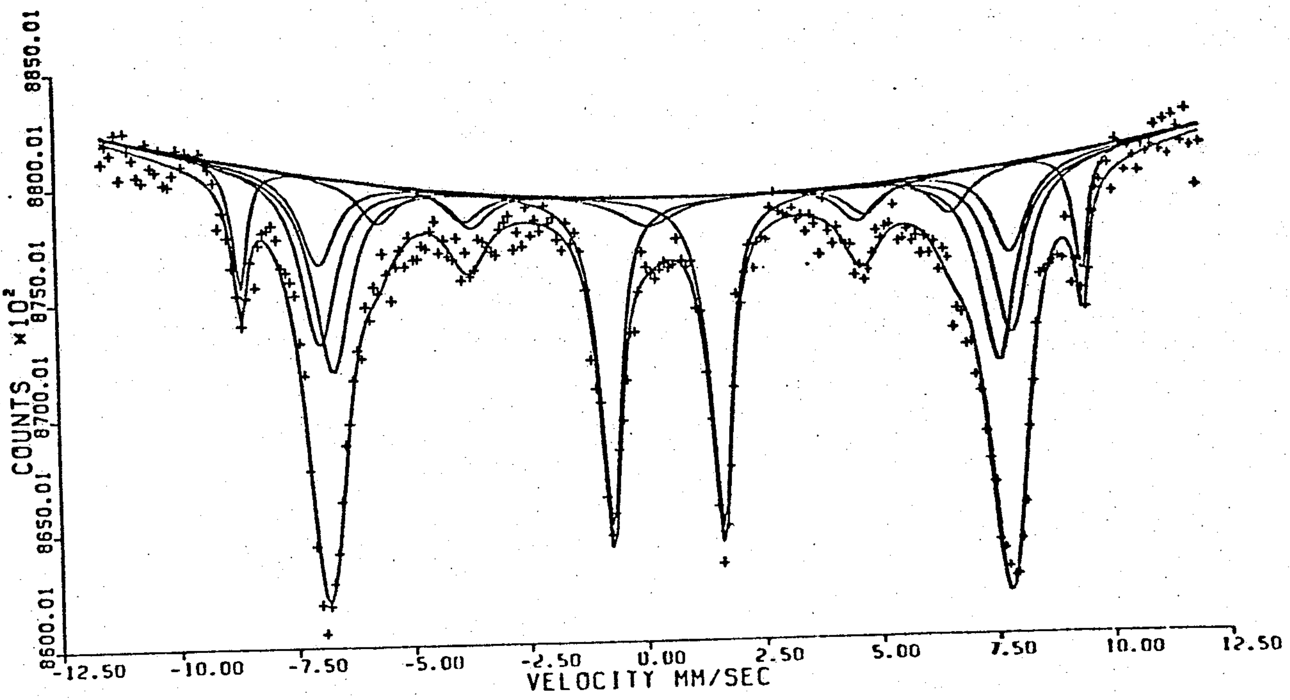

Fig. 4.25 Mössbauer spectrum of x = 0.8 at 20K, 50kOe.

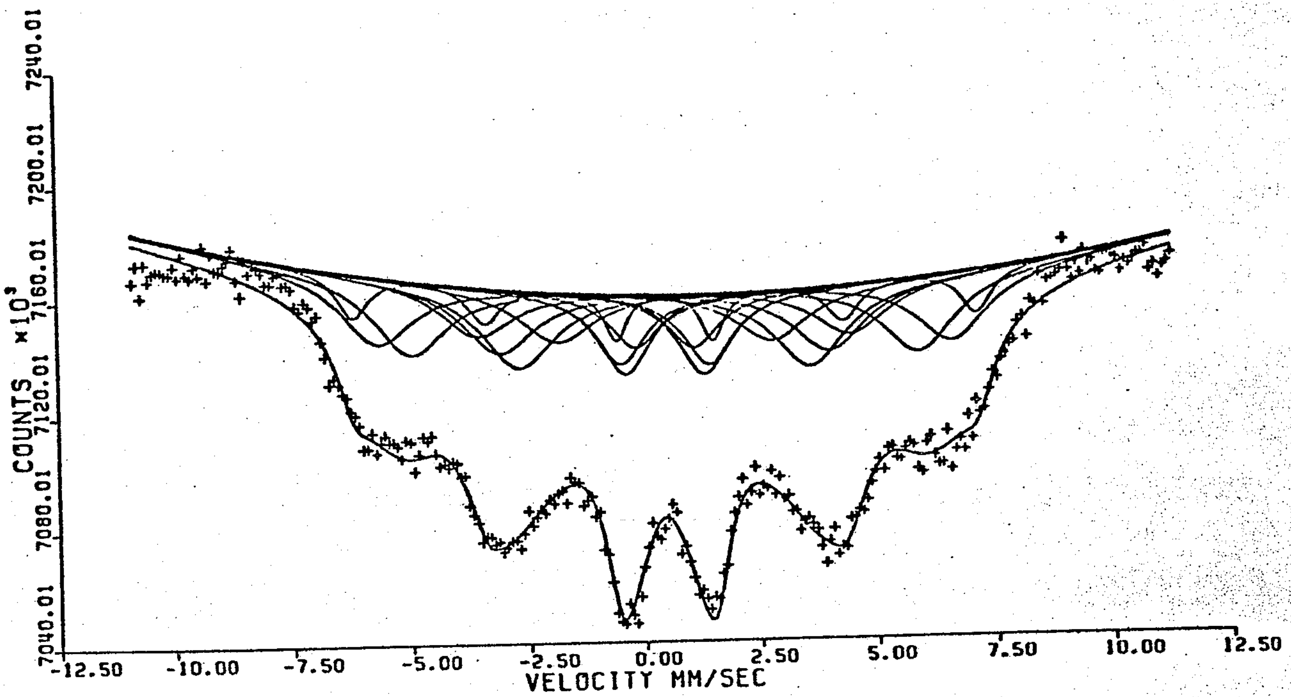

Fig. 4.26 Mössbauer spectrum of x = 0.8 at 40K, 0kOe.

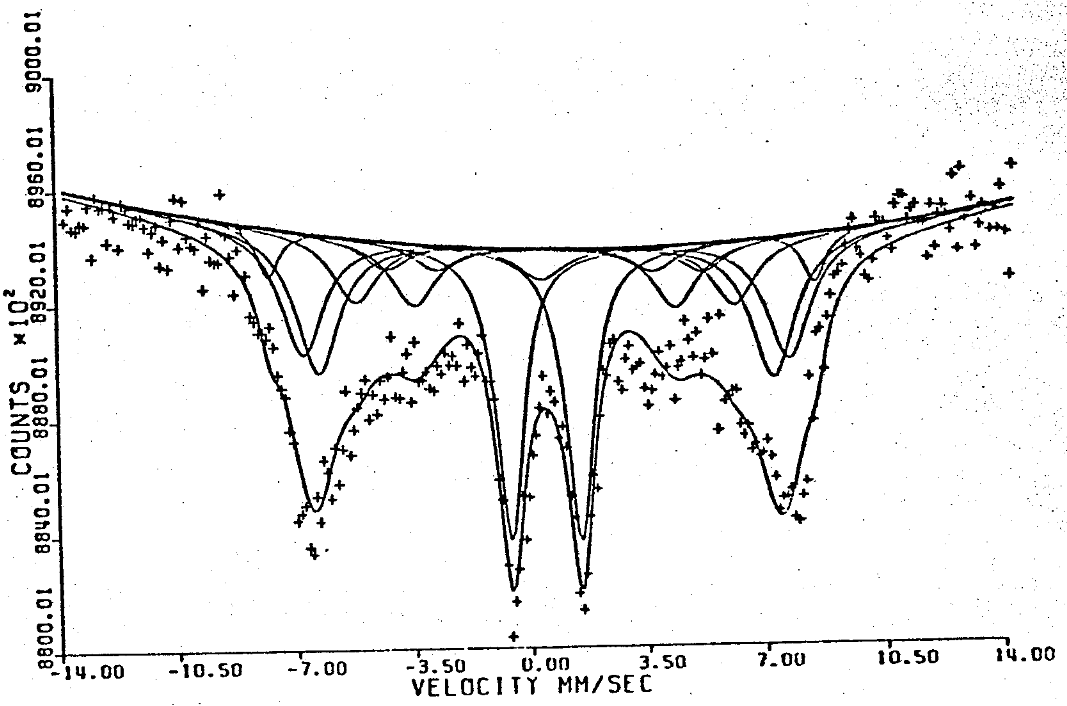

Fig. 4.27 Mössbauer spectrum of x = 0.8 at 40K, 30kOe.

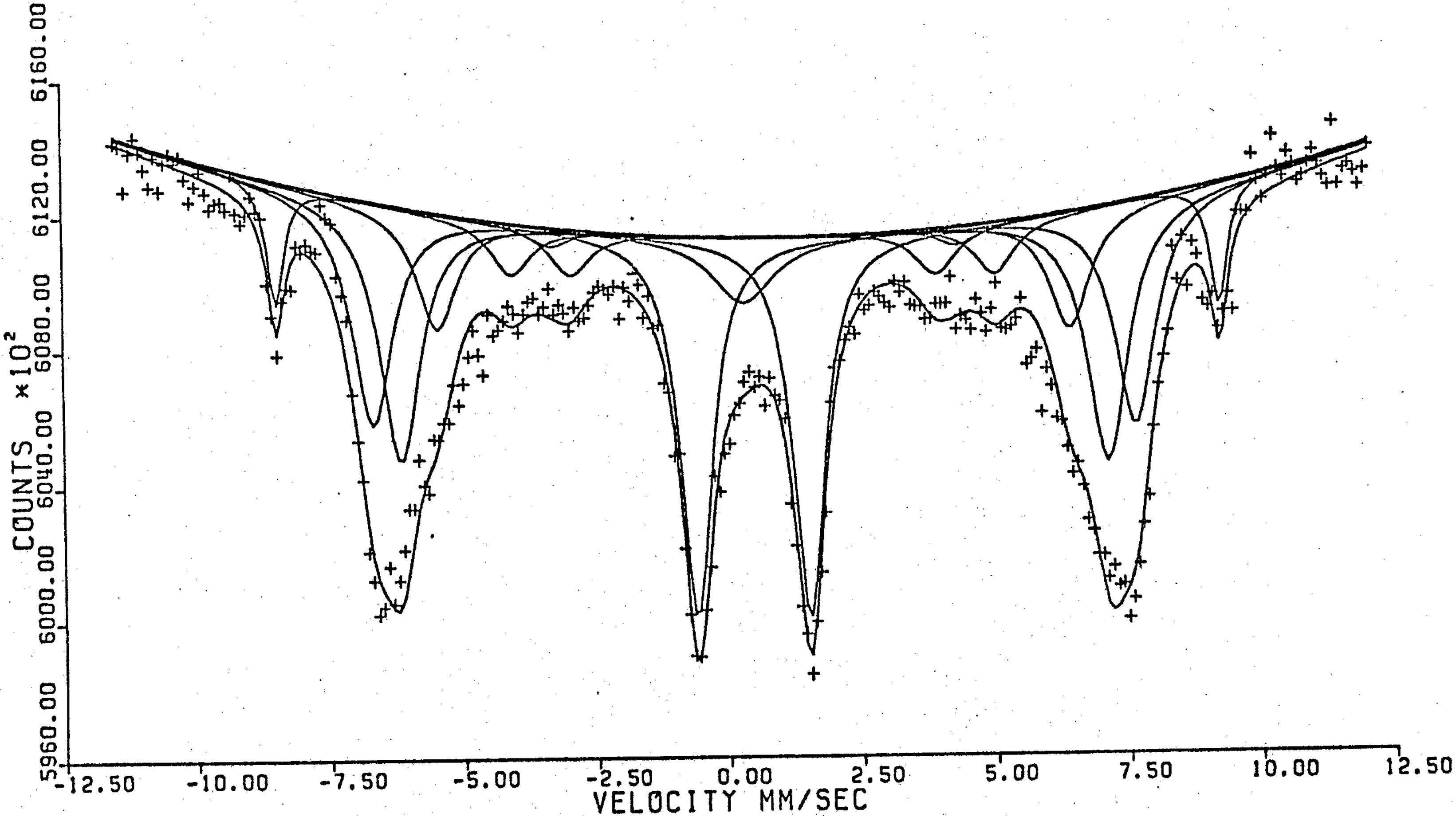

Fig. 4.28 Mössbauer spectrum of x = 0.8 at 40K, 50kOe.

intensities calculations. This was probably due to relaxation effects, which increased with temperature but were suppressed with a magnetic field. As the temperature increased, linewidth increased (from 0.6 mm/sec. at 11.6K to 1.9 mm/sec. at 40K), and the intensity of the inner lines began to increase at the expense of the outer (2.9: 2.3:1 at 11.6K changing to 1.3: 1.3: 1 at 40K). The magnetic field measurements at 40K showed that the linewidth decreased from 19 mm/sec. in zero field to 0.92 mm/sec. in 50kOe while the area ratio changed from 1.3: 1.3: 1.0 at zero field to 2.4: 0.27: 1.0 at 50kOe. These were indications that relaxation phenomena were participating in the spin structure at this temperature and that they were dependant on the applied magnetic field. The magnetic field had the effect of increasing the ordering of the partially ordered structure, making the sample act as if it were at a lower temperature. The molecular field for this sample decreased very quickly with increasing temperature, and thus the ordering effect was quite large. As the material become ordered, spin-waves characteristic of an ordered solid gave motionally narrowed lines with an increased hyperfine field.

REFERENCES

1.) J. G. Stevens and V. E. Stevens (Eds.), Mössbauer Effect Data Index Covering the 1974 Literature. Plenum Publ. Corp., N. Y., N. Y., 1975.

CHAPTER 5

DISCUSSION

The Mössbauer results have been compared with the magnetization data as a function of field, Zn concentration, and temperature. The cause of the large high field susceptibilities for high Zn concentrations was established and the magnetization as a function of concentration was reconciled with the spin structure. The maxima in the magnetization versus temperature curves of $x = 0.6, 0.8$ were also explained.

5.1 MAGNETIZATION AS A FUNCTION OF COMPOSITION:

The saturation magnetization $M_S(x)$ at 4.2K (fig. 3.4) was also plotted in the reduced form $M_S(x)/M_S(x=0)$ for each of the fields (fig. 5.1). In order to compare these experimental values with theoretical values, we first assumed the free ion magnetic moments of $\mu = 4\mu_B$ for Fe^{2+} ions and $\mu = 5\mu_B$ for Fe^{3+} ions independant of the site occupied. These values were used to calculate the moments for $x \lesssim 0.4$ which were also plotted in fig. 5.1. The considerable deviation of the theoretical from the experimental values has been explained in the past[1] by assuming a canted spin structure having canting angles of $\sim 11^{\circ}$ at $x = 0.2$, 25° at $x = 0.4$, 40° at $x = 0.6$, and 60° at $x = 0.8$. Our magnetization measurements for the samples $x = 0.0$ and 0.2 (fig. 3.3) however, showed a very small susceptibility at high fields, allowing us to place an upper limit of 5° on the canting. This indicates that the

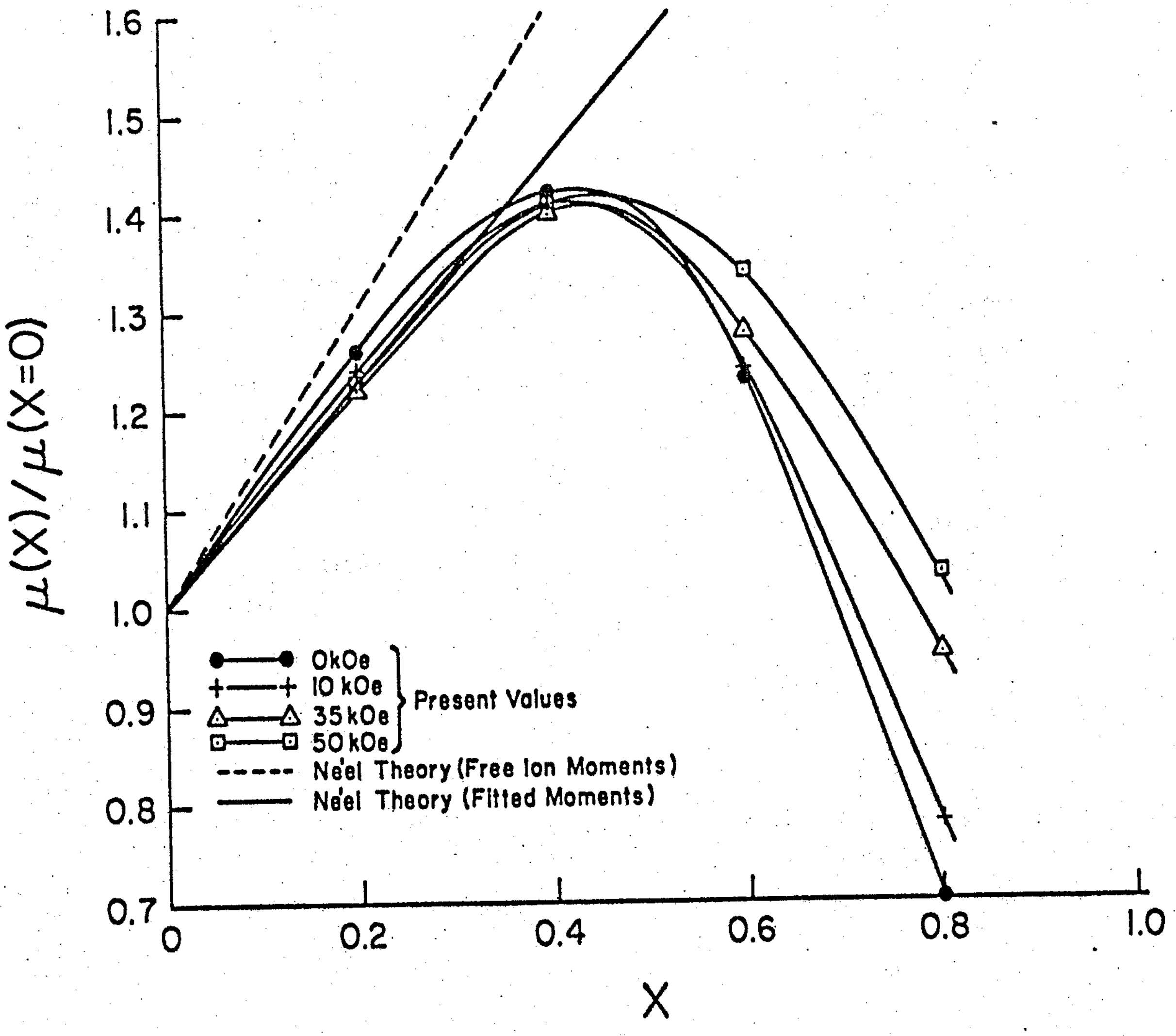

Fig. 5.1 Reduced magnetization versus Zn concentration

canting was not the cause of the discrepancy in magnetic moments in this region. The x = 0.4 sample showed a small high field susceptibility which, if assumed to be entirely due to decreases in canting angle, gave a value for the canting of $17\pm5^{\circ}$, in reasonable agreement with the Mössbauer effect measured value of $21\pm2^{\circ}$ at 10kOe.

The discrepancy in moments would be explained if the values of the magnetic moments of Fe^{2+} and Fe^{3+} ions in the lattice were found to be different from the free ion values assumed above. Such differences could be explained with two effects:

1. The quenching of the orbital moment might not have been complete, increasing the moment of Fe^{2+} ions.
2. Covalency effects could have caused a change in the magnetic moments due to the transfer of electrons into empty 3d orbitals, thus decreasing the magnetic moments for both Fe^{2+} and Fe^{3+}. Calculations were made for Fe^{3+} ions on both A and B sites, giving values of $4.31\mu_B$ and $4.62\mu_B$ respectively[2]. No values for Fe^{2+} ions were available.

We fitted the saturation magnetization of H = 15, 20, 25, 30, 40, 45, and 50kOe for x = 0.0 and 0.2 using the moments of Fe^{3+} ions on B sites, and the difference between Fe^{3+} ion moments on A sites and Fe^{2+} ion moments on B sites as variables (see Table 5.1).

TABLE 5.1

Fitted values of moments.

H (kOe)	B^{3+}	$A^{3+} - B^{2+}$	B^{2+} (assuming $\mu(A)=4.31\mu_B$)
15	4.57	0.43	3.88
20	4.56	0.39	3.92
25	4.53	0.33	3.98
30	4.53	0.32	3.99
35	4.56	0.35	3.96
40	4.52	0.29	4.02
45	4.52	0.29	4.02
50	4.61	0.39	3.92
average	4.55±.06	0.35±0.10	3.96±0.10

The moment of the Fe^{3+} ions on B sites agreed with the value from the covalency calculation, and thus we assumed the value calculated for the A site Fe^{3+} ions in order to fix that moment and that of the B site Fe^{2+} ions. We obtained

$\mu(Fe^{3+}, B) = \mu_\beta^{3+} = 4.55 \pm 0.06\ \mu_B$, $\mu(Fe^{3+}, A) = \mu_\alpha = 4.31\ \mu_B$,

and $\mu(Fe^{2+}, B) = \mu_\beta^{2+} = 3.96 \pm 0.10\ \mu_B$. The expected magnetization as a function of Zn substitution using these values is shown in fig. 5.1. Mössbauer results for the samples x = 0.0 and 0.2 are given in table 5.2.

TABLE 5.2

Internal hyperfine fields for x = 0.0 and 0.2 at 4.2K.

		Fe^{3+}	Fe^{2+}
Figure	Sample	H_{int}	H_{int}
4.2	0.0	515(1)	502(1)
4.3	0.2	512(1)	463(1)

Table 5.3

Internal hyperfine fields for x = 0.4 at 4.2K.

		B Fe^{3+}		B Fe^{2+}		A Fe^{3+}
Figure	Field	H_{int}	θ	H_{int}	θ	H_{int}
4.4	0	511(5)	-	450(1)	-	511(5)
4.5	10	530(5)	21(2)	464(2)	21(2)	511(5)
4.6	50	521(2)	$0^{(10)}$	472(5)	$0^{(10)}$	511(1)

For larger values of x ($x \gtrsim 0.4$), the experimental points deviated more and more from this theoretical fit. Further, the spread in $\mu(x)/\mu(x=0)$ for various applied fields increased with increasing Zn substitution. This was explained in terms of the localized canting of the spin structure found in this region.

The sample x = 0.4 was analysed at 0, 10 and 50kOe (Table 5.3). It was assumed that canting was uniform over the B site, although no B-site Fe^{2+} canting was allowed for in the fit due to the poor resolution of that subspectrum. Using the calculated values for the ionic moments and the formula

$$(1.4\mu_\beta{}^{3+} + 0.6\mu_\beta{}^{2+}) \cos \theta_B - 0.6\mu_\alpha = \mu(x=0.4,\ T=4.2),$$

we calculated the moments for the bulk magnetization, and compared them with the experimental results as shown in table 5.4.

TABLE 5.4

Magnetic moment of x = 0.4 at 4.2K as measured by magnetization and calculated from Mössbauer results.

Field	0	10	50
Magnetiz.	5.72 (6)	5.82 (6)	6.07 (6)
Mössbauer	----	5.6 (3)	6.2 (2)

These results clearly agree within the calculated errors.

The sample x = 0.6 was analysed at fields of 0, 10, 25 and 50kOe, the results of which are shown in Table 5.5. Assuming that all canting occurs on the B_5 and B_6' sites, values were calculated for the moments using the formula:

$$\mu(x,T=4.2) = \sum_{m=0}^{5}\Big\{P_{(m,x)}\cos[\theta_{(m,x)}] + P_{(6,x)}\cos[\theta_{(6,x)}]$$

$$+ P_{(6',x)}\cos[\theta_{(6',x)}]\Big\}\, 2\mu_\beta(x) - (1-x)\,\mu_\alpha(x)$$

derived in Chapter 2. The magnetization and Mössbauer-calculated results are shown in Table 5.6

TABLE 5.6

Magnetic moment of x = 0.6 at 4.2K as measured by magnetization and calculated from Mössbauer results.

Field (kOe)	0	10	25	50
Magnetization	4.99 (5)	5.16 (5)	5.40 (5)	5.78 (6)
Mössbauer	----	5.5 (3)	6.0 (3)	6.4 (3)

The Mössbauer values are an average of 10% higher than the measured magnetization values. No reasons for this discrepancy have been established. It can neither be explained in terms of absorber thickness effects nor in terms of an inaccuracy in the nominal Zn concentration.

For x = 0.8, moments were calculated (Table 5.8) using the

TABLE 5.5

Internal hyperfine fields and canting angles for x = 0.6 at 4.2K

		B_{04}	B_5		B'_6		A
Figure	Field	H_{int}	H_{int}	θ_5	H_{int}	θ_6	H_{int}
4.7	0	510(5)	510(5)	-	523(1)	-	510(5)
4.8	10	513(5)	508(5)	59(2)	511(5)	140*	509(5)
4.9	25	517(1)	511(2)	40(5)	518(3)	140*	512(3)
4.10	50	512(2)	514(3)	0	538(4)	140*	509(2)

TABLE 5.7

Internal hyperfine fields and canting angles for x = 0.8 at 4.2K

		B_{04}	B_5		B'_6		B_6	A
Figure	Field	H_{int}	H_{int}	θ_5	H_{int}	θ_6	H_{int}	H_{int}
4.11	0	509(5)	509(5)	-	522(1)	-	522(1)	509(5)
4.12	8.6	520(10)	515(5)	$65^{(12)}$	$504^{(10)}$	140*	520(10)	502(10)
4.13	15.4	517(5)	512(5)	$60^{(2)}$	$493^{(10)}$	140*	517(5)	501(5)
4.14	30	506(4)	512(5)	$54^{(5)}$	$517^{(4)}$	$140^{(5)}$	525(6)	510(4)
4.15	50	510(1)	513(1)	$46^{(1)}$	$527^{(5)}$	$142^{(1)}$	$527^{(1)}$	$516^{(5)}$

data in table 5.7, the assumption that canting only occurs on the B_5 and B'_6 sites, and the formula given above.

TABLE 5.8

Magnetic moment of x = 0.8 at 4.2K as measured by magnetization and calculated from Mössbauer results.

Field (kOe)	0	8.6	15.4	2.5	50
Magnetization	2.84 (3)	3.22 (3)	3.54 (4)	3.77 (4)	4.47 (5)
Mössbauer	----	3.2 (3)	3.5 (2)	3.8 (2)	4.2 (2)

The model clearly gives good agreement between the Mössbauer and magnetization measurements.

The magnetization at 4.2K as a function of Zn concentration was explained in terms of two different effects: a change in magnetic moments from the free ion values due to covalency effects; and localized canting. Below x = 0.4, no canting takes place and the results were explained using the Néel theory of ferrimagnets and fitting values for the moments of the various ions on different sites. These fitted values were then used over the entire sample range. At x = 0.4, an average canting angle on the B site was also used to explain the data. Above x = 0.4, the localized canting model, modified to allow the multiple reversals that can be caused by second and third B-site nearest neighbour interactions, allows a satisfactory explanation of the results. The spin structure for this region is shown in fig. 5.2.

5.2 The 0kOe Canting Angles and High Field Susceptibility at 4.2K:

We calculated the canting angles in zero field required to fit the observed (fig. 3.4) concentration dependence of the spontaneous magnetization. An average canting angle for the entire B site was calculated for all the samples, and for the x = 0.6, 0.8 samples a B_5 canting angle was calculated assuming a canting angle for B_6' of 140^o (Table 5.9).

TABLE 5.9

Canting angles calculated to fit H = 0kOe, T = 4.2K magnetization data.

x	0.0	0.2	0.4	0.6	0.8
$\theta_{ave.}$	<15	<15	18(15)	41(7)	66(3)
θ_5	-	-	-	70(3)	71(6)
θ_6'	-	-	-	140*	140*

The excellent agreement in calculated θ_5 angles between x = 0.6 and 0.8 supports the assumption that the B_6' canting angle was the same for x = 0.6 and 0.8.

The cause of the increase in the 4.2K high field susceptibility with increasing Zn concentration was also revealed by this data. At high fields, the canting angles were decreased, and the magnetization increased. A comparison of the canting angles estimated by assuming that all high field susceptibility was due to changing canting angles, and the average canting angles of table 5.9 is given in table 5.10.

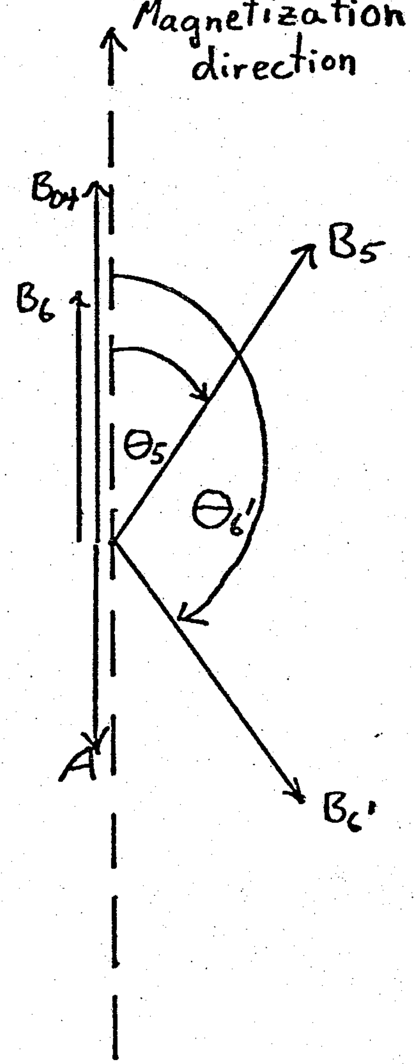

Fig. 5.2 Spin structure of $Zn_xF_{3-x}O_4$ for x = 0.6, 0.8.

TABLE 5.10

Average canting angles estimated from 4.2K high field susceptibility and from H = 0kOe, T = 4.2K magnetization fit.

x	0.0	0.2	0.4	0.6	0.8
$\theta_{ave.}$	<15	<15	18(15)	41(7)	66(3)
$\theta_{suscept.}$	<10	<10	17(5)	32(5)	75(8)

These values are in good agreement, indicating that the high field susceptibility at 4.2K was due to the decrease in canting angles with applied field.

5.3. The Magnetization as a Function of Temperature:

The Mössbauer results were compared with the magnetization results at various temperatures, and the canting angles and hyperfine field decreases were used to calculate the bulk magnetization. Studies on iron absorbers[3,4,5] have shown that the temperature dependence of the hyperfine field closely parallels that of the magnetization. Relaxation processes, characterized by a broadening of the outside lines and an increase in the area of the inner lines at the expense of the outer, were found for some compounds.

At 85K, the magnetization values for x = 0.2 and 0.4 were 4.95 and 5.55 μ_B/formula unit, representing a decline to 0.98±0.02 and 0.97±0.02 of the 4.2K values respectively. Mössbauer spectra for these samples were analysed at this temperature (see Table 5.11). These results showed a decline to 0.995±0.008 of the 4.2K value for the x = 0.2 sample, and a decline to 0.993±0.008 of the 4.2K value for the x = 0.4 sample, in agreement within the errors.

TABLE 5.11

Internal hyperfine fields for x = 0.2 and 0.4 at 85K

Figure	Sample	Fe^{3+} H_{int}	Fe^{2+} H_{int}
4.16	0.2	$506^{(1)}$	$466^{(1)}$
4.17	0.4	$502^{(1)}$	$454^{(1)}$

TABLE 5.12

Internal hyperfine fields for x = 0.6 above 4.2K.

Figure	Spectrum Temp.	Field	B_{04} H_{int}	B_5 H_{int}	θ_5	B_6' H_{int}	θ_6'	A H_{int}
4.18	20	0	$497^{(1)}$	$457^{(1)}$	-	$406^{(2)}$	-	$519^{(1)}$
4.19	32	10	$511^{(1)}$	$456^{(3)}$	$37^{(5)}$	383	140*	$513^{(1)}$
4.20	32	50	$510^{(1)}$	$456^{(6)}$	$23^{(10)}$	298	140*	$509^{(9)}$
4.21	85	0	$482^{(1)}$	$429^{(1)}$	-	$381^{(1)}$	-	$502^{(1)}$

TABLE 5.14

Internal hyperfine fields for x = 0.8 above 4.2K

Figure	Temp.	Field	B_{04} H_{int}	B_5 H_{int}	θ_5	B_6' H_{int}	θ_6'	B_6 H_{int}	A H_{int}
4.22	11.6	0	$500^{(5)}$	$500^{(5)}$	-	473(5)	-	473(5)	500(5)
4.23	20.7	0	$478^{(5)}$	$469^{(1)}$	-	435(5)	-	433(5)	478(5)
4.24	20	30	$506^{(1)}$	487(4)	$48^{(8)}$	$407^{(8)}$	$138^{(20)}$	408(2)	502(1)
4.25	20	50	$509^{(2)}$	$485^{(3)}$	$30^{(3)}$	$421^{(3)}$	$140^{(4)}$	430(2)	508(1)
4.26	40	0	$381^{(2)}$	$337^{(3)}$	-	$249^{(4)}$	-	249(4)	413(2)
4.27	40	30	$479^{(3)}$	$441^{(4)}$	$45^{(2)}$	$328^{(8)}$	$138^{(4)}$	324(6)	474(3)
4.28	40	50	$493^{(1)}$	$458^{(2)}$	$19^{(2)}$	$331^{(2)}$	$137^{(2)}$	331(6)	498(1)

For the x = 0.6 sample, Mössbauer data were gathered at 32K for 10kOe and 50kOe (see Table 5.12). The magnetization values at this temperature and these fields were compared with the values calculated from the Mössbauer measurements in Table 5.13.

TABLE 5.13

Magnetic moment of x = 0.6 above 4.2K as measured by magnetization and calculated from Mössbauer results.

Field	10kOe	50kOe
Magnetization	5.23(5)	5.80(5)
Mössbauer	6.0 (4)	6.2 (4)

The calculations were done by using the canting angles and hyperfine field decreases for each of the subspectra to calculate the moments on various sublattices, and then summing these values. Once again, the calculated values for x = 0.6 were approximately 10% higher than the measured values.

For x = 0.8, Mössbauer data were gathered at several temperatures and fields (see Table 5.14) and the calculated magnetization values compared with the measured values (see Table 5.15).

TABLE 5.15

Magnetic moment of x = 0.8 above 4.2K as measured by magnetization and calculated from Mössbauer results.

Temp	20K		40K	
Field	30kOe	50kOe	30kOe	50kOe
Magnetization	4.11(4)	4.61(5)	4.15(4)	4.66(5)
Mössbauer	4.1 (3)	4.7 (3)	4.0 (3)	4.9 (3)

The Mössbauer values were calculated by using the canting angle and hyperfine field decrease for each of the individual subspectra to calculate the moment for that subspectra, and then summing all the subspectra. The model here gives excellent agreement with the experimental results.

The peak in the magnetization for x = 0.6 and 0.8 (figs. 3.6-3.7) can now be seen as being due to the decrease in the B_5 canting angle. For the x = 0.6 sample, this is the situation for all fields. For the x = 0.8 sample, the decrease in moment due to the disordering caused by the increasing temperature more than offsets any increase in the moment due to the decreasing B_5 canting angle in fields of less than 10kOe. Where the applied field was larger than this, the field began to suppress the relaxation (see Chapter 4) resulting in a relatively sharp increase in the ordering. This allows the moment increase due to the decreasing B_5 canting angle to be observed.

The increase in the amount of ordering can also be observed by comparing the average high field susceptibility above 10kOe for 4.2K and 40K (table 3.2) with the Mössbauer results (table 5.14). The high field susceptibility was due to two possible phenomena: the decrease in the B_5 canting angle with applied field; and the increase in the $\langle S_z \rangle$ value due to field induced increases in the ordering. At 4.2K, all of the high field susceptibility above 10kOe was due to the decrease in B_5 canting angle as the sample is almost completely ordered at that temperature. At 40K however, significant disordering had occurred, and the high field susceptibility was due to both a decrease in the canting angle and an increase in the ordering of the sample with applied field.

REFERENCES

1. C. M. Srivastava et al, Phys. Rev. B, 14 (1976) 2032.
2. G. A. Sawatzky and F. Van der Woude, J. de Physique, 35 (1974) C_6.
3. H. H. Potter, Proc. Roy. Soc. (London), A146 (1934) 362.
4. R. S. Preston et al, Phys. Rev, 128 (1962) 2207.
5. M. A. Butler et al, Phys. Rev. B, 5 (1973) 990.

CONCLUSIONS

The localized canting model of Rosencwaig[1] was modified to allow for second and third nearest neighbour interactions under certain conditions. This model was used to compare magnetization and Mössbauer results.

It was found that the magnetic moment of the sample could be best fitted using moments other than free ion moments for Fe^{2+} and and Fe^{3+} ions. Canting angles were found only for samples with $x \gtrsim 0.4$, and accounted for the peak in the magnetization versus Zn concentration curve.

The high field susceptibility was found to increase with increasing Zn concentration for $x \gtrsim 0.4$, and this was found to be due to the field dependence of the canting angles.

The peak in the magnetization vs temperature curves for $x = 0.6, 0.8$ was found to be due to a decrease in canting angle with temperature. For $x = 0.8$, this peak could not be seen with an applied field of less than 10kOe due to the predominance of the relaxation effects in this region. These relaxation effects were found to be suppressed by increasing the applied field.

This study could be further pursued by:

1) trying to find the sizes of the exchange parameters by finding the field required to completely suppress the canting; and
2) quantitatively characterizing the relaxation processes and conclusively establishing their source.

APPENDIX A

Multiple Reversal Probabilities

In this appendix, the probabilities for multiple reversals of B site spins have been calculated. A model of the spinel structure has been constructed and was frequently referred to during the analysis. The reader may find such a model useful to follow the argument.

In magnetite, each B site ion is surrounded by 6 N N (nearest neighbour) oxygen ions at 2.066 Å, six N N N (next nearest neighbour) B site ions at 2.969 Å (hereafter referred to as B* sites), and six N N N N (next-next nearest neighbour) A site ions at 3.481 Å (hereafter referred to as A* sites). We assume (since $J_{AB} >> J_{BB}$) that only B sites with 6 Zn N N N N can have canting angles $> 90^{o}$. Each of the B* sites also has 6 N N N N A site ions (referred to as A** sites). Three of these A** sites coincide with three of the A* sites.

If we choose a B site ion (hereafter referred to as B_6) which has Zn ions in all six of the A* sites (hereafter referred to as Zn* ions), then all the B* sites will have three Zn* ions as N N N N in A** sites. If any one of the B* sites has more Zn N N N N, they will be designated as Zn** ions.

The six B* sites can be divided into two equal groups, each sharing 4 independent A** sites which are not also A* sites. No such A** sites are shared by members of both groups. This makes it possible to calculate the probability of each combination of numbers of Zn N N N N for a group of 3 B* sites, and then combine these probabilities to determine the probabilities for various combinations of B* sites having various numbers of Zn nearest neighbours. The results are shown in tables A.1 and A.2.

If a B site ion has six Zn N N N N, then the B-B* interaction will align it antiparallel to the B* sites. Such a spin may be referred to as being reversed, and the probability of this occurring is given in table A.3. The probability for more than half of the B* sites in such a case being themselves reversed (either six out of six reversed or four out of six reversed with the other two having five Zn N N N N) can be seen in table A.2. In this case, the B site is reversed with respect to the majority of the B* sites, and doubly reversed with respect to the B lattice. For the x = 0.6 sample, we can therefore determine the multiple reversal probabilities as shown in table A.4.

TABLE A.4

x = 0.6 multiple reversal probabilities

Unreversed	B sites with 0 - 5 Zn N N N N	0.95334
Singly reversed	B sites with 6 Zn N N N N	0.04274
Doubly reversed	B sites with 6 Zn N N N N	0.00392

TABLE A.1

Probability for Zn A-site substitution in one group.

	x = 0.6	x = 0.8
The probability for all 3B* sites to have 3 Zn N N N N	0.0256	0.0016
The probability for 2B* sites to have 4 Zn N N N N and 1 B* site to have 3 Zn N N N N	0.1152	0.0192
The probability for 3B* sites to have 4 Zn N N N N	0.0384	0.0064
The probability for 2B* sites to have 4 Zn N N N N and 1 B* site to have 5 Zn N N N N	0.1728	0.0768
The probability for 2B* sites to have 5 Zn N N N N and 1 B* site to have 4 Zn N N N N	0.1728	0.0768
The probability for 3B* sites to have 5 Zn N N N N	0.0864	0.1024
The probability for 2B* sites to have 5 Zn N N N N and 1 B* site to have 6 Zn N N N N	0.2592	0.3072
The probability for 3B* sites to have 6 Zn N N N N	0.1296	0.4096

TABLE A.2

Probability for Zn A site substitution for two groups together

# B Sites with 6 Zn N N N N	# B Sites with 5 Zn N N N N	Prob x = 0.6	Prob x = 0.8
6	0	0.01680	0.16777
4	2	0.06718	0.25166
3	3	0.02236	0.08389
2	4	0.06718	0.09437

TABLE A.3

The probability for a B site spin to have m Zn A site neighbours for a concentration of x.

x \ m	0	1	2	3	4	5	6
0.0	$1.\overline{0}$	-	-	-	-	-	-
0.2	.26214	.39322	.24576	.08192	.01536	.00154	.00006
0.4	.04666	.18662	.32104	.27648	.13824	.03686	.00410
0.6	.00410	.03686	.13824	.27648	.32104	.18662	.04666
0.8	.00006	.00154	.01536	.08192	.24576	.39322	.26214
1.0	-	-	-	-	-	-	$1.\overline{0}$

In the case of x = 0.8, it is profitable to carry this calculation one step further, to triple reversals. The intermediate results are given in table A.5.

TABLE A.5

x = 0.8 multiple reversal probabilities

Unreversed	B sites with 0 - 5 Zn N N N N	-	0.73786
Singly reversed	B sites with 6 Zn N N N N	-	0.15219
Doubly reversed	B sites with 6 Zn N N N N	-	0.10995

Each of the 6 B* sites has 6 B site N N N. One of these is the B_6 site, and two more are other B* sites. The remaining three sites are referred to as B** sites. No B* site shares any B** sites with another B* site, so the three B** sites associated with each B* site can be treated as an independent group. Each group of 3 B** sites shares A site N N N N consisting of 3 Zn* sites, 3 Zn** sites and 4 A*** sites. The probability of any B** group being reversed is thus analgous to the probability of any B* group being reversed.

For those double reversals where all 6 B* sites have 6 Zn N N N N, the probability of doubly reversing 4 or more such B* sites, and thus triply reversing B_6 is 0.20713. For those double reversals where 4 B* sites have 6 Zn N N N N and 2 B* sites have 5 Zn N N N N, the probability of doubly reversing two of the 4 B_6^* while leaving the B_5^* sites unreversed, or doubly reversing 3 of the 4 B_6^* sites and either one or none of the B_5^* sites, or doubly reversing all 4 B_6^* sites is 0.29757. Any such combination will result in a majority of doubly reversed and unreversed B* sites, and thus a triply reversed B_6 site. The multiple reversal probabilities for both samples x = 0.6 and x = 0.8 are shown in table A.6.

TABLE A.6

Multiple reversal probabilities for x = 0.6, 0.8

		x=0.6	x=0.8
Unreversed	(B sites with 0-5 Zn N N N N)	0.95334	0.73786
Single reversed	(B sites with 6 Zn N N N N)	0.04274	0.15219
Doubly reversed	(B sites with 6 Zn N N N N)	0.00392	0.08121
Triply reversed	(B sites with 6 Zn N N N N)	----	0.02874

We can use these numbers and calculate probabilities for 8 different kinds of sites, in a way analgous to table A.3, by adding a distinction that separates the sites with 6 Zn N N N N into a reversed (singly and triply) site called B_6' and an unreversed (doubly reversed) site called B_6. This is shown in table A.7.

TABLE A.7

Probabilities for various differentiated B sites

m x	0	1	2	3	4	5	6	6′
0.0	$1.\overline{0}$	---	---	---	---	---	---	---
0.2	0.26214	0.39322	0.24576	0.08192	0.01536	0.00154	---	0.000006
0.4	0.04666	0.18662	0.32104	0.27648	0.13824	0.03686	---	0.00410
0.6	0.00410	0.03686	0.13824	0.27648	0.32104	0.18662	0.00392	0.04274
0.8	0.00006	0.00154	0.01536	0.08192	0.24576	0.39322	0.08121	0.18093

APPENDIX B.

The calculation of the moments of the sample with x = 0.8 can also be made using the free ion magnetic moments for the Fe^{2+} and Fe^{3+} ions. This is done to show that the general characteristics of the magnetization curves, such as the peak of the magnetization versus temperature curve, are not a function of the moments fitted in Chapter 5 but that these moments give better quantitative results. The values calculated are shown in Table B.1 which gives the magnetization values, the free ion calculated values, and the fitted calculated values for the moment at the various temperatures and fields where Mössbauer spectra were analysed.

The magnetization calculated using the free ion values of the magnetic moments shows a clear rise with increasing magnetic field at all temperatures, and an increase with increasing temperature at both 30kOe and 50kOe, but the values themselves are not all in good agreement with the measured values. The magnetization calculated using the fitted values gives good agreement over the entire temperature and field ranges.

TABLE B.1

Measured magnetization values, free ion calculated values and fitted ion calculated values and fitted ion calculated values for the moment of $x = 0.8$ at various temperatures and fields

TEMPERATURE (K)	4.2					20		40	
FIELD (kOe)	0	8.6	15.4	25	50	30	50	30	50
Magnetization	2.84(3)	3.22(3)	3.54(4)	3.77(4)	4.47(5)	4.11(4)	4.61(5)	4.15(4)	4.66(5)
Free ion calc.	---	3.4 (7)	3.7 (1)	4.1 (3)	4.5 (5)	4.4 (1)	5.1 (1)	4.3 (1)	5.2 (1)
Fitted calc.	---	3.2 (3)	3.5 (2)	3.8 (2)	4.2 (2)	4.1 (3)	4.7 (3)	4.0 (3)	4.9 (3)

APPENDIX C

Several models were used in attempts to analyse the data from Mössbauer and magnetization measurements. The models used were: the localized canting model with no reversed spins; the localized canting model with reversed spins; and the modified localized canting model with multiply-reversed spins. These models were all compared with the Mössbauer data at 4.2K, 50kOe and 40K, 50kOe, and the magnetization value of 4.47±.04 μ_B/formula unit at 4.2K, 50kOe.

The 4.2K, 50kOe spectrum (fig. C.1) was fitted with lines corresponding to the A site in line a and the B site in line b. Line c was assumed to be due to canting on the B site alone. This yielded an A:B ratio of 0.30:1, a value much higher than the expected ratio of 0.10:1. In addition, the calculated magnetization using this model was 7.2±2 μ_B/formula unit, a value 60% higher than the measured value. The possibility that this indicated the presence of Zn atoms on the B sites could be eliminated because at 40K, 50kOe, the spectrum had the shape shown in fig. C.2, and an area ratio of 0.08:1. At 40K, only A-site ions contributed to the absorption of peak a, but at 4.2K, some B-site spins must have been reversed and contributing to the absorption of peak a. The two Mössbauer spectra showed that peak a broadened with increasing temperature as one would have expected, but that peak b decreased in linewidth. This also indicated the presence of an additional component at 4.2K.

Reversal behaviour could be expected of B sites with large numbers of Zn nearest neighbours, according to the localized canting model. We assumed that all B site spins with six Zn nearest neighbours were reversed and contributing to the area ot peak a and peak c. This gave a theoretical area ratio of 0.49:1, a value in disagreement with the measured value of 0.35:1 (this value was different from the measured value above because of the intensity from peak c). The magnetization calculated using this model was 2.7±.2μ_B/formula unit, a value 40%too low.

When we allowed for multiple reversals as calculated in appendix A, we got a theoretical area ratio 0.36:1, in good agreement with the experimental value of 0.35:1. The B_6 spins could be expected to have a larger temperature dependance of the hyperfine field than the A site spins, and thus would contribute to peak b at 40K. The value calculated for the magnetization using this model is 4.2±0.2μ_B/formula unit, a difference of 6% from the measured value. This model clearly gives by far the best agreement between the Mössbauer and magnetization data.

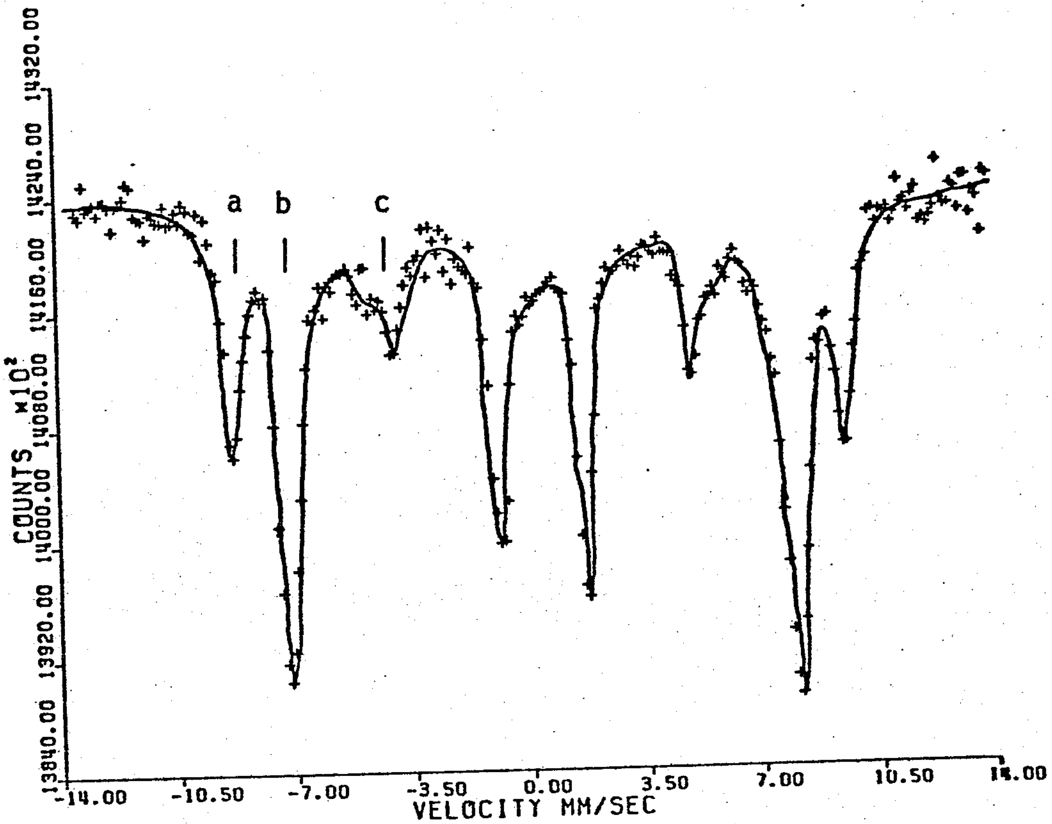

Fig. C.1 Mössbauer spectrum of x = 0.8 at 4.2K, 50kOe.

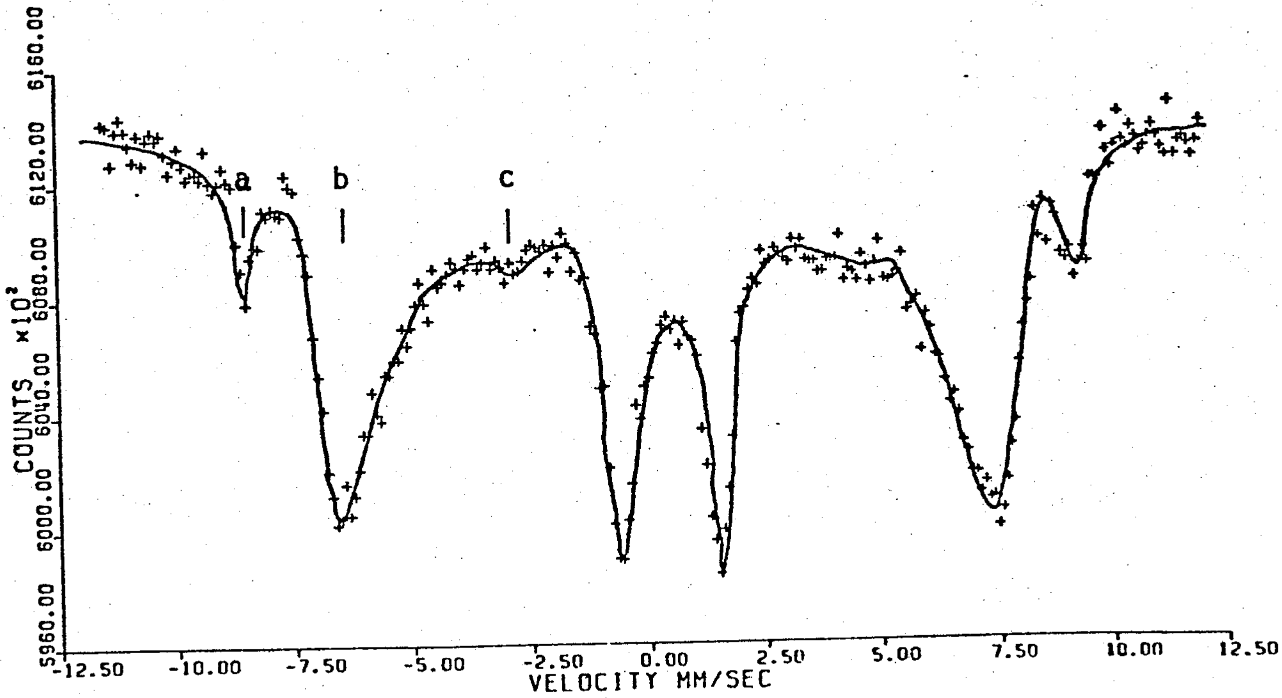

Fig. C.2 Mössbauer spectrum of x = 0.8 at 40K, 50kOe.